

IFSCOM-E 2023
9TH IFS AND CONTEMPORARY MATHEMATICS AND ENGINEERING CONFERENCE
08-11 JULY 2023 TARSUS, MERSİN, TÜRKİYE
ISBN: 978-605-68670-8-8
pp: 95-102

GENERALIZED SYMMETRIC BI-DERIVATIONS OF UP(BCC)-ALGEBRAS

DAMLA YILMAZ

ABSTRACT. In this paper, we define the notions of generalized (l, r) -symmetric bi-derivations and generalized (r, l) -symmetric bi-derivations on UP-algebras. We also explore some of the properties these derivations.

1. INTRODUCTION

Algebraic logic emerged as a subdiscipline of algebra in the nineteenth century. In the following years, studies on the relationship between logic and ordered systems such as Boolean algebras, lattice ordered groups, MV-algebras, etc. have been the subject of many researchers. For example, BCK-algebras and BCI-algebras are two classes of logic algebras introduced in [10], [11] and extensively investigated by many researchers. It is known that BCK-algebras form a proper subclass of BCI-algebras. That is, every BCK-algebra is a BCI-algebra but not vice versa [6].

In the theory of rings, the notion of derivation was given by Posner in [19] and the notion of symmetric bi-derivation was introduced by Gy. Maksa [13], [14]. Many researchers applied these notions of different derivations to BCI-algebras (see [1], [2], [3], [4], [15], [12], [17], [9]).

UP-algebras, introduced by Iampan as a generalization of KU-algebras in [7], have actually been studied since the early 1980s. Since they turn out to be just the residuated on one side, they are sometimes called left residuation algebras (see [16] and its references). Also, they have been called BCC-algebras in some papers. In [18], authors studied left-right derivations and right-left derivations of BCC-algebras. For different derivations studies in BCC-algebras, references [5] can be consulted. In 2016, Sawika et al introduced the notions of (l, r) -derivations, (r, l) -derivations and derivations in UP-algebras [20]. Later, different derivations were studied in UP-algebras (see [8], [21],[22]).

This paper presents the notions of generalized (l, r) -symmetric bi-derivations and generalized (r, l) -symmetric bi-derivations on UP-algebras. Moreover, we investigate some properties of the trace of this derivations and the set $Ker_\phi(U)$.

Date: July, 8, 2023.

Key words and phrases. UP-algebra, Generalized symmetric bi-derivation, Trace, BCC-algebras.

2. PRELIMINARIES

Definition 2.1. [7] An algebra $\mathcal{U} = (U; \odot, 0)$ of type $(2, 0)$ is called a UP-algebra if for all $u, v, w \in U$ the following conditions hold:

- (UP-1) $(v \odot w) \odot ((u \odot v) \odot (u \odot w)) = 0$
- (UP-2) $0 \odot u = u$
- (UP-3) $u \odot 0 = 0$
- (UP-4) $u \odot v = v \odot u = 0$ implies $u = v$

Example 2.2. [7] Suppose that E is a universal set. Define a binary operation \otimes on the power set of E by putting $E_1 \otimes E_2 = E_2 \cap E_1' = E_1' \cap E_2 = E_2 - E_1$ for all $E_1, E_2 \in P(E)$. Then, $(P(E); \otimes, \emptyset)$ is a UP-algebra and it is called the power UP-algebra of type 1.

Example 2.3. [7] Suppose that E is a universal set. Define a binary operation \ominus on the power set of E by putting $E_1 \ominus E_2 = E_2 \cup E_1' = E_1' \cup E_2$ for all $E_1, E_2 \in P(E)$. Then, $(P(E); \ominus, E)$ is a UP-algebra and it is called the power UP-algebra of type 2.

In a UP-algebra $\mathcal{U} = (U; \odot, 0)$, the following properties hold: for any $u, v, w \in U$,

- (1) $u \odot u = 0$
- (2) $u \odot v = 0$ and $v \odot w = 0$ imply $u \odot w = 0$
- (3) $u \odot v = 0$ implies $(w \odot u) \odot (w \odot v) = 0$
- (4) $u \odot v = 0$ implies $(v \odot w) \odot (u \odot w) = 0$
- (5) $u \odot (v \odot u) = 0$
- (6) $(v \odot u) \odot u = 0$ if and only if $u = v \odot u$
- (7) $u \odot (v \odot v) = 0$ ([7])

On a UP-algebra $\mathcal{U} = (U; \odot, 0)$, we define a binary relation \leq on U as follows:

$$u \leq v \text{ if and only if } u \odot v = 0, \text{ for all } u, v \in U$$

In a UP-algebra $\mathcal{U} = (U; \odot, 0)$, for any $u, v, w \in U$,

- (1) $u \leq u$
- (2) $u \leq v$ and $v \leq u$ imply $u = v$
- (3) $u \leq v$ and $v \leq w$ imply $u \leq w$
- (4) $u \leq v$ implies $w \odot u \leq w \odot v$
- (5) $u \leq v$ implies $v \odot w \leq u \odot w$
- (6) $u \leq v \odot u$
- (7) $u \leq v \odot v$ ([7])

Definition 2.4. [7] Let $\mathcal{U} = (U; \odot, 0)$ be a UP-algebra. A subset W of U is called a UP-subalgebra of U if the constant 0 of U is in W and $(W; \odot, 0)$ is a UP-algebra.

Clearly, U and $\{0\}$ are UP-subalgebras of U .

Theorem 2.5. [7] A non-empty subset W of a UP-algebra $\mathcal{U} = (U; \odot, 0)$ is a UP-subalgebra of U if and only if W is closed under the \odot multiplication on U .

Definition 2.6. [7] Let $\mathcal{U} = (U; \odot, 0)$ be a UP-algebra. A subset V of U is called a UP-ideal of U if it satisfies the following properties:

- (1) The constant 0 of U is in V ,
- (2) For any $u, v, w \in U$, $u \odot (v \odot w) \in V$ and $v \in V$ imply $u \odot w \in V$.

Clearly, U and $\{0\}$ are UP-ideals of U .

Definition 2.7. [20] Let $\mathcal{U} = (U; \odot, 0)$ be a UP-algebra. We define a binary operation \wedge by $u \wedge v = (v \odot u) \odot u$.

Definition 2.8. [20] A UP-algebra U is called meet-commutative if $u \wedge v = v \wedge u$ for all $u, v \in U$, i.e., $(v \odot u) \odot u = (u \odot v) \odot v$.

Theorem 2.9. [20] Let U be a UP-algebra. For any $u \in U$, the following properties hold:

- (1) $0 \wedge u = 0$
- (2) $u \wedge 0 = 0$
- (3) $u \wedge u = u$

Definition 2.10. [20] Let U be a UP-algebra. A self map $d : U \rightarrow U$ is called an (l, r) -derivation of U if it satisfies the identity

$$d(u \odot v) = (d(u) \odot v) \wedge (u \odot d(v))$$

for all $u, v \in U$. Similarly, a self map $d : U \rightarrow U$ is called an (r, l) -derivation of U if it satisfies the identity

$$d(u \odot v) = (u \odot d(v)) \wedge (d(u) \odot v)$$

for all $u, v \in U$.

Definition 2.11. [5] Let U be a UP-algebra. A mapping $D : U \rightarrow U$ is called a generalized (l, r) -derivation of U if there exists an (l, r) -derivation $d : U \rightarrow U$ such that

$$D(u \odot v) = (D(u) \odot v) \wedge (u \odot d(v))$$

for all $u, v \in U$; if there exists an (r, l) -derivation $d : U \rightarrow U$ such that

$$D(u \odot v) = (u \odot D(v)) \wedge (d(u) \odot v)$$

for all $u, v \in U$, the mapping $D : U \rightarrow U$ is called a generalized (r, l) -derivation of U .

Definition 2.12. [22] Let U be a UP-algebra. A map $F : U \times U \rightarrow U$ is called symmetric if $F(u, v) = F(v, u)$ holds for all $u, v \in U$.

Definition 2.13. [22] Let U be a UP-algebra and $f : U \rightarrow U$ be a map defined by $f(u) = F(u, u)$. Then, f is called the trace of F , where $F : U \times U \rightarrow U$ is a symmetric mapping.

Definition 2.14. [22] Let U be a UP-algebra and $F : U \times U \rightarrow U$ be a symmetric map. If F satisfies the identity $F(u \odot v, w) = (F(u, w) \odot v) \wedge (u \odot F(v, w))$ for all $u, v, w \in U$, then F is called left-right symmetric bi-derivation (briefly (l, r) -symmetric bi-derivation). If F satisfies the identity $F(u \odot v, w) = (u \odot F(v, w)) \wedge (F(u, w) \odot v)$ for all $u, v, w \in U$, then we say that F is right-left symmetric bi-derivation (briefly (r, l) -symmetric bi-derivation). If F is both (l, r) -symmetric bi-derivation and (r, l) -symmetric bi-derivation, it is called symmetric bi-derivation.

3. GENERALIZED SYMMETRIC BI-DERIVATIONS OF UP(BCC)-ALGEBRAS

Throughout this section, U is a UP-algebra.

Definition 3.1. Let $F : U \times U \rightarrow U$ be an (l, r) -symmetric bi-derivation and $\Phi : U \times U \rightarrow U$ be a symmetric map. We say that Φ is a generalized (l, r) -symmetric bi-derivation related to F , if it satisfies

$$\Phi(u \odot v, w) = (\Phi(u, w) \odot v) \wedge (u \odot F(v, w))$$

for all $u, v, w \in U$. If $F : U \times U \rightarrow U$ is an (r, l) -symmetric bi-derivation and $\Phi : U \times U \rightarrow U$ is a symmetric map such that

$$\Phi(u \odot v, w) = (u \odot \Phi(v, w)) \wedge (F(u, w) \odot v)$$

for all $u, v, w \in U$, then we say that Φ is a generalized (r, l) -symmetric bi-derivation related to F .

Example 3.2. Let $U = \{0, u, v, w, z\}$ be a set with a binary operation \odot is defined by the following Cayley table:

\odot	0	u	v	w	z
0	0	u	v	w	z
u	0	0	0	0	0
v	0	v	0	0	0
w	0	v	v	0	0
z	0	v	v	z	0

Then, $(U; \odot, 0)$ is a UP-algebra. The mappings $F : U \times U \rightarrow U$ defined by

$$F(a, b) = \begin{cases} z, & (a, b) = (u, u) \\ 0, & \text{otherwise} \end{cases}$$

and $\Phi : U \times U \rightarrow U$ defined by

$$\Phi(a, b) = \begin{cases} z, & (a, b) \in \{(u, u), (w, w)\} \\ 0, & \text{otherwise} \end{cases}$$

It can be seen that F is an (r, l) -symmetric bi-derivation and Φ is a generalized (r, l) -symmetric bi-derivation related to F . Since $\Phi(0 \odot u, u) = (\Phi(0 \odot u) \odot u) \wedge (0 \odot F(u, u)) = (0 \odot u) \wedge (0 \odot z) = u \wedge z = v \neq \Phi(u, u) = z$, Φ is not a generalized (l, r) -symmetric bi-derivation.

Theorem 3.3. Let Φ be a generalized (l, r) -symmetric bi-derivation on U related to (l, r) -symmetric bi-derivation F with its trace f and ϕ be the trace of Φ . Then, for all $u, v, w \in U$

- (1) $\Phi(0, u) = 0$
- (2) $\Phi(u, v) = u \wedge F(u, v)$
- (3) $u \leq \Phi(u, v)$
- (4) $\Phi(u, v) \odot w \leq \Phi(u \odot w, v)$

Proof. (1) For all $u \in U$. We have

$$\begin{aligned} \Phi(0, u) &= \Phi(u \odot 0, u) \\ &= (\phi(u) \odot 0) \wedge (u \odot F(0, u)) \\ &= 0 \wedge (u \odot F(0, u)) \\ &= 0 \end{aligned}$$

(2) For all $u, v \in U$, we get

$$\begin{aligned}\Phi(u, v) &= \Phi(0 \odot u, v) \\ &= (\Phi(0, v) \odot u) \wedge (0 \odot F(u, v)) \\ &= (0 \odot u) \wedge F(u, v) \\ &= u \wedge F(u, v)\end{aligned}$$

(3) Let $u, v \in U$. By using (2), we have

$$\begin{aligned}u \odot \Phi(u, v) &= u \odot (u \wedge F(u, v)) \\ &= u \odot ((F(u, v) \odot u) \odot u) \\ &= 0\end{aligned}$$

Thus, $u \leq \Phi(u, v)$ for all $u, v \in U$.

(4) Let $u, v, w \in U$. We have

$$\begin{aligned}(\Phi(u, v) \odot w) \odot (\Phi(u \odot w, v)) &= (\Phi(u, v) \odot w) \odot [(\Phi(u, v) \odot w) \wedge (u \odot F(w, v))] \\ &= (\Phi(u, v) \odot w) \odot [(u \odot F(w, v)) \odot (\Phi(u, v) \odot w)] \odot (\Phi(u, v) \odot w) \\ &= 0\end{aligned}$$

□

Theorem 3.4. *Let Φ be a generalized (r, l) -symmetric bi-derivation on U related to (r, l) -symmetric bi-derivation F with the trace f and ϕ be the trace of Φ . Then, for all $u, v, w \in U$,*

- (1) $\Phi(0, u) = 0$
- (2) $\Phi(u, v) = \Phi(u, v) \wedge u$
- (3) $u \odot \Phi(v, w) \leq \Phi(u \odot v, w)$

Proof. (1) For all $u \in U$, we have

$$\begin{aligned}\Phi(0, u) &= \Phi(u \odot 0, u) \\ &= (u \odot \Phi(0, u)) \wedge (f(u) \odot 0) \\ &= (u \odot \Phi(0, u)) \wedge 0 \\ &= 0\end{aligned}$$

(2) Let $u, v \in U$. Using Proposition 3.7 in [22], we find

$$\begin{aligned}\Phi(u, v) &= \Phi(0 \odot u, v) \\ &= (0 \odot \Phi(u, v)) \wedge (F(0, v) \odot u) \\ &= \Phi(u, v) \wedge u\end{aligned}$$

(3) Let $u, v, w \in U$. Then, we get

$$\begin{aligned}(u \odot \Phi(v, w)) \odot \Phi(u \odot v, w) &= (u \odot \Phi(v, w)) \odot [(u \odot \Phi(v, w)) \wedge (F(u, w) \odot v)] \\ &= (u \odot \Phi(v, w)) \odot [(F(u, w) \odot v) \odot (u \odot \Phi(v, w))] \odot (u \odot \Phi(v, w)) \\ &= 0\end{aligned}$$

□

Definition 3.5. Let W be a non-empty subset of U . If $\Phi(W, W) \subseteq W$, then W is said to be Φ -invariant, where $\Phi(W, W) = \{\Phi(w_1, w_2) \mid w_1, w_2 \in W\}$.

Theorem 3.6. *Let Φ be a generalized (l, r) -symmetric bi-derivation on U related to (l, r) -symmetric bi-derivation F . Then, every UP-ideal W of U is Φ -invariant.*

Proof. Let $a \in \Phi(W, W)$. Thus, $a = \Phi(w_1, w_2)$ for some $w_1, w_2 \in W$. By Theorem 3.3 (3), we have $w_1 \leq \Phi(w_1, w_2)$ and so $w_1 \odot \Phi(w_1, w_2) = 0$. Since $w_1 \in W$, W is a UP-ideal and $0 \odot (w_1 \odot \Phi(w_1, w_2)) = 0$, we get $\Phi(w_1, w_2) = a \in W$. Thus, we obtain $\Phi(W, W) \subseteq W$. \square

Definition 3.7. [22] Let Φ be an (l, r) - (or (r, l) -) symmetric bi-derivation of U . For a fixed element $a \in U$, we define a map $d_a : U \rightarrow U$ by $d_a(u) = F(u, a)$ for all $u \in U$.

Theorem 3.8. [22] Suppose that F is an (l, r) - (resp. (r, l) -) symmetric bi-derivation of U . Then, the map d_a is an (l, r) - (resp. (r, l) -) derivation of U , for all $a \in U$.

Theorem 3.9. Let Φ be a generalized (l, r) - (resp. (r, l) -) symmetric bi-derivation of U . For a fixed element $a \in U$, we define a map $D_a : U \rightarrow U$ by $D_a(u) = \Phi(u, a)$ for all $u \in U$. Then, the map D_a is a generalized (l, r) - (resp. (r, l) -) derivation of U , for all $a \in U$.

Proof. For all $u, v \in U$, we have

$$\begin{aligned} D_a(u \odot v) &= \Phi(u \odot v, a) \\ &= (\Phi(u, a) \odot v) \wedge (u \odot F(v, a)) \\ &= (D_a(u) \odot v) \wedge (u \odot d_a(v)) \end{aligned}$$

\square

Definition 3.10. Let Φ be a generalized $((l, r)$ - or (r, l) -) symmetric bi-derivation on U and ϕ be the trace of Φ . We define a subset of U by

$$Ker_\phi(U) = \{u \in U \mid \phi(u) = 0\}$$

Theorem 3.11. Let Φ be a generalized (r, l) -symmetric bi-derivation of U related to (r, l) -symmetric bi-derivation F . If $u \in U$ and $v \in Ker_\phi(U)$, then $v \wedge u \in Ker_\phi(U)$.

Proof. Let $u \in U$ and $v \in Ker_\phi(U)$. Then, we have $\phi(v) = 0$. Hence,

$$\begin{aligned} \phi(v \wedge u) &= \Phi(v \wedge u, v \wedge u) = \Phi((u \odot v) \odot v, v \wedge u) \\ &= ((u \odot v) \odot \Phi(v, v \wedge u)) \wedge (F(u \odot v, v \wedge u) \odot v) \\ &= ((u \odot v) \odot \Phi(v, (u \odot v) \odot v)) \wedge (F(u \odot v, v \wedge u) \odot v) \\ &= ((u \odot v) \odot ((u \odot v) \odot \phi(v) \wedge F(u \odot v, v) \odot v)) \wedge (F(u \odot v, v \wedge u) \odot v) \\ &= 0 \wedge (F(u \odot v, v \wedge u) \odot v) \\ &= 0 \end{aligned}$$

Thus, we get $v \wedge u \in Ker_\phi(U)$ for all $u \in U$ and $v \in Ker_\phi(U)$. \square

Theorem 3.12. Let Φ be a generalized (r, l) -symmetric bi-derivation of U related to (r, l) -symmetric bi-derivation F . If $v \in Ker_\phi(U)$, then we have $u \odot v \in Ker_\phi(U)$ for all $u \in U$.

Proof. Let $u \in U$ and $v \in Ker_\phi(U)$. Then, $\phi(v) = 0$. Hence, we get

$$\begin{aligned} \phi(u \odot v) &= \Phi(u \odot v, u \odot v) \\ &= ((u \odot \Phi(v, u \odot v)) \wedge (F(u, u \odot v) \odot v)) \\ &= (u \odot ((u \odot \phi(v)) \wedge (F(v, u) \odot v))) \wedge (F(u, u \odot v) \odot v) \\ &= 0 \wedge (F(u, u \odot v) \odot v) \\ &= 0 \end{aligned}$$

Thus, we find that $u \odot v \in Ker_f(U)$ for all $u \in U$ and $v \in Ker_f(U)$. \square

Theorem 3.13. *Let Φ be a generalized (r, l) -symmetric bi-derivation of U related to (r, l) -symmetric bi-derivation F . Then, $Ker_\phi(U)$ is a UP-subalgebra of U .*

Proof. Directly from Theorem 3.12. \square

Theorem 3.14. *Assume that U is a meet-commutative UP-algebra, Φ is a generalized (r, l) -symmetric bi-derivation related to (r, l) -symmetric bi-derivation F . If $v \leq u$ and $v \in Ker_\phi(U)$ for all $u, v \in U$, then $u \in Ker_\phi(U)$.*

Proof. Let $v \leq u$ and $v \in Ker_\phi(U)$. Then, we have $v \odot u = 0$ and $\phi(v) = 0$. Hence, we get

$$\begin{aligned}
 \phi(u) &= \phi(0 \odot u) \\
 &= \phi((v \odot u) \odot u) \\
 &= \phi((u \odot v) \odot v) \\
 &= \Phi((u \odot v) \odot v, (u \odot v) \odot v) \\
 &= ((u \odot v) \odot \Phi(v, (u \odot v) \odot v)) \wedge (F(u \odot v, (u \odot v) \odot v) \odot v) \\
 &= ((u \odot v) \odot ((u \odot v) \odot \phi(v)) \wedge (F(u \odot v, v) \odot v)) \wedge (F(u \odot v, (u \odot v) \odot v) \odot v) \\
 &= 0 \wedge (F(u \odot v, (u \odot v) \odot v) \odot v) \\
 &= 0
 \end{aligned}$$

Therefore, we obtain $u \in Ker_\phi(U)$. \square

4. CONCLUSION

Some characterizations of algebraic structures are determined by derivations. In this paper, we define generalized (l, r) - and (r, l) -symmetric bi-derivations of UP-algebras and we examine some properties of them. After this paper, some type of generalized symmetric bi-derivations, permuting tri-derivations can be studied on UP-algebras.

REFERENCES

- [1] H. A. Abujabal, N. O. Al-Shehri, Some results on derivations of BCI-algebras, Journal of natural sciences and mathematics-Lahore, 46(1/2), 13 (2006).
- [2] H. A. Abujabal, N. O. Al-Shehri, On left derivations of BCI-algebras, Soochow Journal of Mathematics, 33(3), 435 (2007).
- [3] A. M. Al-Roqi, On generalized (α, β) -derivations in BCI-algebras, Journal of applied mathematics and informatics, 32(1,2), 27-38 (2014).
- [4] L. K. Ardekani, B. Davvaz, On generalized derivations of BCI-algebras and their properties, Journal of Mathematics, 2014 (2014).
- [5] S. M. Bawazeer, N. O. Alshehri, R. S. Babusail, Generalized derivations of BCC-algebras, International Journal of Mathematics and Mathematical Sciences, 2013 (2013).
- [6] Q. P. Hu, On some classes of BCI-algebras, Math. Japon., 29, 251-253 (1984).
- [7] A. Iampan, A new branch of the logical algebra: UP-algebras, Journal of Algebra and Related Topics, 5(1), 35-54 (2017).
- [8] A. Iampan, Derivations of UP-algebras by means of UP-endomorphisms, Algebraic Structures and Their Applications, 3(2), 1-20 (2016).
- [9] S. Ilbira, A. Firat, Y. B. Jun, On symmetric bi-derivations of BCI-algebras, Applied Mathematical Sciences, 5(57-60), 2957-2966 (2011).

- [10] Y. Imai, K. Iséki, On axiom systems of propositional calculi, I. Proceedings of the Japan Academy, 41(6), 436-439 (1965).
- [11] K. Iséki, An algebra related with a propositional calculus, Proceedings of the Japan Academy, 42(1), 26-29 (1966).
- [12] Y. B. Jun, X. L. Xin, On derivations of BCI-algebras, Information Sciences, 159(3-4), 167-176 (2004).
- [13] Gy. Maksa, A remark on symmetric bi-additive functions having nonnegative diagonalization, Glasnik Math, 15(35), 279-282 (1980).
- [14] Gy. Maksa, On the trace of symmetric bi-derivations, CR Math. Rep. Acad. Sci. Canada, 9: 303-307 (1987).
- [15] G. Muhiuddin, A. M. Al-roqi, Y. B. Jun, Y. Ceven, On symmetric left bi-derivations in BCI-algebras, International Journal of Mathematics and Mathematical Sciences, 2013, 1-6 2013.
- [16] H. Ono, Y. Komori, Logics without the contraction rule, The Journal of Symbolic Logic, 50(1), 169-201 (1985).
- [17] M. A. Ozturk, Y. Ceven, Y. B. Jun, Generalized derivations of BCI-algebras, Honam Mathematical Journal, 31(4), 601-609 (2009).
- [18] C. Prabpayak, U. Leerawat, On derivations of BCC-algebras, Agriculture and Natural Resources, 43(2), 398-401.
- [19] E. C. Posner, Derivation in prime rings, Proc. Am. Math. Soc. 8, 1093-1100, (1957).
- [20] K. Sawika et al. Derivations of UP-algebras, The Korean Journal of Mathematics, 24(3), 345-367 (2016).
- [21] T. Tippanya et al. A new derivation of UP-algebras by means of UP-endomorphisms, Algebra Lett., 2017: Article ID 4, 2017.
- [22] D. Yilmaz, Symmetric Bi-derivations of UP(BCC)-Algebras, Submitted to the Journal of Applied Non-Classical Logics, (2023).

ERZURUM TECHNICAL UNIVERSITY, FACULTY OF SCIENCE, DEPARTMENT OF MATHEMATICS,
ERZURUM, TURKEY

Email address: `damla.yilmaz@erzurum.edu.tr`

IFSCOM-E 2023

9TH IFS AND CONTEMPORARY MATHEMATICS AND ENGINEERING CONFERENCE

08-11 JULY 2023 TARSUS, MERSİN, TÜRKİYE

ISBN: 978-605-68670-8-8

pp: 103-108

SOME RESULTS ON DEFERRED CESÀRO STATISTICAL CONVERGENCE OF ORDER α IN THE PROBABILITY SPACES

U.DEĞER AND K.UZUN

ABSTRACT. The idea of statistical convergence, which is a generalization of the concept of convergence and is based on the natural density of positive integers, was first given independently in 1951 by H. Steinhaus and H. Fast ([1],[2]). In 2010, the concept of α order statistical convergence was considered by R. Çolak [8]. Afterwards the concept of deferred Cesàro statistical convergence was discussed by M. Küçükaslan and M. Yılmaztürk in 2016 [10]. In this study, by considering these two facts, the concept of deferred Cesàro statistical convergence of order α has been discussed in probability spaces.

1. INTRODUCTION AND PRELIMINARIES

The concept of convergence is one of the fundamental elements of analysis and theory of functions. The idea of statistical convergence, which is a generalization of this concept and is based on the concept of natural density, was first introduced by H. Fast and H. Steinhaus independently in 1951 ([1],[2]). If (x_n) is a sequence with real terms and x is a real number, for any $\epsilon > 0$,

$$\lim_{n \rightarrow \infty} \frac{1}{n} |\{k \leq n : |x_k - x| \geq \epsilon\}| = 0,$$

it is said that the sequence (x_n) is statistically convergent to the number x . In this case, we write $x_n \xrightarrow{S} x$. The concept of statistical convergence, which has applications in many fields, has been studied by many mathematicians in fields such as summability theory, functional analysis, probability theory, and measure theory. One way refer to [3],[4],[5],[6],[7], etc. for more details.

In 2010, R. Çolak defined the concept of statistical convergence of order α , which is a generalization of statistical convergence [8]. On the other hand, in 1932, R.P. Agnew gave the definition of deferred Cesàro summability, which is a generalization of the Cesàro submethod [9]. Considering this definition, the concept of deferred statistical convergence was first discussed by Küçükaslan and Yılmaztürk in 2016 [10]. If (x_n) is a sequence with real terms and x is a real number, for any $\epsilon > 0$,

$$\lim_{n \rightarrow \infty} \frac{1}{b_n - a_n} |\{k : a_n < k \leq b_n \text{ and } |x_k - x| \geq \epsilon\}| = 0,$$

Date: July, 8, 2023.

Key words and phrases. Statistical convergence in probability, Deferred Cesàro method.

it is said that the sequence (x_n) is deferred Cesàro statistically convergent to the number x . In this case, we write $x_n \xrightarrow{DS} x$.

The concept of statistical convergence is also considered for sequences with random variables in probability spaces with a similar logic. In this framework, the definition of statistical convergence for convergence in the known sense in probability spaces was given by Ghosal in 2013 [11].

Accordingly, if $(X_n)_{n \in \mathbb{N}}$ is a sequence with random variables and X is a random variable, for any $\epsilon, \delta > 0$,

$$\lim_{n \rightarrow \infty} \frac{1}{n} |\{k \leq n : P(|X_k - X| \geq \epsilon) \geq \delta\}| = 0,$$

then (X_n) is a sequence with random variables and X is a random variable with probability that is said to be statistically convergent. In this case, we write $X_n \xrightarrow{PS} X$.

In 2015, Das, Ghosal and Som gave some results regarding this by considering the definition of statistical convergence of α in probability [12]. In the light of these studies, the definition of deferred Cesàro statistical convergence in probability was given by Srivastava, Jena and Paikray in 2019 [13].

2. MAIN RESULTS

In this section, considering statistical convergence of real numbers, we define the method of deferred Cesàro statistical convergent of order α in probability. Also, existing results in the literature are adapted for this method.

Definition 2.1. Let $(a_n), (b_n)$ be sequences of non-negative integers such that $a_n < b_n$ for each $n \in \mathbb{N}$ and $\lim_{n \rightarrow \infty} b_n = +\infty$. Let $0 < \alpha \leq 1$. A given sequence (X_n) of random variables is deferred Cesàro statistical convergent of order α in probability to random variable X , if for any $\epsilon, \delta > 0$

$$\lim_{n \rightarrow \infty} \frac{1}{(b_n - a_n)^\alpha} |\{k : a_n < k \leq b_n \text{ and } P(|X_k - X| \geq \epsilon) \geq \delta\}| = 0.$$

In this case, we write $X_n \xrightarrow{PDS^\alpha} X$. Also, if $a_n = 0, b_n = n$, then statistically convergent sequence of order α in probability is obtained from the above definition. Moreover, taking $\alpha = 1$, we obtain the definition of deferred Cesàro statistical convergent in probability.

Theorem 2.2. Let (x_n) be a sequence of real numbers such that $x_n \xrightarrow{DS^\alpha} x$. Assuming (x_n) as a sequence of random variables (X_n) having a one-point distribution at that point and x as a random variable X having a one point distribution then we can write $X_n \xrightarrow{PDS^\alpha} X$.

Proof. For any $\epsilon > 0$, we can write

$$\lim_{n \rightarrow \infty} \frac{1}{(b_n - a_n)^\alpha} |\{k : a_n < k \leq b_n \text{ and } |x_k - x| \geq \epsilon\}| = 0.$$

Now let $\delta > 0$. Since

$$K = \{k : a_n < k \leq b_n \text{ and } |x_k - x| \geq \epsilon\},$$

we have

$$\{k : a_n < k \leq b_n \text{ and } P(|X_k - X| \geq \epsilon) \geq \delta\} \subseteq K.$$

From the last statement, we conclude that the sequence of random variable X_n is deferred Cesàro statistically convergent of order α in probability to a random variable X . \square

Corollary 1. Let x_n be sequence with real terms such that $x_n \xrightarrow{S^\alpha} x$. Assuming (x_n) as a sequence of random variables (X_n) having a one-point distribution at that point and x as a random variable X having a one point distribution then we have $X_n \xrightarrow{PDS^\alpha} X$.

Theorem 2.3. Let $\alpha, \beta \in (0, 1]$ be any real numbers. If $X_n \xrightarrow{PDS^\alpha} X$ and $X_n \xrightarrow{PDS^\beta} Y$, then $P(X = Y) = 1$.

Proof. For any $\epsilon, \delta > 0$, we have

$$\begin{aligned} & |\{k : a_n < k \leq b_n \text{ and } P(|X - Y| \geq \epsilon) \geq \delta\}| \\ &= |\{k : a_n < k \leq b_n \text{ and } P(|X - X_k + X_k - Y| \geq \epsilon) \geq \delta\}| \\ &\leq |\{k : a_n < k \leq b_n \text{ and } P(|X_k - X| \geq \frac{\epsilon}{2}) \geq \frac{\delta}{2}\}| \\ &+ |\{k : a_n < k \leq b_n \text{ and } P(|X_k - Y| \geq \frac{\epsilon}{2}) \geq \frac{\delta}{2}\}|. \end{aligned}$$

Without loss of generality, let $\beta \leq \alpha$ and $P(X = Y) \neq 1$. Then, there are positive real numbers ϵ and δ such that $P(|X - Y| \geq \epsilon) = \delta > 0$. Therefore, we can write

$$\begin{aligned} & \frac{1}{(b_n - a_n)^\alpha} |\{k : a_n < k \leq b_n \text{ and } P(|X - Y| \geq \epsilon) \geq \delta\}| \\ &\leq \frac{1}{(b_n - a_n)^\alpha} |\{k : a_n < k \leq b_n \text{ and } P(|X_k - X| \geq \frac{\epsilon}{2}) \geq \frac{\delta}{2}\}| \\ &+ \frac{1}{(b_n - a_n)^\beta} |\{k : a_n < k \leq b_n \text{ and } P(|X_k - Y| \geq \frac{\epsilon}{2}) \geq \frac{\delta}{2}\}|. \end{aligned}$$

Consequently, taking the limit of both sides of inequality, we obtain

$$\begin{aligned} & \lim_{n \rightarrow \infty} \frac{b_n - a_n}{(b_n - a_n)^\alpha} \\ &\leq \lim_{n \rightarrow \infty} \frac{1}{(b_n - a_n)^\alpha} |\{k : a_n < k \leq b_n \text{ and } P(|X_k - X| \geq \frac{\epsilon}{2}) \geq \frac{\delta}{2}\}| \\ &+ \lim_{n \rightarrow \infty} \frac{1}{(b_n - a_n)^\beta} |\{k : a_n < k \leq b_n \text{ and } P(|X_k - Y| \geq \frac{\epsilon}{2}) \geq \frac{\delta}{2}\}|. \end{aligned}$$

While the right-hand side of inequality is zero, left-hand side is non zero. This contradicts the assumption that $P(X = Y) \neq 1$ Hence $P(X = Y) = 1$. \square

Theorem 2.4. Let $\alpha \in (0, 1]$ be any real number. If $X_n \xrightarrow{PDS^\alpha} X$ and $Y_n \xrightarrow{PDS^\alpha} Y$, then $X_n + Y_n \xrightarrow{PDS^\alpha} X + Y$.

Proof. Since $X_n \xrightarrow{PDS^\alpha} X$ and $Y_n \xrightarrow{PDS^\alpha} Y$, for all $\epsilon, \delta > 0$, we have

$$\lim_{n \rightarrow \infty} \frac{1}{(b_n - a_n)^\alpha} |\{k : a_n < k \leq b_n \text{ and } P(|X_k - X| \geq \frac{\epsilon}{2}) \geq \frac{\delta}{2}\}| = 0$$

and

$$\lim_{n \rightarrow \infty} \frac{1}{(b_n - a_n)^\alpha} |\{k : a_n < k \leq b_n \text{ and } P(|Y_k - Y| \geq \frac{\epsilon}{2}) \geq \frac{\delta}{2}\}| = 0.$$

Also, since

$$\begin{aligned} & \{k : a_n < k \leq b_n \text{ and } P(|(X_k + Y_k) - (X + Y)| \geq \epsilon) \geq \delta\} \subseteq \\ & \{k : a_n < k \leq b_n \text{ and } P(|X_k - X| \geq \frac{\epsilon}{2}) \geq \frac{\delta}{2}\} \cup \\ & \{k : a_n < k \leq b_n \text{ and } P(|Y_k - Y| \geq \frac{\epsilon}{2}) \geq \frac{\delta}{2}\} \end{aligned}$$

the following inequality holds :

$$\begin{aligned} & \frac{1}{(b_n - a_n)^\alpha} |\{k : a_n < k \leq b_n \text{ and } P(|(X_k + Y_k) - (X + Y)| \geq \epsilon) \geq \delta\}| \\ & \leq \frac{1}{(b_n - a_n)^\alpha} |\{k : a_n < k \leq b_n \text{ and } P(|X_k - X| \geq \frac{\epsilon}{2}) \geq \frac{\delta}{2}\}| \\ & \quad + \frac{1}{(b_n - a_n)^\alpha} |\{k : a_n < k \leq b_n \text{ and } P(|Y_k - Y| \geq \frac{\epsilon}{2}) \geq \frac{\delta}{2}\}|. \end{aligned}$$

Then, taking the limit of both sides of inequality, we get

$$\lim_{n \rightarrow \infty} \frac{1}{(b_n - a_n)^\alpha} |\{k : a_n < k \leq b_n \text{ and } P(|(X_k + Y_k) - (X + Y)| \geq \epsilon) \geq \delta\}| = 0,$$

that is, $X_n + Y_n \xrightarrow{PDS^\alpha} X + Y$. \square

Theorem 2.5. *Let $\alpha \in (0, 1]$ be any real number and $c \in \mathbb{R}$ be given. If $X_n \xrightarrow{PDS^\alpha} X$, then $c \cdot X_n \xrightarrow{PDS^\alpha} c \cdot X$.*

Proof. Suppose that $X_n \xrightarrow{PDS^\alpha} X$ and $c \in \mathbb{R}$. In case $c = 0$, proof is clear. If $c \neq 0$, then desired result is obtained from the following equality:

$$\begin{aligned} & \frac{1}{(b_n - a_n)^\alpha} |\{k : a_n < k \leq b_n \text{ and } P(|c \cdot X_k - c \cdot X| \geq \epsilon) \geq \delta\}| \\ & = \frac{1}{(b_n - a_n)^\alpha} |\{k : a_n < k \leq b_n \text{ and } P(|X_k - X| \geq \frac{\epsilon}{|c|}) \geq \delta\}|. \end{aligned}$$

\square

Theorem 2.6. *Let $0 < \alpha \leq \beta \leq 1$. If $X_n \xrightarrow{PDS^\alpha} X$ then $X_n \xrightarrow{PDS^\beta} X$.*

Proof. Let $0 < \alpha \leq \beta \leq 1$. Since

$$\frac{1}{(b_n - a_n)^\beta} \leq \frac{1}{(b_n - a_n)^\alpha}$$

this implies

$$\begin{aligned} & \frac{1}{(b_n - a_n)^\beta} |\{k : a_n < k \leq b_n \text{ and } P(|X_k - X| \geq \epsilon) \geq \delta\}| \\ & \leq \frac{1}{(b_n - a_n)^\alpha} |\{k : a_n < k \leq b_n \text{ and } P(|X_k - X| \geq \epsilon) \geq \delta\}| \end{aligned}$$

for any $\epsilon, \delta > 0$. Hence, every deferred Cesàro statistical convergent sequence of order α in probability is deferred Cesàro statistical convergent of order β in probability. \square

The following example shows that the converse of Theorem 2.6 is not true:

Example

Let $a_n = 0$, $b_n = n$ and $\frac{r}{s}$ be a rational number between α and β . Let the probability density function of X_n be given by,

If $n = \lfloor m^{\frac{s}{r}} \rfloor$ for some $m \in \mathbb{N}$,

$$f_n(x) = \begin{cases} 1, & 0 < x < 1 \\ 0, & \text{otherwise} \end{cases}$$

If $n \neq \lfloor m^{\frac{s}{r}} \rfloor$ for each $m \in \mathbb{N}$,

$$f_n(x) = \begin{cases} \frac{nx^{n-1}}{5^n}, & 0 < x < 5 \\ 0, & \text{otherwise} \end{cases}$$

Let $0 < \epsilon, \delta < 1$. Then,

$$P(|X_n - 5| \geq \epsilon) = \begin{cases} 1, & \text{if } n = \lfloor m^{\frac{s}{r}} \rfloor \text{ for some } m \in \mathbb{N} \\ (1 - \frac{\epsilon}{5})^n, & \text{if } n \neq \lfloor m^{\frac{s}{r}} \rfloor \text{ for every } m \in \mathbb{N}. \end{cases}$$

Therefore, we obtain

$$\lim_{n \rightarrow \infty} \frac{n^{\frac{r}{s}} - 1}{n^\alpha} \leq \lim_{n \rightarrow \infty} \frac{1}{n^\alpha} |\{k : a_n < k \leq b_n \text{ and } P(|X_k - X| \geq \epsilon) \geq \delta\}|$$

and

$$\lim_{n \rightarrow \infty} \frac{1}{n^\alpha} |\{k : a_n < k \leq b_n \text{ and } P(|X_k - X| \geq \epsilon) \geq \delta\}| \leq \lim_{n \rightarrow \infty} \frac{n^{\frac{r}{s}} + 1}{n^\beta} + \lim_{n \rightarrow \infty} \frac{c}{n^\beta}$$

where c is fixed positive integer. This shows that the sequence (X_n) is deferred Cesàro statistical convergent of order β in probability to 5 but is not deferred Cesàro statistical convergent of order α in probability to 5 for any $\alpha < \beta$.

Corollary 2. In Example, if we take $\beta = 1$, then the sequence (X_n) is deferred Cesàro statistical convergent in probability to 5 but is not deferred Cesàro statistical convergent of order α in probability to 5 for any $0 < \alpha < 1$.

Theorem 2.7. Let $0 < \alpha \leq 1$. If $X_n \xrightarrow{PS^\alpha} X$ then $X_n \xrightarrow{PDS^\alpha} X$.

Proof. Let $X_n \xrightarrow{PS^\alpha} X$. Then it follows that

$$\lim_{n \rightarrow \infty} \frac{1}{n^\alpha} |\{k \leq n : P(|X_k - X| \geq \epsilon) \geq \delta\}| = 0$$

for all $\epsilon, \delta > 0$. Hence we can write ([?])

$$\lim_{n \rightarrow \infty} \frac{1}{(b_n)^\alpha} |\{k \leq b_n : P(|X_k - X| \geq \epsilon) \geq \delta\}| = 0.$$

Since

$$\{a_n < k \leq b_n : P(|X_k - X| \geq \epsilon) \geq \delta\} \subseteq \{k \leq b_n : P(|X_k - X| \geq \epsilon) \geq \delta\},$$

we obtain the inequality

$$\begin{aligned} & \frac{1}{(b_n - a_n)^\alpha} |\{a_n < k \leq b_n : P(|X_k - X| \geq \epsilon) \geq \delta\}| \\ & \leq \frac{1}{(b_n - a_n)^\alpha} |\{k \leq b_n : P(|X_k - X| \geq \epsilon) \geq \delta\}| \end{aligned}$$

$$= \frac{1}{(b_n)^\alpha \left(1 - \frac{a_n}{b_n}\right)^\alpha} |\{k \leq b_n : P(|X_k - X| \geq \epsilon) \geq \delta\}|.$$

Then, taking the limit of both sides of inequality

$$\lim_{n \rightarrow \infty} \frac{1}{(b_n)^\alpha} |\{k \leq b_n : P(|X_k - X| \geq \epsilon) \geq \delta\}| = 0$$

and due to the following inequality

$$\lim_{n \rightarrow \infty} \frac{1}{\left(1 - \frac{a_n}{b_n}\right)^\alpha} < \infty$$

we get

$$\lim_{n \rightarrow \infty} \frac{1}{(b_n - a_n)^\alpha} |\{a_n < k \leq b_n : P(|X_k - X| \geq \epsilon) \geq \delta\}| = 0.$$

That is, $X_n \xrightarrow{PDS^\alpha} X$. □

REFERENCES

- [1] H. Steinhaus, Sur la convergence ordinaire et la convergence asymptotique, Colloquium Mathematicum, Vol. 2, No. 1, pp. 73-74 (1951).
- [2] H. Fast, Sur la convergence statistique, Colloquium Mathematicum, Vol. 2, No. 3-4, pp. 241-244 (1951).
- [3] I.J. Schoenberg, The integrability of certain functions and related summability methods, The American Mathematical Monthly, Vol. 66, No. 5, pp. 361-375 (1959)
- [4] J. Kline, The T-statistically convergent sequences are not an FK-space, International Journal of Mathematics and Mathematical Sciences, Vol. 18, No. 4, pp. 825-827 (1995).
- [5] J. Fridy, and M.K. Khan, Tauberian theorems via statistical convergence, Journal of Mathematical Analysis and Applications, Vol. 228, No. 1, pp. 73-95 (1998).
- [6] M. Küçükaslan, U. Değer and O. Dovgoshey, On the statistical convergence of metric-valued sequences, Ukrainian Mathematical Journal, Vol. 66, No. 5, pp. 712-720 (2014).
- [7] B.T. Bilalov and T.Y. Nazarova, Statistical convergence of functional sequence, Rocky mountain journal of mathematics, Vol. 45, No. 5, pp. 1413-1423 (2015).
- [8] R. Çolak, 'Statistical convergence of order α , Modern Methods in Analysis and Its Applications, Vol. 1, pp. 121-129 (2010).
- [9] R.P. Agnew, On deferred Cesàro means, Annals of Mathematics, Vol. 33, No. 3, pp. 413-421 (1932).
- [10] M. Küçükaslan and M. Yılmaztürk, On deferred statistical convergence of sequences, Kyungpook Mathematical Journal, Vol. 56, No. 2, pp. 357-366 (2016).
- [11] S. Ghosal, Statistical convergence of a sequence random variables and limit theorems, Applications of Mathematics, Vol. 58, No. 4, pp. 423-437 (2013).
- [12] P. Das, S. Ghosal and S. Som, Statistical convergence of order α in probability, Arab Journal of Mathematical Science, Vol. 21, No. 2, pp. 253-265 (2015).
- [13] H.M. Srivastava, B.B. Jena and S.K. Paikray, Deferred Cesàro statistical probability convergence and its applications to approximation theorems, Journal of Nonlinear and Convex Analysis, Vol. 20, No. 9, pp. 1777-1792 (2019).

(U.Değer) MERSIN UNIVERSITY, DEPARTMENT OF MATHEMATICS, 33330, MERSIN, TURKEY
Email address: udeger@mersin.edu.tr; degpar@gmail.com

(K.Uzun) MERSIN UNIVERSITY, INSTITUTE OF SCIENCE, 33330, MERSIN, TURKEY
Email address: kubraasoytok@gmail.com

IFSCOM-E 2023

9TH IFS AND CONTEMPORARY MATHEMATICS AND ENGINEERING CONFERENCE

08-11 JULY 2023 TARSUS, MERSİN, TÜRKİYE

ISBN: 978-605-68670-8-8

pp: 109-116

FRACTIONAL PREY-PREDATOR MODEL WITH LINEAR FUNCTIONAL RESPONSE, PREY REFUGE, FEAR AND CARRY-OVER EFFECT

ERCAN BALCI

0000-0002-8530-7073

ABSTRACT. This paper presents a prey-predator model that incorporates the trait-mediated fear effect and its carry-over effect, as well as the prey defense mechanism of prey refuge. The functional response considered in the model is the Holling-I type. Additionally, to account for memory within the system, we analyze the Caputo fractional order version of the proposed model. The obtained results are also supported by numerical simulations.

1. INTRODUCTION

Understanding prey-predator interactions and predation process is one of the most essential part in maintaining balance and biodiversity in an ecosystem. We first consider the following basic predator-prey model and then make some refinements to it. Let u and v be the density of the population of prey and predator at any time t respectively.

$$(1) \quad \begin{cases} \frac{du}{dt} = ru - \frac{u^2}{k} - p(u)v, \\ \frac{dv}{dt} = ap(u)v - dv. \end{cases}$$

Here, prey populations grows logistically with a growth rate of r and a maximum capacity of k . Predator populations grows with rate conversion rate of prey and predator a , but faces a natural death with a rate of d . The function $p(u)$ takes different forms depending on the specific characteristics of the prey and predator populations and the interactions between them and is called the predator functional response. Many different functional responses such as Holling I-II-III functional responses, ratio dependent functional responses and Beddington–DeAngelis functional response etc. have been used in mathematical models. However, this

Date: July, 8, 2023.

2000 Mathematics Subject Classification. 37N25; 92B05 .

Key words and phrases. Prey-predator, Fear effect, Carry-over effect, Prey refuge, Caputo fractional.

functional response is only a term that describes the direct predation effect of the predator on the prey. However, studies have shown that the predator has some effects on the prey other than direct predation, which change the behaviour of the prey. These effects on prey are called trait-mediated effects. Due to these effects, the growth of the prey is reduced. To reflect this biological fact, a fear factor $g(\gamma, v) = \frac{1}{1 + \gamma v}$ is added as a factor to the prey growth rate, r , in mathematical models. When we consider the linear functional response $p(u) = \lambda u$ together with the fear factor $g(\gamma, v)$ for the above model (1), we get the following model:

$$(2) \quad \begin{cases} \frac{du}{dt} = \frac{r}{1 + \gamma v} u - \frac{u^2}{k} - \lambda uv, \\ \frac{dv}{dt} = a\lambda uv - dv. \end{cases}$$

Here γ represents the level of fear. For the properties and biological interpretation of the fear factor $g(\gamma, v)$, we refer to the pioneering work of Wang et al. [1]. Furthermore, the concept of the carry-over effect relates to the phenomenon in which an individual's previous experiences and background exert an influence on their present performance within a specific context. Proceeding from this idea, some works have proposed the revised fear factor to comprise the carry-over effect related that fear of predation [2, 3]. The revised fear factor term is as follows:

$$g(c, \gamma, u, v) = \frac{1 + cu}{1 + cu + \gamma v}$$

where c is the carry-over effect parameter associated to fear. For the properties and biological interpretation of the $g(c, \gamma, u, v)$, we refer to [2, 3]. Moreover, the dynamics of predator-prey populations can be significantly influenced by the existence of prey refuges [4]. These refuges can take various forms, and in our study, we consider that a certain proportion of the prey population, denoted as $(1 - \epsilon)$, can evade predation by either seeking shelter or migrating to protected areas. Here, $\epsilon \in [0, 1)$ denotes the prey refuge rate. By incorporating this parameter into the aforementioned system (2) with the revised fear factor term, we obtain the following system:

$$(3) \quad \begin{cases} \frac{du}{dt} = r \frac{1 + cu}{1 + cu + \gamma v} u - \frac{u^2}{k} - \lambda(1 - \epsilon)uv, \\ \frac{dv}{dt} = a\lambda(1 - \epsilon)uv - dv. \end{cases}$$

Now, we apply following rescaling $\tau = rt$, $\bar{v} = \frac{\lambda v}{r}$. Dropping the bars and still denoting τ by t , we get the following system:

$$(4) \quad \begin{cases} \frac{du}{dt} = u \frac{1 + cu}{1 + cu + fv} - \frac{u^2}{m} - (1 - \epsilon)uv, \\ \frac{dv}{dt} = \rho(1 - \epsilon)uv - \delta v, \end{cases}$$

where $f = \frac{\gamma r}{\lambda}$, $m = rk$, $\rho = \frac{a\lambda}{r}$, and $\delta = \frac{d}{r}$. Lastly, mathematical models employ fractional order derivatives to capture the memory and hereditary characteristics of the system being studied, as they possess a non-local nature. This concept is also applicable in biological systems, as many of them exhibit the phenomenon

of memory effect [5, 6]. To delve into the intricate relationship between hereditary traits, life cycle factors, and prey-predator interactions, we will investigate a modified model that incorporates fractional order dynamics. The fractional order version of the system (4) is given as follows:

$$(5) \quad \begin{cases} {}^C D_t^\alpha u(t) = u \frac{1 + cu}{1 + cu + fv} - \frac{u^2}{m} - (1 - \epsilon)uv, \\ {}^C D_t^\alpha v(t) = \rho(1 - \epsilon)uv - \delta v, \end{cases}$$

where ${}^C D_t^\alpha$ denotes Caputo fractional differentiation of order $\alpha \in (0, 1)$, and is defined as

$${}^C D_t^\alpha F(t) = \frac{1}{\Gamma(1 - \alpha)} \int_0^t \frac{F'(\eta)}{(t - \eta)^\alpha} d\eta.$$

2. STABILITY AND HOPF BIFURCATION ANALYSIS

In this section, we make stability and bifurcation analysis of equilibrium points of system (5). The system (5) can have three non-negative equilibrium:

- i. The extinction equilibrium $E_0 = (0, 0)$.
- ii. The predator-extinction equilibrium $E_1 = (m, 0)$.
- iii. If the condition

$$(6) \quad \rho > \frac{\delta}{m(1 - \epsilon)}$$

are satisfied, the model (5) has unique positive equilibrium point $E^* = (u^*, v^*)$ where

$$u^* = \frac{\delta}{\rho(1 - \epsilon)},$$

and v^* is the positive root of the equation

$$A_1 v^2 + A_2 v + A_3 = 0$$

where $A_1 = u^* f m (-1 + \epsilon) u^*$, $A_2 = u^* (u^* f + (1 - \epsilon)(m + u^* c m))$, and $A_3 = u^* (u^* - m - u^* c m + (u^*)^2)$.

For the fundamental theorems on dynamical analysis fractional order systems, we refer to [5, 7, 8].

Theorem 1. (i) *The trivial equilibrium $E_0 = (0, 0)$ is always saddle point, consequently unstable.*

(ii) *The predator-extinction equilibrium point $E_1 = (m, 0)$ of system (5) is locally asymptotically stable if $\rho < \frac{\delta}{m(1 - \epsilon)}$. Otherwise, it is a saddle point.*

Proof. (i) The eigenvalues of the Jacobien matrix $J(E_0)$ corresponding to the system (5) evaluated at the equilibrium point $E_0 = (0, 0)$ are $\lambda_1 = 1 > 0$, $\lambda_2 = \delta < 0$. This implies that $E_0 = (0, 0)$ is a saddle point. (ii) The eigenvalues of the Jacobien matrix $J(E_1)$ corresponding to the system (5) evaluated at the equilibrium point $E_1 = (m, 0)$ are $\lambda_1 = -1 < 0$, $\lambda_2 = -\delta + m(1 - \epsilon)\rho$. Under the condition $\rho < \frac{\delta}{m(1 - \epsilon)}$, we have $\lambda_2 < 0$ and this implies that $E_1 = (m, 0)$ is locally asymptotically stable . \square

The jacobian matrix corresponding to linearization of the system (5) around the coexistence equilibrium point $E^* = (x^*, y^*)$ is

$$J(E^*) = \begin{pmatrix} a_{11} & a_{12} \\ a_{21} & 0 \end{pmatrix}$$

with the corresponding characteristic equation

$$\lambda^2 + b_1\lambda + b_0 = 0$$

where $b_1 = -a_{11}$, $b_0 = -a_{12}a_{21}$

Theorem 2. *Assuming the existence condition $\rho > \frac{\delta}{m(1-\epsilon)}$ of the positive equilibrium $E^* = (x^*, y^*)$ holds, $E^* = (x^*, y^*)$ is locally asymptotically stable if one of the following conditions holds:*

- i) $b_1 \geq 0$,
- ii) $b_1 < 0$, $b_1^2 - 4b_0 < 0$, $\left| \tan^{-1}\left(\frac{\sqrt{4b_0 - b_1^2}}{b_1}\right) \right| > \frac{\alpha\pi}{2}$.

Proof. Under the positivity condition (6), $a_{12} < 0$, $a_{21} > 0$, and consequently $b_0 > 0$. i) For $b_1 \geq 0$, the eigenvalues of $J(E^*)$ are either complex numbers with negative real parts or negative real numbers. In both cases, they satisfy the inequality $|\arg(\lambda_{1,2})| > \frac{\alpha\pi}{2}$. ii) The conditions $b_1 < 0$, $b_1^2 - 4b_0 < 0$ implies that the eigenvalues of $J(E^*)$ are complex numbers with positive real parts. Last condition $\left| \tan^{-1}\left(\frac{\sqrt{4b_0 - b_1^2}}{b_1}\right) \right| > \frac{\alpha\pi}{2}$ is equivalent to the inequality $|\arg(\lambda_{1,2})| > \frac{\alpha\pi}{2}$ which ensures local asymptotica stability. \square

Theorem 3. *Assume that the existence condition $\rho > \frac{\delta}{m(1-\epsilon)}$ of the positive equilibrium $E^* = (x^*, y^*)$, the inequalities $b_1 < 0$ and $b_1^2 - 4b_0 < 0$ holds. Then the system (5) undergoes a Hopf bifurcation around $E^* = (x^*, y^*)$ as fractional order parameter α goes through the critical value $\alpha_h = \frac{2}{\pi} \left| \tan^{-1}\left(\frac{\sqrt{4b_0 - b_1^2}}{b_1}\right) \right|$.*

Proof. The inequalities $b_1 < 0$ and $b_1^2 < 4b_0$ guarantees that the characteristic polynomial has complex conjugate roots with strictly positive real parts which implies that the stability of $E^* = (x^*, y^*)$ is contingent on the fractional order parameter $\alpha \in (0, 1)$. Moreover, $\min_{1 \leq j \leq 2} |\arg(\lambda_i)| = \left| \tan^{-1}\left(\frac{\sqrt{4\rho_0 - \rho_1^2}}{\rho_1}\right) \right|$ and for $\alpha = \alpha_h = \frac{2}{\pi} \left| \tan^{-1}\left(\frac{\sqrt{4b_0 - b_1^2}}{b_1}\right) \right|$, the function $m(\alpha_h) = 0$ where where $m(\alpha) = \frac{\alpha\pi}{2} - \min_{1 \leq j \leq 2} |\arg(\lambda_i)|$. The transversality condition

$$\left. \frac{dm(\zeta)}{d\zeta} \right|_{\zeta=\alpha_h} = \frac{\pi}{2} \neq 0,$$

is also satisfied. So, the system (5) goes through a Hopf bifurcation at $E^* = (x^*, y^*)$ as α passes through α_h . \square

3. NUMERICAL EXAMPLES

For the numerical simulations, we use the parametric values given in Table 1 unless otherwise stated. For numerical simulations we use the PECE algorithm [9] and MATLAB software.

TABLE 1. Parametric values used for numerical simulations

c	f	m	ϵ	ρ	δ
1.5	2.3	6	0.5	0.45	0.06

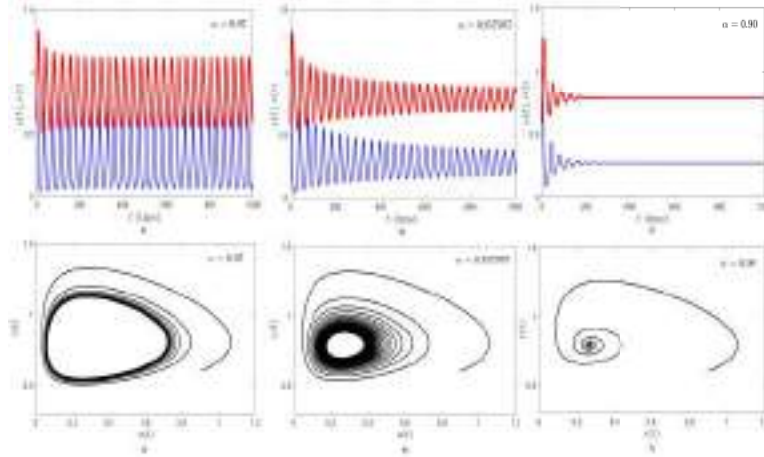


FIGURE 1. Time series solutions of prey (blue) and predator (red) populations and the corresponding phase portraits with varying α

In Figure 1, we fix the parameter values as in Table 1 and we vary the fractional order parameter α . The presence of equilibrium points remains unaffected by changes in the fractional order parameter α . However, variations in α can impact the stability characteristics of these equilibrium points. Specifically, when the eigenvalues of the Jacobian matrix, evaluated at the equilibrium point, possess complex eigenvalues with positive real parts, decreasing α expands the region of stability. As the value of α decreases, the memory effect in the system becomes more powerful. The critical Hopf bifurcation value for fractional order is calculated as $\alpha_h \approx 0.957937$ (Figure 1,b,e). Above this value, the amplitude of oscillations in the solutions of the system (5) increases (Figure 1,a,d, Figure 2). Below which, the coexistence equilibrium point E^* becomes locally asymptotically stable (Figure 1,c,f). Biologically speaking, it can be inferred that both species utilize the knowledge gained from their past interactions within the ecosystem to establish a sustainable position.

In Figure 3 and Figure 4, we fix the parameter values as in Table 1 and we take the fractional order parameter as $\alpha = 0.96$. The fear effect term acts as a growth suppressor for the prey population, and as the level of fear increases, the prey population decreases. The decrease in the prey population can be expected to negatively affect the predator population. However, in fact, the addition of the fear effect to the system leads to a more conservative demand for food by the predator population, resulting in a prolonged food supply. This contributes to stability of coexistence equilibrium point. The critical Hopf bifurcation value of the level of fear parameter is calculated as $f_h \approx 3.187$ (Figure 3,b,e, Figure 4). Above which, the coexistence equilibrium point E^* becomes locally asymptotically stable E^* (Figure 3,c,f).

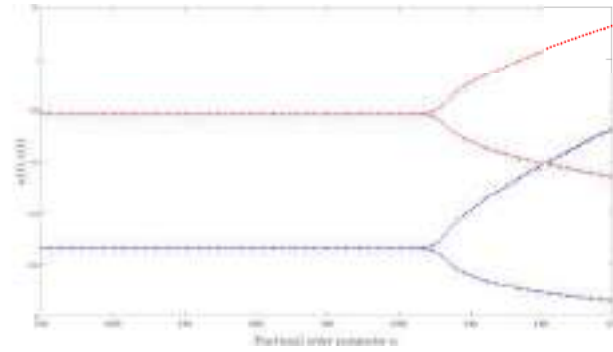


FIGURE 2. Bifurcation diagram with varying the fractional order α

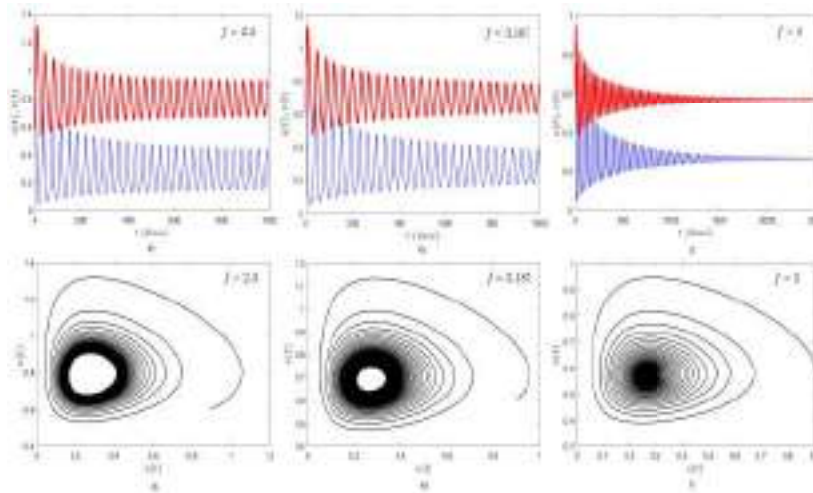


FIGURE 3. Time series solutions of prey (blue) and predator (red) populations and the corresponding phase portraits with varying the level of fear f

In Figure 5 and Figure 6, we fix the parameter values as in Table 1 and we take $\alpha = 0.95$. The critical Hopf bifurcation value of the carry-over parameter is calculated as $c_h \approx 1.649$. Increase in the carry-over parameter c , slightly promotes predator population. For $c \approx 0.1649$, the coexistence equilibrium E^* loses its stability and there exist a limit cycle around E^* (Figure 5,b,e, Figure 6). The term fear effect suppresses the growth of the prey population and an increase in the level of fear reduces the prey population, while contributing to a more stable and permanent food supply for predators and, consequently, to a more stable system. The carry-over parameter, which weakens the impact of the fear effect on the prey population, has the opposite influence on the system. So, increase in the carry-over parameter c leads instability of the coexistence equilibrium E^* (Figure 5,c,f).

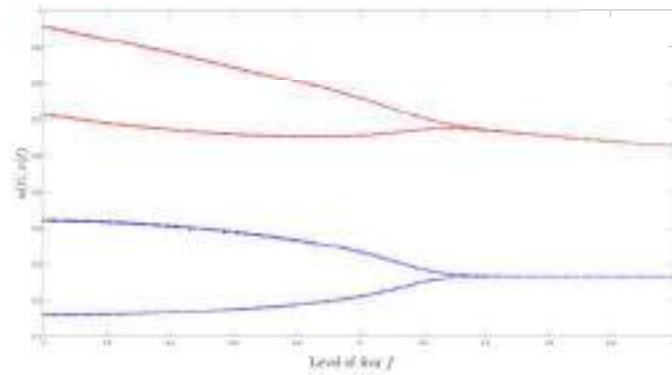


FIGURE 4. Bifurcation diagram with varying the level of fear f

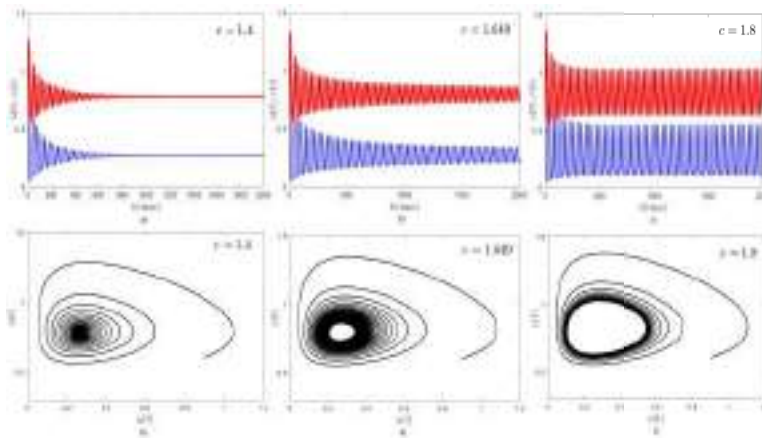


FIGURE 5. Time series solutions of prey (blue) and predator (red) populations and the corresponding phase portraits with varying the carry-over parameter c

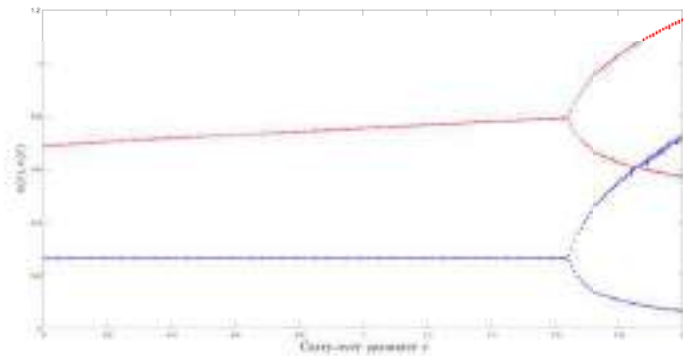


FIGURE 6. Bifurcation diagram with varying the carry-over parameter c

4. CONCLUSION

In this paper, a prey-predator model that incorporates the fear effect and its carry-over effect, as well as the prey defense mechanism of prey refuge is investigated. The carry-over effect can be used as a parameter to balance the suppressive effect of the fear effect term on prey growth. In addition, the inclusion of the memory effect in the system with the Caputo fractional order derivative provides richer dynamical behaviour. Finally, the use of other functional responses instead of the Holling-I type functional response considered in this study may provide more comprehensive and interesting results. New studies can be conducted in this context.

REFERENCES

- [1] X. Wang, L. Zanette, X. Zou, Modelling the fear effect in predator–prey interactions, *Journal of mathematical biology*, 73(5), 1179-1204 (2016).
10.1007/s00285-016-0989-1
- [2] S.K. Sasmal, Y. Takeuchi, Modeling the Allee effects induced by cost of predation fear and its carry-over effects, *Journal of Mathematical Analysis and Applications*, 505(2), 125485 (2022).
10.1016/j.jmaa.2021.125485
- [3] S. Mondal, G.P. Samanta, A comparison study of predator–prey system in deterministic and stochastic environments influenced by fear and its carry-over effects, *European Physical Journal Plus*, 137(1), (2022).
10.1140/epjp/s13360-021-02219-9
- [4] Li, Hong-Li, et al., Dynamical analysis of a fractional-order predator-prey model incorporating a prey refuge, *Journal of Applied Mathematics and Computing*, 54, 435-449 (2017).
10.1007/s12190-016-1017-8
- [5] K. Baisad, S. Moonchai, Analysis of stability and hopf bifurcation in a fractional Gauss-type predator-prey model with Allee effect and Holling type-III functional response, *Advances in Difference equations*, 2018, 82. (2018)
10.1007/s12190-016-1017-8
- [6] E. Balci, S. Kartal, I. Ozturk, Comparison of dynamical behavior between fractional order delayed and discrete conformable fractional order tumor-immune system, *Mathematical Modelling of Natural Phenomena* 16 (3), (2021).
10.1051/mmnp/2020055
- [7] I. Petras, *Fractional-Order Nonlinear Systems: Modeling, Analysis and Simulation*, Springer, Berlin, (2011).
- [8] A.S. Deshpande, V. Daftardar-Gejji, Y.V. Sukale, On Hopf bifurcation in fractional dynamical systems, *Chaos, Solitons and Fractals*, 98: 189-198 (2017).
- [9] K. Diethelm, N.J. Ford, A.D. Freed, A predictor-corrector approach for the numerical solution of fractional differential equations, *Nonlinear Dynamics*, 29: 3-22 (2002).

ERCIYES UNIVERSITY, DEPARTMENT OF MATHEMATICS, 38039, KAYSERI, TURKEY
Email address: ercanbalci@erciyes.edu.tr

NONLINEAR DIFFERENTIAL EQUATIONS ACCORDING TO THE BISHOP PARALLEL TRANSPORT FRAME

Fatma BULUT

0000-0002-7684-6796

ABSTRACT

Bishop created a curve-specific alternative to Frenet's frame and named it Bishop frame. It is known that for a given constant vector field concerning Bishop parallel transport frame $\{T, M_1, M_2, M_3\}$, there are no $(1, k)$ -type slant helices for $1 \leq k \leq 4$ in [23].

The aim of this paper nonlinear differential equations according to Bishop parallel transport frame $\{T, M_1, M_2, M_3\}$, for (k, m) -type slant helices (2,3)-, (2,4)-, and (3,4)-type slant helices in 4-dimensional Euclidean space. It then provides characterizations of (k, m) -type slant helices in accordance with the Bishop parallel transport frame in 4-dimensional Euclidean space.

1. INTRODUCTION

A generic helix is a curve with a tangent vector that forms a continuous angle facing in one direction. A slant helix, a new type of helix, is a curve whose principal normal vector field makes a constant angle with a fixed direction. This definition was first proposed by Izumiya and Takeuchi [1] in 2004. The concept of Darboux helix in 3-dimensional Euclidean space was introduced and studied by Yaylı et al. [2] in 2012. Darboux helices in Euclidean space were investigated by İlarıslan and Yıldırım [3] in 2018. In addition, in recent years, numerous researchers [4,5] have conducted studies on this subject, focusing on the principal normal vector field of the curve.

Curves, where the angle between the curve and a fixed direction is constant, are called slant helices. In curve theory, the most exciting curves recently are helices, slant helices, and related curves [6]. A curve may be referred to as a geodesic, circle, or helix, depending on the values of its curvatures. The differential geometry of curves is an important concept for different frames in various spaces. For example, in 3-dimensional Euclidean space, the Frenet frame, which consists of a curve's tangent, principal normal, and binormal vectors, is the best-known orthonormal frame for studying the differential geometry of that curve. The local behavior of a space curve, or its shape, is fully determined by the curvature and torsion of the curve. Therefore, for a curve to be thoroughly studied, it must be continuously differentiable, at least up to the third order.

Date: July, 11, 2023.

2000 Mathematics Subject Classification. 14H50, 53A04

Key words and phrases. Helix, slant helix, type-3 Bishop frame, (k, m) -type slant helix.

Many researchers use the Frenet frame to characterize and calculate the properties of curves. However, the Frenet frame is defined only for differentiable curves, and at some points, the second derivative of the curve may be zero. In this case, an alternative frame is needed for the curve. For this reason, in 1975, Bishop [7] defined an alternative frame or parallel translation frame for curves in 3-dimensional Euclidean space with the help of parallel vector fields. This frame is a well-defined movable frame even when the second derivative of a curve is completely zero. Bishop found an alternative way to describe a movable frame thanks to this frame. This frame is formed by keeping the tangent vector in the Frenet frame constant and rotating the normal vectors at a certain angle [7]. With the discovery of this alternative frame, researchers aimed to examine basic subjects according to this new frame, and many studies on Bishop frame were conducted [8,9]. Bükcü and Karacan [10] investigated some special curves according to Bishop frame. Yılmaz et al. [10] studied the global images of the components of Bishop frame. Macit and Düldül [11] characterized the curvatures of each associated curve in E^3 and described some new associated curves. In 2015, Büyükkütük and Öztürk [12] obtained some results for curves relative to Bishop frame in E^4 .

Elzawy [13] studied Bishop and Frenet frames in 4-dimensional Euclidean space. Choi and Kim [14], in 2012, defined some connected curves for a given Frenet curve with the help of integral curves. These connected curves can be listed as the principal-direction curve, the binormal strike curve, the principal-donor curve, and the binormal-donor curve [14]. Körpınar's [15] associated curves concerning Bishop frame in 3-dimensional Euclidean space have also been studied. Additionally, (k, m) -type slant helices have been investigated in 4-dimensional Euclidean space and 4-dimensional Minkowski space [16-23].

2. PRELIMINARIES

This section provides some basic notions to be needed in the following sections.

Definition 2.1 [24] Let $\gamma: I \subseteq \mathbb{R} \rightarrow E^4$ be a regular curve given in E^4 , where $I \subseteq \mathbb{R}$ is an open interval. The set $\{T, M_1, M_2, M_3\}$ with the unit normal vector field $T(U)$ perpendicular to the tangent vector field of γ is called the parallel translation frame of γ , Bishop frame, or the parallel transport frame.

This study uses the name parallel transport frame instead of Bishop frame. Let $\{T, M_1, M_2, M_3\}$ be the parallel transport frame, U being a constant vector, it was established in the previous thesis that there were no $(1, 2)$ -, $(1, 3)$ -, or $(1, 4)$ -type slant helices in the parallel transport frame [23].

Let $\{T, M_1, M_2, M_3\}$ be the parallel transport frame of the regular curve γ . Let k_1, k_2, k_3 denote the curve's first, second, and third curvatures, respectively. In E^4 , for every $s \in I \subset \mathbb{R}$ and $k_3 \neq 0$, the Frenet formulas are as follows [24]:

$$\begin{bmatrix} T' \\ M'_1 \\ M'_2 \\ M'_3 \end{bmatrix} = \begin{bmatrix} 0 & k_1 & k_2 & k_3 \\ -k_1 & 0 & 0 & 0 \\ -k_2 & 0 & 0 & 0 \\ -k_3 & 0 & 0 & 0 \end{bmatrix} \begin{bmatrix} T \\ M_1 \\ M_2 \\ M_3 \end{bmatrix} \quad (1)$$

3. INCLUSION RESULTS FOR THE FRAME

In this section, we obtained (k, m) -type slant helices, specifically $(2, 3)$ -, $(2, 4)$ -, and $(3, 4)$ -type slant helices in 4-dimensional Euclidean space, based on nonlinear differential equations according to parallel transport frame.

Theorem 3.1. Let $\gamma: I \subseteq \mathbb{R} \rightarrow E^4$ be a regular curve given in E^4 . If γ is a $(2,3)$ -type slant helix according to parallel transport frame $\{T, M_1, M_2, M_3\}$, the following nonlinear equation is obtained:

$$y' - 2 \left(\frac{k_1 k_2}{k_3^2 + k_2^2} \right) y' + \frac{k_1^2 - \mu k_3^2}{k_3^2 + k_2^2} = 0$$

and there

$$y' = \frac{\left(\frac{k_1}{k_3} \right)'}{\left(\frac{k_2}{k_3} \right)'}, \text{ and } \mu = \frac{K^2}{b^2} - 1$$

are constants.

PROOF.

Suppose that γ is a $(2,3)$ -type slant helix according to parallel transport frame $\{T, M_1, M_2, M_3\}$ and U is a constant nonzero vector field, then

$$\langle M_1, U \rangle = b$$

$$\langle M_2, U \rangle = u_1$$

are constants along the $\gamma = \gamma(s)$ curve, and if we derivative the above equations concerning s , we get

$$\text{for } k_1 \neq 0, \langle T, U \rangle = 0.$$

If we take derivating concerning s again, we have

$$\langle T', U \rangle = 0$$

From Equation 1, using the Frenet formulas, we find the following equations:

$$\begin{aligned} k_1 \underbrace{\langle M_1, U \rangle}_b + k_2 \underbrace{\langle M_2, U \rangle}_{u_1} + k_3 \langle M_3, U \rangle &= 0 \Rightarrow \\ \langle M_3, U \rangle &= -\frac{k_1}{k_3} b - \frac{k_2}{k_3} u_1 \end{aligned} \quad (2)$$

If we take derivating Equality 2 concerning s , we find

$$k_3 \underbrace{\langle T, U \rangle}_0 = 0 = \left(\frac{k_1}{k_3} b + \frac{k_2}{k_3} u_1 \right)'$$

In this way, $\frac{k_1}{k_3}b + \frac{k_2}{k_3}u_1 = \text{constant}$ and $\frac{u_1}{b} = -\frac{k_1}{k_2} = \text{constant}$ is obtained from here. If U is a nonzero constant vector field, we can write $U = aT + bM_1 + u_1M_2 + u_2M_3$. From here, we get

$$a = \langle T, U \rangle = 0$$

$$b = \langle M_1, U \rangle$$

$$u_1 = \langle M_2, U \rangle = \frac{-\left(\frac{k_1}{k_3}\right)' b}{\left(\frac{k_2}{k_3}\right)'}$$

$$u_2 = \langle M_3, U \rangle = -\frac{k_1}{k_3}b - \frac{k_2}{k_3}u_1 = \left(-\frac{k_1}{k_3} + \frac{k_2}{k_3} \left(\frac{\left(\frac{k_1}{k_3}\right)'}{\left(\frac{k_2}{k_3}\right)'} \right) \right) b$$

We write U using the substitutions for the a, b, u_1 and u_2 , as follows:

$$U = 0T + bM_1 + \frac{-\left(\frac{k_1}{k_3}\right)' b}{\left(\frac{k_2}{k_3}\right)'} M_2 + \left(-\frac{k_1}{k_3} + \frac{k_2}{k_3} \left(\frac{\left(\frac{k_1}{k_3}\right)'}{\left(\frac{k_2}{k_3}\right)'} \right) \right) b M_3$$

If we multiply both sides of $U = aT + bM_1 + u_1M_2 + u_2M_3$ by the inner product of U and $\langle U, U \rangle = K^2$ is for a constant K , we get

$$K^2 = b^2 + \left(-\frac{k_1}{k_3} + \frac{k_2}{k_3} \left(\frac{\left(\frac{k_1}{k_3}\right)'}{\left(\frac{k_2}{k_3}\right)'} \right) \right)^2 b^2 + \left(\frac{-\left(\frac{k_1}{k_3}\right)'}{\left(\frac{k_2}{k_3}\right)'} \right)^2 b^2$$

If we divide both sides of the equation by b^2 for the constant $\mu = \frac{K^2}{b^2} - 1$, and we get the following nonlinear differential equation for $y' = \frac{\left(\frac{k_1}{k_3}\right)'}{\left(\frac{k_2}{k_3}\right)'}$

$$y' - 2 \left(\frac{k_1 k_2}{k_3^2 + k_2^2} \right) y' + \frac{k_1^2 - \mu k_3^2}{k_3^2 + k_2^2} = 0.$$

Theorem 3.2. Let $\gamma: I \subseteq \mathbb{R} \rightarrow E^4$ be a regular curve given in E^4 . If the γ curve is a (2,4)- type slant helix according to parallel transport frame $\{T, M_1, M_2, M_3\}$, then, following nonlinear equation is obtained:

$$(y')^2 - 2 \left(\frac{k_1 k_3}{k_2^2 + k_3^2} \right) y' + \frac{k_1^2 - \mu k_2^2}{k_2^2 + k_3^2} = 0$$

where $y' = \frac{\left(\frac{k_1}{k_2}\right)'}{\left(\frac{k_3}{k_2}\right)'}$ and $\mu = \frac{K^2}{b^2} - 1$ are constants.

PROOF.

Suppose that the curve γ is a (2,4)-type slant helix according to parallel transport frame $\{T, M_1, M_2, M_3\}$, and U is a constant nonzero vector field, then we have

$$\langle M_3, U \rangle = u_2$$

$$\langle M_1, U \rangle = b$$

are constants. If we take derivating of the above equations concerning s , we get

$$k_1 \neq 0, k_3 \neq 0 \text{ için } \langle T, U \rangle = 0$$

and if we take derivating again with respect to s , we find

$$\langle T', U \rangle = 0$$

Using the Frenet formulas in Equality 1, we find the following equations:

$$\begin{aligned} k_1 \underbrace{\langle M_1, U \rangle}_b + k_2 \langle M_2, U \rangle + k_3 \underbrace{\langle M_3, U \rangle}_{u_2} = 0 \Rightarrow \\ \langle M_2, U \rangle = -\frac{k_1}{k_2} b - \frac{k_3}{k_2} u_2 \end{aligned} \quad (3)$$

If we take derivating Equality 3, concerning s , we have $-k_2 \frac{\langle T, U \rangle}{0} = 0 = -\left(\frac{k_1}{k_2} b + \frac{k_3}{k_2} u_2\right)'$. Therefore,

$\frac{k_1}{k_2} b + \frac{k_3}{k_2} u_2$ is a constant and $\left(\frac{k_1}{k_2}\right)' b + \left(\frac{k_3}{k_2}\right)' u_2 = 0$ is obtained. If U is a nonzero constant vector field, we can write $U = aT + bM_1 + u_1M_2 + u_2M_3$. Then, we get the following coefficients:

$$a = \langle T, U \rangle = 0$$

$$b = \langle M_1, U \rangle$$

$$u_1 = \langle M_2, U \rangle = -\frac{k_1}{k_2} b - \frac{k_3}{k_2} u_2 = \left(-\frac{k_1}{k_2} + \frac{k_3}{k_2} \left(\frac{\left(\frac{k_1}{k_2}\right)'}{\left(\frac{k_3}{k_2}\right)'} \right) \right) b$$

$$u_2 = \langle M_3, U \rangle = \frac{-\left(\frac{k_1}{k_2}\right)' b}{\left(\frac{k_3}{k_2}\right)'}$$

We write $U = aT + bM_1 + u_1M_2 + u_2M_3$ using the substitutions, for a, b, u_1 and u_2 ,

$$U = 0T + bM_1 + \left(-\frac{k_1}{k_2} + \frac{k_3}{k_2} \left(\frac{\left(\frac{k_1}{k_2}\right)'}{\left(\frac{k_3}{k_2}\right)'} \right) \right) b M_2 + \left(\frac{-\left(\frac{k_1}{k_2}\right)' b}{\left(\frac{k_3}{k_2}\right)'} \right) M_3$$

If we get inner product with U on both sides of the last equation above, and $\langle U, U \rangle = K^2$ for a constant K , we get

$$K^2 = b^2 + \left(-\frac{k_1}{k_2} + \frac{k_3}{k_2} \left(\frac{\left(\frac{k_1}{k_2}\right)'}{\left(\frac{k_3}{k_2}\right)'} \right) \right)^2 b^2 + \left(\frac{-\left(\frac{k_1}{k_2}\right)' b}{\left(\frac{k_3}{k_2}\right)'} \right)^2 b^2$$

If we divide both sides of the equation by b^2 for the constant $\mu = \frac{K^2}{b^2} - 1$, and we get the following nonlinear differential equation for $y' = \frac{\left(\frac{k_1}{k_2}\right)'}{\left(\frac{k_3}{k_2}\right)'}$

$$(y')^2 - 2 \left(\frac{k_1 k_3}{k_2^2 + k_3^2} \right) y' + \frac{k_1^2 - \mu k_2^2}{k_2^2 + k_3^2} = 0$$

Theorem 3.3. Let $\gamma: I \subseteq \mathbb{R} \rightarrow E^4$ be a regular curve given in E^4 . If the γ curve is a (3,4)-type slant helix according to parallel transport frame $\{T, M_1, M_2, M_3\}$, then, the following nonlinear equation is obtained:

$$(y')^2 - 2 \left(\frac{k_2 k_3}{k_1^2 + k_3^2} \right) y' + \frac{k_2^2 - \mu k_1^2}{k_1^2 + k_3^2} = 0$$

where $y' = \frac{\left(\frac{k_3}{k_1}\right)'}{\left(\frac{k_2}{k_1}\right)'}$ and $\mu = \frac{K^2}{u_2^2} - 1$ are constants.

PROOF. Let's assume that the γ curve is a (2,4)-type slant helix according to parallel transport frame $\{T, M_1, M_2, M_3\}$, and U is a constant nonzero vector field, then

$$\langle M_2, U \rangle = u_1$$

$$\langle M_3, U \rangle = u_2$$

are constants. If we derivative the above equations concerning s , for $k_2 \neq 0$, $k_3 \neq 0$, we get $\langle T, U \rangle = 0$. If we take derivating with respect to s again, we have

$$\langle T', U \rangle = 0$$

Using the Frenet formulas in Equality 1, we find the following equations:

$$\begin{aligned} k_2 \underbrace{\langle M_2, U \rangle}_{u_1} + k_1 \langle M_1, U \rangle + k_3 \underbrace{\langle M_3, U \rangle}_{u_2} &= 0 \Rightarrow \\ \langle M_1, U \rangle &= -\frac{k_3}{k_1} u_2 - \frac{k_2}{k_1} u_1 \end{aligned} \quad (4)$$

If we derivative Equation 4 with respect to s again, $-k_1 \underbrace{\langle T, U \rangle}_0 = 0 = -\left(\frac{k_3}{k_1} u_2 + \frac{k_2}{k_1} u_1\right)'$. Then, $\frac{k_3}{k_1} u_2 + \frac{k_2}{k_1} u_1$

is a constant. If U is a nonzero constant vector field, we can write $U = aT + bM_1 + u_1M_2 + u_2M_3$. Thus, we get the following coefficients:

$$a = \langle T, U \rangle = 0$$

$$b = \langle M_1, U \rangle = -\frac{k_3}{k_1} u_2 - \frac{k_2}{k_1} u_1 = \left(-\frac{k_3}{k_1} + \frac{k_2}{k_1} \left(\frac{\left(\frac{k_3}{k_1}\right)'}{\left(\frac{k_2}{k_1}\right)'} \right) \right) u_2$$

$$u_1 = \langle M_2, U \rangle = \frac{-\left(\frac{k_3}{k_1}\right)' u_2}{\left(\frac{k_2}{k_1}\right)'}$$

$$u_2 = \langle M_3, U \rangle$$

We write $U = aT + bM_1 + u_1M_2 + u_2M_3$ using the substitutions, for a, b, u_1 and u_2 :

$$U = 0T + \left(-\frac{k_3}{k_1} + \frac{k_2}{k_1} \left(\frac{\left(\frac{k_3}{k_1} \right)'}{\left(\frac{k_2}{k_1} \right)'} \right) \right) u_2 M_1 + \frac{-\left(\frac{k_3}{k_1} \right)' u_2}{\left(\frac{k_2}{k_1} \right)'} M_2 + u_2 M_3$$

If we get inner product with U on both sides of the last equation above, and $\langle U, U \rangle = K^2$ for a constant K , we get

$$K^2 = u_2^2 + \left(-\frac{k_3}{k_1} + \frac{k_2}{k_1} \left(\frac{\left(\frac{k_3}{k_1} \right)'}{\left(\frac{k_2}{k_1} \right)'} \right) \right)^2 u_2^2 + \left(\frac{-\left(\frac{k_3}{k_1} \right)'}{\left(\frac{k_2}{k_1} \right)'} \right)^2 u_2^2$$

If we divide both sides of the equation by u_2^2 for the constant $\mu = \frac{K^2}{u_2^2} - 1$, and we have the following

nonlinear differential equation for $y' = \frac{\left(\frac{k_3}{k_1} \right)'}{\left(\frac{k_2}{k_1} \right)'}$

$$(y')^2 - 2 \left(\frac{k_2 k_3}{k_1^2 + k_3^2} \right) y' + \frac{k_2^2 - \mu k_1^2}{k_1^2 + k_3^2} = 0.$$

4. CONCLUSION

This study obtained new nonlinear differential equations according to this frame by using the frame provided in [23], known as Bishop parallel transport frame $\{T, M_1, M_2, M_3\}$. Since there are no (1,2)-, (1,3)-, and (1,4)-type slant helices according to the Bishop parallel transport frame $\{T, M_1, M_2, M_3\}$ in [23], they do not have nonlinear equations. In addition, such slant helices can be investigated in different spaces and according to other frames. Nonlinear differential equations for (k, m) -type slant helices can be obtained by analyzing the equivalents of these studies in three-dimensional, four-dimensional spaces or in different dimensional spaces and in different frames in E^4 according to the Bishop frame.

REFERENCES

- [1] N. Takeuchi, S. İzumiya, *New Special Curves and Developable Surfaces*, Turkish Journal of Mathematics (28) (2004) 153-163.
- [2] E. Zıplar, A. Şenol, Y. Yaylı, *On Darboux Helices in Euclidean 3-Space*, Global Journal of Science Frontier Research: (F) Mathematics and Decision 12 (13) (2012) 73-80.
- [3] K. İlarıslan, M. Yıldırım, *On Darboux Helices in Euclidean 4-Space*, Mathematical Methods in the Applied Sciences 42 (16) (2018) 5184-5189.
- [4] Y. Forterre, J. Duamaj, *Generating Helices in Nature*, Science 333 (6050) (2011) 1715-1716.
- [5] L. Kula, N. Ekmekci, Y. Yaylı, *Characterizations of Slant Helices in Euclidean 3-Space*, Turkish Journal of Mathematics (33) (2009) 1-13.
- [6] X. Yang, *High Accuracy Approximation of Helices by Quintic Curve*, Computer Aided Geometric Design (20) (2003) 303-317.
- [7] R. L. Bishop, *There is No More Than One Way to Frame a Curve*, Mathematical 82 (3) (1975) 246-251.
- [8] B. Körpınar, *On Characterization Inextensible Flows of Curves According to Bishop Frame in E^3* , Revista Notas de Matematica 7 (32) (2011) 37-45.
- [9] B. Bükcü, M. K. Karacan, *The Slant Helices According to Bishop Frame*, International Scholarly and Scientific Research & Innovation 3 (11) (2009) 1010-1013.
- [10] S. Yılmaz, E. Özyılmaz, M. Turgut, *New Spherical Indicatrices and Their Characterizations*, Analele Stiintifice ale Universitatii Ovidius Constanta 18 (2) (2010) 337-354.
- [11] N. Macit, M. Döldül, *Some New Associated Curves of a Frenet Curve in E^3 and E^4* , Turkish Journal of Mathematics (38) (2014) 1023-1037.
- [12] S. Buyukkutuk, G. Öztürk, *Constant Ratio Curves According to Parallel Transport Frame in Euclidean 4-space E^4* , New Trends in Mathematica Sci 3 (4) (2015) 171-178.
- [13] M. Elzawy, *Smarandache Curves in Euclidean 4-Space*, Journal of the Egyptian Mathematical Society 25 (3) (2017) 268-271.

- [14] J. H. Choi, Y. H. Kim, *Associated Curves of a Frenet Curve and Their Applications*, Applied Mathematics and Computation 218 (18) (2012) 9116-9124.
- [15] T. Körpınar, M. T. Sariaydn, *Associated Curves According to Bishop Frame in Euclidean 3-Space*, Advanced Modeling and Optimization 15 (3) (2013) 713-717.
- [16] F. Bulut, *Slant Helices of (k, m) -Type According to the ED-frame in Minkowski 4-Space*, Symmetry 13 (11) (2021) 2185.
- [17] F. Bulut, *Special Helices on Equiform Differential Geometry of Timelike Curves in E_1^4* , Cumhuriyet Science Journal 42 (4) (2021) 906-915.
- [18] F. Bulut, F. Tartık, *(k, m) -type Slant Helices According to Parallel Transport Frame in Euclidean 4- Space*, Turkish Journal of Mathematics and Computer Science 13 (2) (2021) 261-269.
- [19] M. Y. Yıldırım, M. Bektaş, *Slant Helices of (k, m) -type in E^4* , Acta Universitatis Sapientiae Mathematica (10) (2018) 395-401.
- [20] Z. Özdemir, İ. Gök, N. Ekmekci, Y. Yaylı, *A New Approach on Type-3 Slant Helices in E^4* , General Mathematics Notes 28 (1) (2015) 40-49.
- [21] Y. Ünlütürk, H. Tozak, C. Ekici, *On k -Type Slant Helices Due to Bishop Frame in Euclidean 4-Space*, International Journal of Combinatorics (1) (2020) 1-9.
- [22] Ç. Camcı, H. H. Hacısalihoğlu, İ. Gök, *V_n -Slant Helices in Euclidean n -Space*, Mathematical Communications 2 (14) (2009) 317-329.
- [23] G. Cihangir, *On Type-3 Slant Helices Due to Bishop Frame in Euclidean 4-Space*, Master's Thesis, Fırat University (2022) Elazığ.
- [24] F. Gökçelik, Z. Bozkurt, I. Gök, F. N. Ekmekci, Y. Yaylı, *Parallel Transport Frame in 4- dimensional Euclidean Space E^4* , Caspian J. of Math. Sci. 3(1) (2014) 91-102.

DEPARTMENT OF MATHEMATICS, FACULTY OF ARTS AND SCIENCES, BİTLİS EREN UNIVERSITY, BİTLİS, TÜRKİYE
E-mail address: fbulut@beu.edu.tr

IFSCOM-E 2023
9TH IFS AND CONTEMPORARY MATHEMATICS AND ENGINEERING CONFERENCE
8-11 JULY 2023, TARSUS, MERSİN, TÜRKİYE
ISBN: 978-605-68670-8-8
pp: 125-131

ALMOST SUPRA B-CONTINUOUS FUNCTIONS

FATMA TALAS and AYNUR KESKIN KAYMAKCI

0000-0003-0808-1805 and 0000-0001-5909-8477

ABSTRACT

In this paper we introduce the notion of almost supra b-continuous function in supra topological spaces. Of course, we obtain some characterizations and several properties of it. The important properties of it that is stronger than both almost supra pre-continuity and almost supra semi-continuity and weaker than almost supra β -continuity

1. INTRODUCTION

The notion of supra topology is basic with respect to the investigation of general topological spaces. Several researchers have studied on this subject in [1,2,3,4,5,7,8,9]. They generalized the notion of open set such as supra-open, supra α -open, supra preopen, supra semi-open, supra b-open and given several results analogous to topological spaces. In 1983, A. S. Mashour et al.[7] introduced the supra topological spaces and studied s-continuous functions and s-continuous functions. In 2008, R. Devi et al.[3] have introduced and investigated the concepts of supra α -open sets and $s\alpha$ -continuous functions. In 2010, O. R. Sayed and Takashi Noiri [9] have defined and studied on supra b-open sets and supra b-continuous functions, respectively. Furthermore, they have introduced the concepts of supra b-open functions and supra b-closed functions and investigate several properties of them. In 2010, O.R.Sayed[8] has given definitions of the notions of supra preopen sets. In 2013, Saeid Jafari and Sanjay Tahiliani[5] have defined and studied of supra β -open sets and supra β -continuous functions. Besides they have introduced a new

Date: July, 8, 2023.

2000 Mathematics Subject Classification. Primary 54 A10; Secondary 54 A20.

Key words and phrases. Supra b-open set, almost supra b-continuity.

type of open functions and closed functions by using supra β -open set and supra β -closed set, respectively. In 2016, T.M. Al-shami[1] has studied the properties of supra limits and supra boundary points and introduce a notion of supra closure operators. They have also introduced and investigated some spaces such that supra Lindelöff, almost supra compact (almost supra Lindelöff) and mildly supra compact (midly supra Lindelöff) spaces. Moreover they have investigated several separation axioms such that supra regular, supra normal and STi-spaces (i=3,4). In 2017, T.M. Al-shami[2] has introduced the notions of supra semi open set, supra semi interior (resp. supra semi closure and supra semi boundary) operator. Based on the supra semi open sets, new types of supra continuous, supra open, supra closed and supra homeomorphism maps are presented and studied. In 2020, M. E. El-shafei et al.[4] have defined some concepts on supra topological spaces using supra preopen sets and investigated main properties. They have given by correcting some results obtained in previous study and presenting further properties of supra preopen sets.

On the other hand, Keskin and Noiri[6] have introduced the notion of almost b-continuous on topological spaces and obtained several properties of these functions.

In this paper we introduce the notion of almost supra b-continuous function in supra topological spaces. Of course, we obtain some characterizations and several properties of it. The important properties of it that is stronger than both almost supra pre-continuity and almost supra semi-continuity and weaker than almost supra β -continuity.

2. PRELIMINARIES

Throught this paper (X, τ) and (Y, σ) (or simply X and Y) denote topological spaces on which no separation axioms are assumed unieess explicitly stated. For a subset A of (X, τ) , the closure and the interior of A in X are denoted by $Cl(A)$ and $int(A)$, respectively. It is known that subset in A of (X, τ) is said to be regular open if $A = int(Cl(A))$ and A is said to be δ – open if for each $x \in A$, there exists a regular open set U such that $x \in U \subseteq A$. The complement of a regular open (resp. δ -open) set is called regular closed (resp. δ -closed). The family of all regular open (resp. regular closed) sets of X will be denoted by $RO(X)$ (resp. $RC(X)$).

Definition 2.1. (Mashour et al., 1983) A family μ of subsets of a nonempty set X is called a supra topology provided that the following two conditions hold: (1) X and $\emptyset \in \mu$, (2) μ is closed under arbitrary union. The pair (X, μ) is called a supra topological space. Every element of μ is called a supra open set and its complement is called a supra closed set.

Remark 2.2. (Mashour et al., 1983) 1. Since $\bigcup_{i \in \emptyset} G_i = \emptyset$, then some authors remove the empty set \emptyset from the first condition of a supra topology.

2. μ is called an associated supra topology with a topology τ if $\tau \subseteq \mu$.

3. Through this paper, we consider (X, μ) and (Y, φ) are associated supra topological spaces with the topological spaces (X, τ) and (X, δ) , respectively.

Definition 2.3. (Mashour et al., 1983) Let A be a subset of (X, μ) . Then, $\text{int}^\mu(A)$ is union of all supra open sets contained in A and $\text{Cl}^\mu(A)$ is the intersection of all supra closed sets containing A . If there is no confusion, we write $\text{int}(A)$ and $\text{Cl}(A)$ in the places of $\text{int}^\mu(A)$ and $\text{Cl}^\mu(A)$, respectively.

Definition 2.4. (Sayed, Noiri, 2010) (X, μ) be a supra topological space, set A is said a **supra b-open set** if $A \subset \text{Cl}^\mu(\text{int}^\mu(A)) \cup \text{int}^\mu(\text{Cl}^\mu(A))$. The complement of a supra b-open set is called a supra b-closed set.

The family of all supra b-open (resp. supra b-closed) sets of X will be denoted by $SBO(X)$ (resp. $SBC(X)$).

Since $\tau \subset \mu$, every open set is supra open Besides, in (Sayed, Noiri, 2010), authors obtained that every supra open set is supra b-open, so, one can conclude that every open set is supra b-open.

Definition 2.5. (Sayed, Noiri, 2010) The supra b-closure of set A , denoted by $\text{Cl}_b^\mu(A)$, is the intersection of supra b-closed sets including A . The supra b-interior of a set A , denoted by $\text{int}_b^\mu(A)$, is the union of supra b-open sets included in A .

Remark 2.6. (Sayed, Noiri, 2010) It is clear that $\text{int}_b^\mu(A)$ is a supra b-open set and $\text{Cl}_b^\mu(A)$ is a supra b-closed set.

Lemma 2.7. (Sayed, Noiri, 2010) The following properties are hold:

1. $A \subseteq \text{Cl}_b^\mu(A)$,
2. $A = \text{Cl}_b^\mu(A)$ iff A is a supra b-closed set,
3. $\text{int}_b^\mu(A) \subseteq A$,
4. $\text{int}_b^\mu(A) = A$ iff A is a supra b-open set,
5. $X - \text{int}_b^\mu(A) = \text{Cl}_b^\mu(X - A)$, 6. $X - \text{Cl}_b^\mu(A) = \text{int}_b^\mu(X - A)$.

3. ALMOST SUPRA B-CONTINUOUS FUNCTIONS

In this section, we introduce a new type of almost continuous maps called an almost supra b-continuous map and obtain some of their properties and characterizations.

Definition 3.1. Let (X, τ) and (Y, σ) be two topological spaces and μ be associated supra topology with τ . A function $f : (X, \tau) \rightarrow (Y, \sigma)$ is called an almost supra b-continuous map for

each $x \in X$ and each $V \in SRO(Y)$ containing $f(x)$, there exists $U \in SBO(X)$ containing x such that $f(U) \subset V$.

Theorem 3.2. For a function $f : (X, \tau) \rightarrow (Y, \sigma)$ (such that μ be an associated supra topology with τ), the following properties are equivalent:

1. f is almost supra b- continuous;
2. For each $x \in X$ and each $V \in \sigma$ containig $f(x)$, there exists $U \in SBO(X)$, containig x such that $f(U) \subset \text{int}(Cl(V))$;
3. $f^{-1}(V) \in SBC(X)$ for every $F \in RC(Y)$;
4. $f^{-1}(V) \in SBO(X)$ for every $F \in RO(Y)$.

Proof: The prof is obvious from Definition 3.1.

Theorem 3.3. For a function $f : (X, \tau) \rightarrow (Y, \sigma)$ (such that μ be an associated supra topology with τ), the following properties are equivalent:

1. f is almost supra b- continuous;
2. $f(Cl_b^\mu(A)) \subset \delta - Cl(f(A))$ for every subset A of X ;
3. $Cl_b^\mu(f^{-1}(B)) \subset f^{-1}(\delta - Cl(B))$ for every subset B of Y ;
4. $f^{-1}(F) \in SBC(X, \tau)$ for every δ -closed set F of Y ;
5. $f^{-1}(V) \in SBO(X, \tau)$ for every δ -open set V of Y ;

Prof: **1 \Rightarrow 2.** Let A be a subset of X . Since $\delta - Cl(f(A))$ is a δ -closed set in Y , it is denoted by

$\cap \{F_\alpha : F_\alpha \in RC(Y, \sigma), \alpha \in \Delta\}$, where Δ is an index set. By theorem 3.2, we have

$A \subset f^{-1}(\delta Cl(f(A))) = \cap \{f^{-1}(F_\alpha) : \alpha \in \Delta\} \in SBC(X, \tau)$ and hence $Cl_b^\mu(A) \subset f^{-1}(\delta Cl(A))$. Hence, we obtain $f(Cl_b^\mu(A)) \subset \delta Cl(f(A))$.

3 \Rightarrow 2. Let B be a subset of Y . We have $f(Cl_b^\mu(f^{-1}(B))) \subset \delta Cl(f(f^{-1}(B))) \subseteq \delta Cl(B)$ and hence $Cl_b^\mu(f^{-1}(B)) \subset f^{-1}(\delta Cl(B))$.

3 \Rightarrow 4. Let F be any δ -closed set of Y . We have $Cl_b^\mu(f^{-1}(F)) \subset f^{-1}(\delta Cl(F)) = f^{-1}(F)$ and $f^{-1}(F)$ is supra b-closed in X .

4 \Rightarrow 5. Let V be any δ -open set of Y . Using (4), we have $f^{-1}(Y - V) = X - f^{-1}(V) \in SBC(X, \tau)$ and so $f^{-1}(V) \in SBO(X)$.

5 \Rightarrow 1. Let V be any regular open set of Y . Since V is δ -open $f^{-1}(V) \in SBO(X)$ and hence according to Theorem 3.2, f is almost supra b-continuous.

It is known that a function $f : (X, \tau) \rightarrow (Y, \sigma)$ is said to be R-map (resp. δ -continuous), if $f^{-1}(V) \in RO(X)$ (resp. $f^{-1}(V) \subset X$ is δ -open) for each $V \in Ro(Y)$.

Theorem 3.4. Let $f : (X, \tau) \rightarrow (Y, \sigma)$ and $g : (Y, \varphi) \rightarrow (Z, \psi)$ be two functions such that μ

be an associated supra topology with τ . For the composition $g \circ f: (X, \tau) \rightarrow (Z, \psi)$, the following properties are hold:

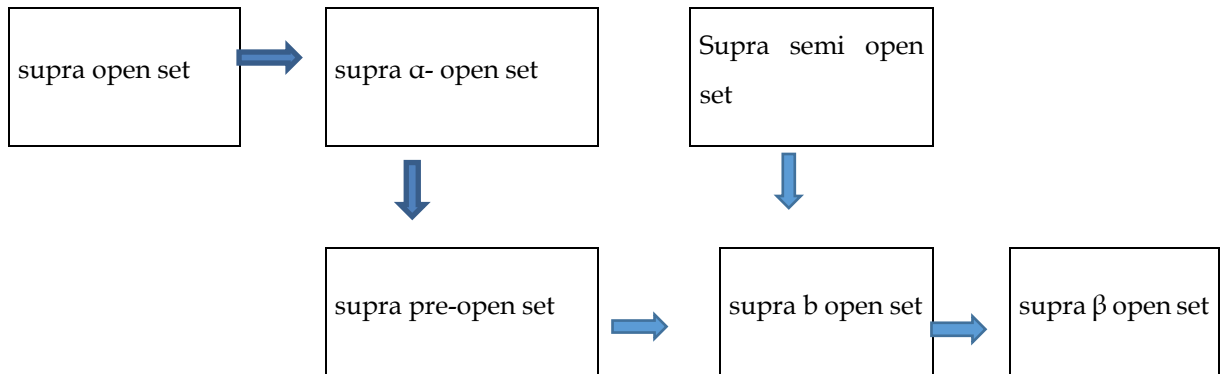
1. If f is an almost supra b-continuous and g is on R-map, then $g \circ f$ is an almost supra b-continuous.
- 2.If f is an almost supra b-continuous and g is δ -continuous, then $g \circ f$ is an almost supra b-continuous.

Proof: The proofs are obtaned immediatly as consequences of the definition and it is thus omitted.

Definition 3.5. Let (X, μ) be a supra topological space A subset X is said to be;

- 1.**supra α -open set** (Devi et al., 2008) if $A \subset \text{int}^\mu(\text{Cl}^\mu(\text{int}^\mu(A)))$
- 2.**supra semi open set** (Sayed ve Noiri , 2010) if $A \subset \text{Cl}^\mu(\text{int}^\mu(A))$
- 3.**supra pre-open set** (Sayed, 2010) if $A \subset \text{int}^\mu(\text{Cl}^\mu(A))$
- 4.**supra β -open set** (Ravi et al.,2012) if $A \subseteq \text{Cl}^\mu(\text{int}^\mu(\text{Cl}^\mu(A)))$.

The family of all supra α -open (resp. supra pre-open, supra semi open, supra β -open) sets of X will be denoted by $S\alpha O(X)$ (resp. $SPO(X), SSO(X), S\beta O(X)$). In [Sayed, Noiri, 2010], authors given the following diagram in which the converses of the implicotions need not be true.



Now, we introduce some almost continuity in supra topological spaces.

Definition 3.6. (X, τ) and (Y, σ) be two topological spaces and μ be an associated supra topology with τ . A map $f : (X, \tau) \rightarrow (Y, \sigma)$ is called an

- 1.**almost supra α - continuous** if $f^{-1}(V) \in S\alpha O(X)$ for every $V \in RO(Y)$
- 2.**almost supra pre-continuous** if $f^{-1}(V) \in SPO(X)$ for every $V \in RO(Y)$
- 3.**almost supra semi continuous** if $f^{-1}(V) \in SSO(X)$ for every $V \in RO(Y)$
- 4.**almost supra β -continuous** if $f^{-1}(V) \in S\beta O(X)$ for every $V \in RO(Y)$

Theorem 3.7. Let $f : (X, \tau) \rightarrow (Y, \sigma)$ a function such that μ be an associated supra topology with τ . Then, the following properties are hold:

1. If is almost supra α - continuous , then it is an almost supra pre-continuous;
2. If is almost supra α - continuous , then it is an almost supra semi-continuous;

3. If f is almost supra pre-continuous, then it is an almost supra b-continuous;
4. If f is almost supra semi-continuous, then it is an almost supra b-continuous;
5. If f is almost supra b-continuous, then it is an almost supra β -continuous.

Prof: 1. $V \in RO(Y)$ while $f^{-1}(V) \subseteq \text{int}^\mu(\text{Cl}^\mu(\text{int}^\mu(f^{-1}(V))))$ because f is an almost supra α -continuous function. Then we have $\text{int}^\mu(f^{-1}(V)) \subseteq f^{-1}(V)$, $\text{Cl}^\mu(\text{int}^\mu(f^{-1}(V))) \subseteq \text{Cl}^\mu(f^{-1}(V))$ and so $\text{int}^\mu(\text{Cl}^\mu(\text{int}^\mu(f^{-1}(V)))) \subseteq \text{int}^\mu(\text{Cl}^\mu(f^{-1}(V)))$. This shows that f is almost supra pre-continuous function.

2. $V \in RO(Y)$ while $f^{-1}(V) \subseteq \text{int}^\mu(\text{Cl}^\mu(\text{int}^\mu(f^{-1}(V))))$ because f is an almost supra α -continuous function. Then we have $f^{-1}(V) \subseteq \text{int}^\mu(\text{Cl}^\mu(\text{int}^\mu(f^{-1}(V)))) \subseteq \text{Cl}^\mu(\text{int}^\mu(f^{-1}(V)))$ and $f^{-1}(V) \subseteq \text{Cl}^\mu(\text{int}^\mu(f^{-1}(V)))$. So, f is an almost supra semi-continuous function.

3. $V \in RO(Y)$ while $f^{-1}(V) \subseteq \text{int}^\mu(\text{Cl}^\mu(f^{-1}(V)))$ because f is an almost supra pre-continuous function. So, we have $f^{-1}(V) \subseteq \text{int}^\mu(\text{Cl}^\mu(f^{-1}(V))) \subseteq \text{int}^\mu(\text{Cl}^\mu(f^{-1}(V))) \cup \text{Cl}^\mu(\text{int}^\mu(f^{-1}(V)))$ and $f^{-1}(V) \subseteq \text{int}^\mu(\text{Cl}^\mu(f^{-1}(V))) \cup \text{Cl}^\mu(\text{int}^\mu(f^{-1}(V)))$. Hence, f is an almost supra b-continuous function.

4. $V \in RO(Y)$ while $f^{-1}(V) \subseteq \text{Cl}^\mu(\text{int}^\mu(f^{-1}(V)))$ because f is an almost supra semi-continuous function. Hence, we have $f^{-1}(V) \subseteq \text{Cl}^\mu(\text{int}^\mu(f^{-1}(V))) \subseteq \text{int}^\mu(\text{Cl}^\mu(f^{-1}(V))) \cup \text{Cl}^\mu(\text{int}^\mu(f^{-1}(V)))$ and $f^{-1}(V) \subseteq \text{int}^\mu(\text{Cl}^\mu(f^{-1}(V))) \cup \text{Cl}^\mu(\text{int}^\mu(f^{-1}(V)))$. So, f is an almost supra b-continuous function.

5. $V \in RO(Y)$ while $f^{-1}(V) \subseteq \text{int}^\mu(\text{Cl}^\mu(f^{-1}(V))) \cup \text{Cl}^\mu(\text{int}^\mu(f^{-1}(V)))$ because f is almost supra b-continuous function. So, $f^{-1}(V) \subseteq \text{Cl}^\mu(\text{int}^\mu(f^{-1}(V))) \subseteq \text{int}^\mu(\text{Cl}^\mu(f^{-1}(V))) \cup \text{Cl}^\mu(\text{int}^\mu(f^{-1}(V)))$ and hence $f^{-1}(V) \subseteq \text{int}^\mu(\text{Cl}^\mu(f^{-1}(V))) \cup \text{Cl}^\mu(\text{int}^\mu(f^{-1}(V)))$. Therefore f is an almost supra β -continuous function.

REFERENCES

- [1] T.M Al-shami, Supra results related to supra topological spaces, *Journal of Advanced Studies in Topology*, 7(4), 283-294, (2016).
- [2] T.M.Al-Shami, On supra semi open sets and some applications on topological spaces, *Journal of Advanced Studies in Topology*, 8(2), 144-153, (2017).
- [3] R.Devi, S.Sampathkumar and M.Caldas, On supra α -open sets and $S\alpha$ -continuous functions, *General Mathematics*, 16(2), 77-84, (2008).
- [4] M. E. El-Shafei, A. H. Zakari and T.M.Al-Shami, Some applications of supra preopen sets, *Hindawi Journal of Mathematics*, Volume 2020, Article ID 9634206, <https://doi.org/10.1155/2020/9634206>.
- [5] S. Jafari and S. Tahiliani, Supra β -open sets and supra β -continuity on topological spaces, *Annales Univ. Sci. Budapest.*, 56, 1-9, (2013).
- [6] A. Keskin (Kaymakci) and T. Noiri, Almost b-continuous functions, *Chaos, Solitons and Fractals*, 41(1), 72-81, (2009).
- [7] A. S. Mashhour, A. A. Allam, F. S. Mahmoud and F. H. Khedr, On supra topological spaces, *Indian J. Pure Appl. Math.*, 14(4), 502-510, (1983).
- [8] O. R. Sayed, Supra pre-open sets and supra pre-continuity on topological spaces, *Series Mathematics and Information*, 20, 79-88,(2010).
- [9] O. R. Sayed and T. Noiri, On supra b-open sets and supra b-continuity on topological spaces, *European Journal of Pure and Applied Mathematics*, 3(2), 295-302, (2010).

SELCUK UNIVERSITY, FACULTY OF SCIENCE, DEPARTMENT OF MATHEMATICS, CAM- PUS, 42031,
KONYA/TÜRKİYE
E-mail address: canfatma8485@gmail.com

SELCUK UNIVERSITY, FACULTY OF SCIENCE, DEPARTMENT OF MATHEMATICS, CAMPUS, 42031,
KONYA/TÜRKİYE
E-mail address: akeskin@selcuk.edu.tr

**CORPORATE CARBON FOOTPRINT CALCULATION AND EVALUATION OF MERSIN
UNIVERSITY ÇİFTLİKKÖY CAMPUS**

HASRET KARAKAYA¹, YASIN ÖZAY² and NADIR DİZGE¹

0000-0002-6154-7427, 0000-0001-5419-6115 and 0000-0002-7805-9315

ABSTRACT

The increasing greenhouse gases present in the troposphere layer, which is located on average eleven kilometers above the atmosphere in our world, and global warming threaten the continuity of the entire ecosystem. In particular, the increase in the use of fossil fuels, the increase in the number of population every day, industrialization and deforestation are all activities that increase global warming by increasing the amount of greenhouse gas emissions. Natural disasters caused by global warming and climate change complicate the life activities of all living things. Recently, increasing to prevent changes in the climate system and thus, if it is to continue in the future the increase of natural disasters, drought, seasonal changes, change in extreme temperature difference Day and night on earth as the change in the amount of naturally occurring gases vital to live with the results, it is envisaged that this will not be a world for 50 years. On an international scale, which is one of the most important environmental problems-climate change, due to all organisms affect all national and international institutions and organizations should do their part. Developed and developing countries in order to prevent the creation of a new energy policy, climate change, carbon emissions and thus the necessity for the provision of a sustainable environment by maintaining a minimum level of the United Nations and is important for studies is located. In order to obtain results in the studies carried out, the expression of carbon footprint appears. Carbon footprint is the indication of greenhouse gas emissions released into the atmosphere as a Tue of activities in terms of carbon dioxide. Mersin University Çiftlikköy Campus has a very important position in the greenhouse gas emission emitted in Mersin province in terms of the area it covers in Mersin province and the excess of the human population. For this reason, in this study, Mersin University Çiftlikköy Campus Corporate Carbon Footprint Calculation was performed. In the

Date: July, 8, 2023.

Key words and phrases. Global Warming, Greenhouse Gas Emissions, Carbon Footprint, Climate Change, Mersin University.

calculation, the amount of carbon dioxide released by using the natural gas consumption data of the campus related to heating for the year 2022, electricity consumption, vehicles belonging to the university and fuel consumption of vehicles entering the campus were calculated. The calculations also revealed a total of 23,614 tons of CO₂e, which accounts for 73.7% of greenhouse gas emissions in Scope 3, including other indirect emissions related to campus entry, academics, guest vehicle fuels, and minibus-bus. This quantity represents the amount of carbon dioxide emitted from fuel. The annual fuel consumption of vehicles owned by the Rectorate, as well as the natural gas consumption for heating, are classified as direct emissions in Scope 1. They have been calculated to be 1,132 tons of CO₂e. Additionally, Scope 2 indirect greenhouse gas emissions, resulting from electricity consumption, have been estimated to be 5,060 tons of CO₂e.

1. INTRODUCTION

The energy source of our world, which is the common living space of all living things, is the sun. The rays coming from the sun to the Earth provide the continuation of the vital activities of all living and non-living beings in the world by using approximately 51% for the continuation of vital activities. The atmosphere of our planet works just like a greenhouse. The gases in the atmosphere and the average temperature on earth provide the temperature level that allows the continuity of life. This natural effect of gases in the atmosphere is called the "Greenhouse Gas Effect" [1].

Compounds, which are defined as greenhouse gases for this reason, cause global warming by creating a greenhouse effect in the atmosphere, especially due to the increase in their quantity resulting from the use of fossil fuels.,

- Carbon dioxide (CO₂)
- Methane (CH₄)
- Diazot oxide (N₂O)
- Hydrofluorocarbons (HFCs)
- Perfluorocarbons (PFCs)
- Gases such as Sulfur hexafluoride (SF₆)

The increase in greenhouse gases in the atmosphere significantly contributes to global warming. The amount of carbon dioxide equivalent emitted into the atmosphere is on the rise due to the development of industrial processes, increasing population, and vital activities such as agriculture, lighting, heating, food consumption, livestock activities, and transportation. The total amount of greenhouse gases emitted into the atmosphere, measured in terms of carbon dioxide, resulting from the activities conducted by an individual, country, or institution, is referred to as the carbon footprint [2]. According to the Intergovernmental Panel on Climate Change (IPCC), the primary cause of the increase in greenhouse gases and carbon dioxide is attributed to the consumption of fossil fuels. Other significant factors include changes in land use, particularly deforestation associated with increased agricultural

practices. The IPCC reports that the primary driver of global warming is the rise in greenhouse gas emissions resulting from human activities [3].

The use of fossil fuels, primarily coal, is the main factor responsible for the increase in carbon dioxide levels in the atmosphere. According to the Intergovernmental Panel on Climate Change (IPCC), greenhouse gas emissions resulting from human activities in 2004,

- 6% of it is attributed to carbon dioxide emissions resulting from the burning of fossil fuels.
- Deforestation accounts for a 17% contribution.
- Among fossil fuels, coal has the most significant impact.
- While coal provides 27% of the global primary energy use, it is responsible for 43% of energy-related greenhouse gas emissions.
- Coal consumption has a greater carbon dioxide release into the atmosphere compared to natural gas consumption, with a unit of energy produced releasing 1.7 times more carbon dioxide.
- The impact of coal consumption is followed by oil with 36% and natural gas with 20% [4].

All living things on Earth rely on specific resources to sustain their vital activities. The world is currently grappling with the crisis of climate change and global warming, primarily caused by factors such as increasing global population, industrialization, and deforestation [1].

2. MATERIAL AND METHODS

In the scope of this study, carbon footprint calculation was conducted using the data obtained from Mersin University Çiftlikköy Campus, one of the largest campuses in Mersin province, located in the Mediterranean region. The study included the area from the campus entrance to the faculties, excluding the Medical Faculty and the Dormitory area.

Tier 1 methodology was used from the methods published in the IPCC guideline. In the IPCC Guideline, there are 3 different calculation methods, namely Tier 1, Tier 2, and Tier 3, for the estimation of fossil fuel emissions. In these methods, the number of data and details in the calculation increase as the method level increases [5].

Calculations have been prepared using the data of the internationally accepted IPCC 2006 guideline in accordance with the provisions of the GHG Protocol document and ISO 14064-1 standard.

In the calculations made with the standard method, the total carbon dioxide emissions are calculated by multiplying the activity data and emission factors [5,6].

Calculations within the scope of the "Regulation on the Monitoring of Greenhouse Gas Emissions", which was published in the Official Gazette dated 17.05.2014 and numbered 29003 by the Ministry of Environment and Urbanization, are given in annex-3 of the regulation in line with these standards [7]. Regulation Annex-3 Calculation is available below and the Ministry has also used the same formula within the scope of IPCC and GHG Protocol.

Regulation ANNEX- 3: Principles of Monitoring and Reporting of Greenhouse Gas Emissions

1. Monitoring of Carbon Dioxide Emissions

Emissions should be monitored by calculation or direct measurement.

The calculation is made with the formula given below in all data:

Emission Amount = Activity data × emission factor × oxidation factor

Activity data (such as fuel used, production rate) should be tracked in the form of supply data or measurement.

Depending on the IPCC guideline, formula (1) is used in the calculation of Tier-1, and the oxidation factor is taken as 1 in natural gas calculations, assuming that there is tanning. In this context, all calculations;

(1) Emission Amount (tCO₂) = Activity Data × Emission Factor. Here, unit conversions and emission factors according to the category to be calculated are used as specified in the IPCC guideline.

3. RESULTS AND DISCUSSION

The carbon emission amount of Mersin University in 2022 has been calculated as 23,614 tCO₂. 73.7% of this consists of other indirect emissions defined as Scope-3, namely the amount of carbon dioxide emitted from academicians, guest vehicle fuels, and minibus-bus fuels entering the campus. Mersin ranks 3rd in terms of quantity, primarily due to its generally hot climate and the use of natural gas solely for heating purposes in the university.

The studies conducted at universities include the following:

Calculation of CO₂ emissions based on students, academicians, and personnel throughout the education period.

Inclusion of CO₂ calculations from university activities such as energy consumption, fuel use, and heating.

This study encompasses CO₂ calculations for energy consumption, fuel use, and heating in Mersin University Çiftlikköy Campus. When all the calculations given in the methodology are made, the following emissions are attributed to our university's Çiftlikköy Campus is given at Table 3.1.

Table 3.1. Carbon Footprint Calculation Quantities

Scope	Natural Gas	Electricity	Vehicles of the Rectorate	Other Vehicles Entering the Campus
Scope-1 Direct Emission Sources	743,232 tCO ₂	-	387,81 tCO ₂	-
Scope-2 Sources of Indirect Emissions	-	5.060 tCO ₂	-	-
Scope-3 Other Indirect Emission Sources	-	-	-	17.422 tCO ₂

As a result of the calculations, the greenhouse gas emission coverage results are presented in Figure 3.1. The CO₂ emission calculation percentages for Mersin University Çiftlikköy Campus are illustrated in Figure 3.2

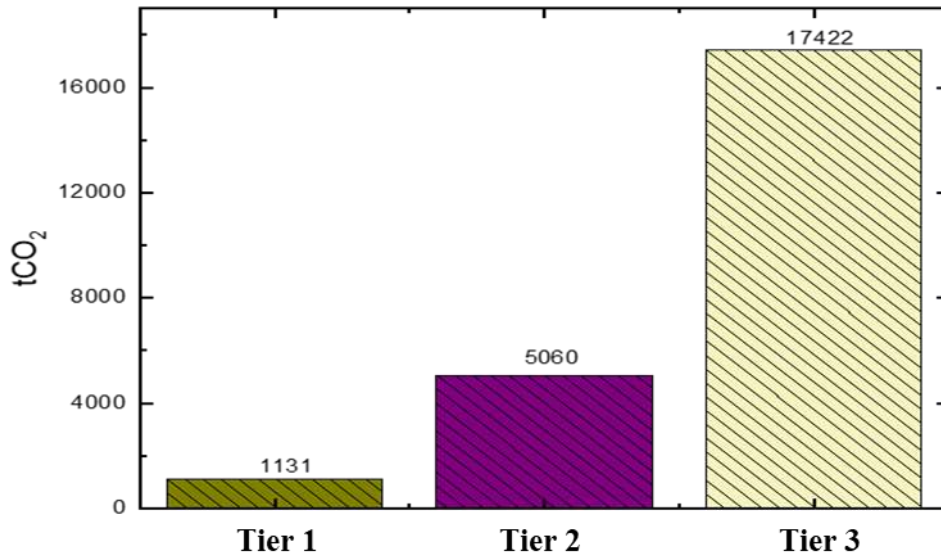


Figure 3.1. Greenhouse Gas Emissions

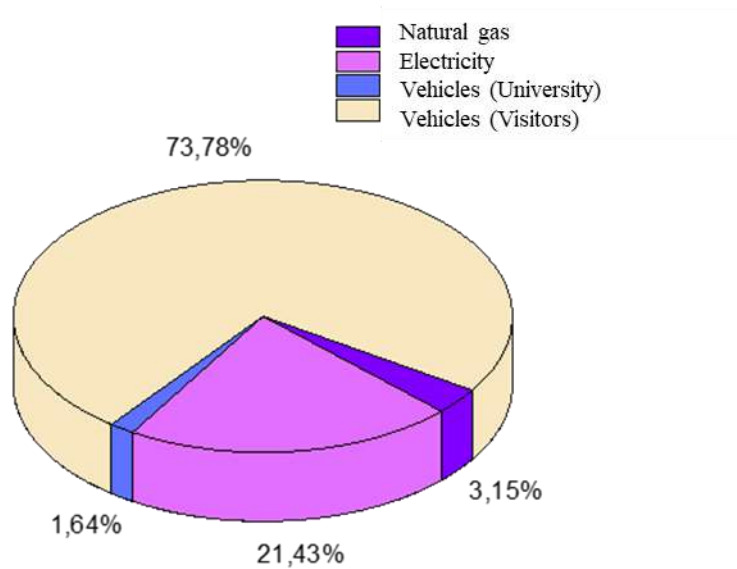


Figure 3.2. Mersin University Çiftlikköy Campus CO₂ Emissions

In a 2017 study by Özçelik, the Terzioğlu Campus of Çanakkale Onsekiz Mart University was examined, and the carbon footprint of various sources was calculated. This calculation encompassed natural gas usage for campus heating, the vehicle fleet owned by the university administration, electricity consumption, as well as emissions from academic, administrative, and student transportation. Based on the calculated data, the carbon footprint was determined to be 19,706.084 tons of CO₂e [8].

In another study conducted by Çerçi in 2021, the carbon footprint of Erzincan Binali Yıldırım University was determined. The study considered the natural gas/coal used for heating, electricity consumption for lighting and classroom/office equipment, as well as gasoline and diesel consumption by university vehicles. The calculated emissions for 2020 amounted to 2,383.74 tCO₂e[9].

The CO₂e values obtained from the Terzioğlu Campus of Çanakkale Onsekiz Mart University are similar to our study's results. However, the calculated emissions for Erzincan Binali Yıldırım University were only 10% of our study's findings. This discrepancy is believed to be related to factors such as university size, the number of academicians, students, and guests[8,9].

The highest greenhouse gas emissions are attributed to fuels used by academicians, guest vehicles, minibusses, and buses entering the campus. The next significant portion is due to electricity consumption. To reduce these emissions, it is necessary to promote the use of public transportation and electric vehicles, encourage walking and cycling for short distances, adopt energy-saving lamps throughout the campus, switch off unnecessary lights, replace electrical devices with eco-labeled ones, and carry out regular maintenance and repair processes.

4. CONCLUSION

As a result of the increasing greenhouse gas emissions and the resulting global warming and climate change, it is crucial for both national and international institutions and organizations to adopt a sustainable environmental approach to ensure the world remains a livable ecosystem. This thesis study focuses on calculating the Carbon Footprint using technical data obtained from Mersin University Çiftlikköy Campus. The carbon dioxide emissions were calculated based on the amount of natural gas, electricity consumption, fuel consumption of vehicles belonging to the rectorate, and other vehicles entering the campus.

Based on the obtained data, the following considerations should be taken into account:

- Transitioning to a hybrid education system would reduce carbon emissions.
- Electric vehicles and buses with low-volume engines and high energy efficiency can replace passenger vehicles belonging to the Rectorate.
- Electricity consumption can be reduced by shutting down all unnecessary electrical systems, allocating a budget for renewable energy sources, and meeting electricity needs through renewable sources to reduce reliance on imported electricity.
- All electrical systems within the university should be replaced with low-power consumption systems. Raising awareness among administrative and technical personnel, as well as students, regarding sustainable environments, greenhouse gas emissions, global warming, and climate change can lead to a reduction in carbon emissions.
- Regular maintenance of vehicles and electronic-mechanical equipment and systems used in the university is essential in preventing an increase in greenhouse gas emissions.

- Placing awareness boards, brochures, and posters in all faculties and social areas of the university to promote actions such as turning off unnecessary lights and encouraging bicycle use within walking distances can effectively raise awareness among staff and students.

- Introducing elective courses in other faculties, such as Global Warming and Climate Change and Environmental Education, will significantly impact the reduction of individual CO₂ emissions by increasing awareness.

- Implementing Solar Photovoltaic (SPP) projects in suitable areas on the university campus to produce energy from renewable sources will play a crucial role in preventing the increase in greenhouse gas emissions and promoting a sustainable environment.

- Installing alternative CO₂ trap filters at the natural gas system outlets is also important.

Considering these factors, it is necessary to develop an action plan, create a roadmap, and work towards implementing it throughout the entire university.

REFERENCES

[1] Lynas, M. "Your Carbon Footprint." Neşet Kutluğ (Trans.). Istanbul: Open Radio Books, (2009).

[2] Tatar, O. "International Carbon Trade and Determination of Izmir's 'Carbon Footprint'." Presentation at ÇŞB, (2010).

[3] Binboğa, G., Ünal, A. "ÜİİİD-IJEAS, 2018 (21): 187-202 ISSN 1307-9832." (2018).

[4] International Standard ISO-14064-1. "Greenhouse Gases - Part 1: Specification with Guidance at the Organization Level for Quantification and Reporting of Greenhouse Gas Emissions and Removals." ISO 14064-1:2018 Training.

[5] IPCC Guidelines. Accessed on December 1, 2022, from <https://www.ipcc-nggip.iges.or.jp/>

[6] Üreden, A., Özden, S. "How to Calculate Corporate Carbon Footprint: A Theoretical Study." Anatolian Journal of Forest Research, 4(2), 98-108, (2018).

[7] Official Gazette dated 17.05.2014 and numbered 29003. "Regulation on Tracking Greenhouse Gas Emissions" by ÇŞB.

[8] Özçelik, G. "EVALUATION of ÇANAKKALE ONSEKİZ MART UNIVERSITY TERZIOĞLU CAMPUS in terms of ENERGY and CARBON FOOTPRINT" Natural and Applied Sciences, Çanakkale Onsekiz Mart University, Çanakkale/Turkey, (2017).

[9] Kurnuç Seyhan, A. & Çerçi, M. Determination of Carbon Footprint Using IPCC Tier 1 and DEFRA Methods: A Case Study of Fuel and Electricity Consumption at Erzincan Binali Yıldırım University. Süleyman Demirel University Journal of Institute of Natural and Applied Sciences, 26 (3), 386-397. DOI: 10.19113/sdufenbed.1061021, (2022).

¹MERSIN UNIVERSITY, DEPARTMENT OF ENVIRONMENTAL ENGINEERING, 33343 MERSIN, TURKEY.
E-mail address: hasret@lotuscevre.com.tr

²TARSUS UNIVERSITY, DEPARTMENT OF ENVIRONMENTAL PROTECTION TECHNOLOGIES, 33400 MERSIN, TURKEY.
E-mail address: yasinozay@tarsus.edu.tr

³MERSIN UNIVERSITY, DEPARTMENT OF ENVIRONMENTAL ENGINEERING, 33343 MERSIN, TURKEY
E-mail address: nadirdizge@gmail.com

IFSCOM-E 2023
9TH IFS AND CONTEMPORARY MATHEMATICS AND ENGINEERING CONFERENCE
8-11 JULY 2023, TARSUS, MERSİN, TÜRKİYE
ISBN: 978-605-68670-8-8
pp: 139-146

PISTACHIO SPECIES IDENTIFICATION USING HISTOGRAM OF ORIENTED GRADIENT DESCRIPTORS AND SUPPORT VECTOR MACHINE

BİRKAN BÜYÜKARIKAN¹

0000-0002-9703-9678

ABSTRACT

Developing intelligent systems, including computer vision and machine learning technologies for classifying agricultural products according to their types, are an interesting research topic. Here, models are obtained with the help of intelligent systems to decide. These models simulate human visual perception for the classification of agricultural products. In this study, an approach combining the histogram of oriented gradients (HOG) technique and support vector machine (SVM) was proposed for pistachio image species classification. In this study, image features were extracted using different cell sizes of the HOG. These features were classified using different kernel functions of SVM with 10-fold cross-validation. Thus, this study investigated the possibility of improving an existing method by making it learnable. In the experimental results, the proposed approach achieved different success with a different number of features. This study showed that the best performance results were obtained in the model where the cell size was 128 x 128 and the kernel type was polynomial. The accuracy of this model was 0.940, sensitivity 0.938, specificity 0.941, F-score 0.930, G-mean 0.931, and AUC value 0.978.

1 INTRODUCTION

Pistachios are highly nutritious fruit with high levels of carbohydrates, potassium, and minerals. This fruit is eaten as a snack as well as used in desserts [5], and it determines the quality of the pistachio by growing it according to world standards [11]. Two pistachio species extensively grown and exported in Turkey are Kırmızı and Siirt. Kırmızı from this species; is used extensively in the pastry industry for reasons such as color, taste, and aroma. Siirt pistachio is preferred as a snack due to its round shape and high cracking rate [18]. Because these species have different nutritional values, shell thickness, size, and width, they enable the pistachios to be visually distinguished [1, 3]. Visually examining pistachios categorizes quality and value. Indeed, visual inspection of pistachios is slow and subjective, as it involves human evaluation. Therefore, it is of great commercial importance to

Date: July, 8, 2023.

Key words and phrases. Histogram of oriented gradient, support vector machine, Pistachio species, detection

distinguish these pistachio species with the help of image processing and machine learning (ML) methods. However, selecting features are important when applying ML methods at the classification stage. Features such as texture, morphology, and shape are extracted from the images for the class labels to be distinctive in the feature space. With the help of these features, pistachios are classified as non-destructive.

This study aims to classify a pistachio species by image processing methods. In this study, a classification approach with the support vector machine (SVM) method based on the histogram of oriented gradients (HOG) technique, which has a wide application in the extraction of texture properties in computer vision studies, was proposed. This study was applied to a data set containing Pistachio Image. This study used different cell sizes in the HOG to extract different features from the image. It was performed with varying types of kernel to provide the best decision boundary in the SVM method. This study was evaluated with the 10-fold cross-validation method.

2 LITERATURE SURVEY

In this subsection, research and ideas for classifying the pistachio image data set by type are reviewed. Here, the researchers used classical and state-of-the-art models. Ozkan, Koklu [13] extracted morphological and shape features from pistachio images and classified pistachio species with an approach based on K-Nearest Neighbor (K-NN) and Principal Component Analysis (PCA) models. Pistachios with K-NN and PCA achieved a classification accuracy of 0.9418. In this approach, the data were trained with the 10-fold cross-validation method. It is also the first study applied to a pistachio image species data set. In recent years, researchers have used convolutional neural network (CNN) models as feature extractors. Kumar, Sigappi [9] classified the features obtained from CNN models and ML methods. They achieved 97.20% classification accuracy with Logistic Regression (LR). Başaran [4] proposed classifying pistachio images based on Wavelet Image Scattering and DarkNet53 deep feature as a result of the classification of 1051 features obtained from the proposed approach with SVM resulting in an accuracy of 97.98%.

On the other hand, it can also perform end-to-end estimation of pistachio images with CNN models. Lisda, Kusriani [12] used Inception V3 and ResNet50 from studies that classify pistachio species with CNN models. In their proposed approach, images were trained with 80% training, 10% testing, and 10% validation. The accuracy of the Inception V3 and ResNet50 models were calculated as 96% and 86%, respectively. Singh, Taspinar [17] used CNN models to classify pistachio species and obtained the best accuracy in the VGG16 model. In this proposed approach, they adopted a transfer learning approach while training CNN models. Özaltın, Köklü [14] classified Pistachio Species with their proposed OzNet model and achieved a classification accuracy rate of 0.9576 according to the 10-fold cross-validation method with this model.

As reviewed above, researchers have generally classified pistachio species images with CNN models. Moreover, researchers used CNN models as feature extractors and classified pistachio species

with the help of ML methods. The lack of classical image processing studies applied in this data set was the starting point of this study.

2 MATERIAL AND METHOD

2.1 Images

The Pistachio Image data set was created by Ozkan, Koklu [13]. This data set contains images of Red and Siirt pistachio species. The images in the data set have 600 x 600 pixels and contain 2148 RGB images in total. There are 1232 images in the Kırmızı type and 916 images in the Siirt type [13]. Some sample images in the data set are given in Fig. 1. In Figure 1, the first line shows the Kırmızı type, and the second line shows the Siirt type.

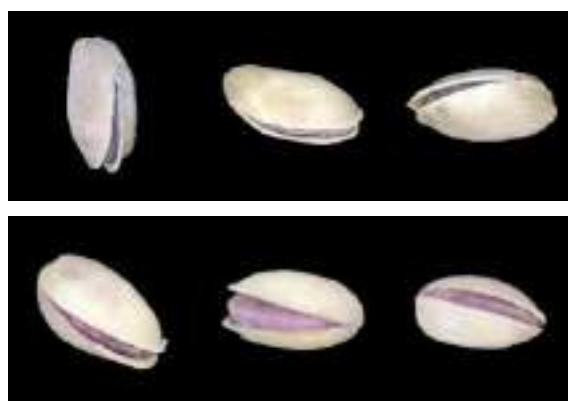


Fig. 1. Sample images in the data set

2.2 HOG

HOG is an image processing technique that is frequently used in image recognition and classification problems. This technique detects the structure and shape of an object. It has advantages such as geometric and light invariance because it uses serial management with a local computation to extract features with the HOG technique [6, 10]. In this technique, images are divided into small cells. A HOG in each cell is then calculated based on the pixels. Here, the division of each cell into angular compartments is related to the direction of the gradient. Adjacent cells are then grouped into blocks. These groups represent the block histogram and the feature descriptor [7, 16].

Example images created with the HOG technique according to different cell sizes are shown in Fig. 2. Reducing cell size increases the HOG's ability to capture small details in the image. However, this also prolongs the image processing process.

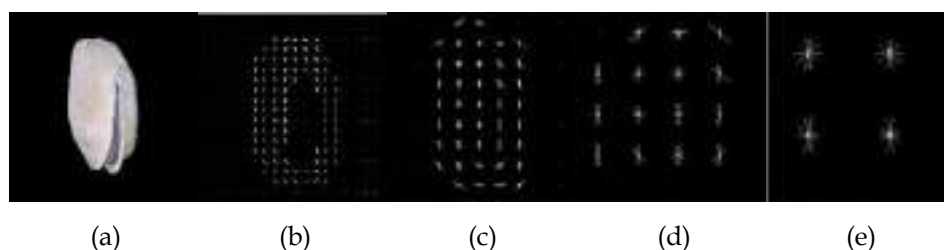


Fig. 2. Representative HOG images of different cell sizes, (a) original, (b) 32 x 32, (c) 64 x 64, (d) 128 x 128, (e) 256 x 256

2.3 SVM

SVM is a binary classification technique that adopts supervised learning and creates a hyperplane in higher-order space. Here, feature transformation is done so the SVM can perform a successful classification operation. It uses various kernel functions for feature transformation. These kernel functions are linear, polynomial, and radial basis function (RBF) [8]. Commonly used kernel functions are shown in Table 1 [2, 19]. With feature transformation, the dimensions of the features are increased significantly. However, this situation also increases the education process [10].

Table 1. Kernel functions

Kernel type	Function
Linear	$K(x_i, x_j) = x_i \cdot x_j$
Polynomial	$K(x_i, x_j) = (\gamma(x_i \cdot x_j) + c)^d$
RBF	$K(x_i, x_j) = \exp(-\gamma x_i - x_j ^2)$

2.4 Proposed approach

Original sizes of RGB images were used in this study. The images were then converted into grayscale. Then, features in different cell sizes were extracted from the HOG technique using the extractHOGFeatures function of MatLab2023a. The cell sizes were 256 x 256, 128 x 128, 64 x 64, and 32 x 32. Using these cell sizes, four data sets of pistachio images were created, and the feature numbers in these data sets are 36, 324, 2304, and 10404, respectively. Using these feature data sets, pistachio species were classified using different kernel types of SVM. This study was evaluated with the 10-fold cross-validation method. Thus, the effects on the classification performance of randomly allocated data were fixed.

Correct matching of features can be achieved by adjusting the parameters of the SVM. The regularization parameter (C) optimizes the model [15]. The C parameter was selected automatically in this study. Figure 3 shows the diagram of the proposed approach. Sensitivity, Specificity, F-score, G-mean, Accuracy, and AUC metrics were used to evaluate the proposed approach models.



Fig. 3. Diagram of the proposed approach

3 EXPERIMENTAL RESULTS

In this study, a computer vision study based on different HOG cell sizes was proposed to extract pistachio species features. Different kernel types of the SVM method were used to classify pistachio species. This study's data sets were classified using the 10-fold cross-validation method. Table 2 lists the average performance results of pistachio species according to cell size and kernel types.

This study obtained better results in the polynomial kernel type than other kernel types. In the type of polynomial kernel type and 128x128 cell size, sensitivity was 0.938, specificity was 0.941, F-score was 0.930, G-mean was 0.939, accuracy was 0.940, and AUC was 0.978.

The high AUC value indicates that it can easily separate the pistachio species. Sensitivity shows the ratio of the Kirmızı species, and specificity shows the ratio of the Siirt species. The high F-score value of the proposed model indicates a good model selection. In this study, the data of the classes are not equal. The high G-mean value of the proposed model indicates that the balance between classification performances between classes is good.

Table 2. Classification performance results of pistachio values

Cell size	SVM kernel type	Sensitivity	Specificity	F-score	G-mean	Accuracy	AUC
256 x 256	Linear	0.807	0.861	0.809	0.833	0.838	0.903
	Polynomial	0.885	0.894	0.873	0.889	0.891	0.946
	RBF	0.834	0.902	0.847	0.867	0.873	0.945
128 x 128	Linear	0.887	0.908	0.882	0.897	0.899	0.965
	Polynomial	0.938	0.941	0.930	0.939	0.940	0.978
	RBF	0.913	0.932	0.912	0.922	0.924	0.978
64 x 64	Linear	0.883	0.909	0.881	0.896	0.899	0.966
	Polynomial	0.925	0.926	0.915	0.925	0.926	0.976
	RBF	0.918	0.901	0.896	0.910	0.909	0.973
32 x 32	Linear	0.888	0.906	0.882	0.897	0.899	0.965
	Polynomial	0.924	0.912	0.905	0.917	0.917	0.975
	RBF	0.909	0.889	0.883	0.898	0.898	0.967

Bold font shows the important scores

Fig. 4 shows the confusion matrix of the experiment, in which the best accuracy result was obtained with a 128 x 128 cell size. Almost all class labels appear to be classified correctly.

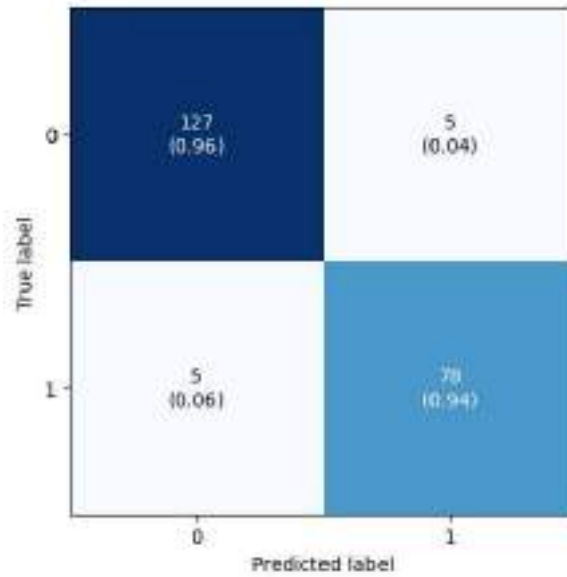


Fig. 4. The confusion matrix, Class 0: Kırmızı species and Class 1: Siirt species

When the proposed approach is compared in terms of accuracy compared to existing systems, the highest accuracy value was obtained in the VGG16 model proposed by Singh, Taspinar [17]. Their proposed study split the data set into 80:20% and had an accuracy value of 98.84%. Lisda, Kusri [12] used known CNN models. They divided the data set into 80% training, 10% testing, and 10% validation and achieved the highest accuracy in the InceptionV3 model. Özeltin, Köklü [14] suggested CNN models and had an accuracy rate of 0.9576. They implemented a proposed model with a 10-fold cross-validation method.

Başaran [4] ve Kumar, Sigappi [9] used CNN models as feature extractors. The accuracy metric obtained from these studies was 97.98% and 97.20%, respectively. It can be said that the classification accuracy is high since the related features of the classes can be extracted more efficiently since the irrelevant features are not taken into account in deep learning. On the other hand, Ozkan, Koklu [13] extracted the morphological and shape features of pistachio images. K-NN and PCA classified the pistachios with an accuracy of 0.9418. The accuracy results obtained for classifying images with different methods may vary. In this proposed approach, the HOG method obtained image features in different cell sizes. Its peanuts are of the Polynomial kernel type of SVM with an average classification accuracy of 0.940.

4 RESULTS

In this study, an approach based on the HOG technique and SVM was proposed for the classification of pistachio species. Here, the HOG features are obtained by dividing the image regions into cells. The HOG measures the gradient direction and strength within the pistachio image region. Features from the HOG technique were obtained according to four cell sizes 256 x 256, 128 x 128, 64 x 64, and 32 x 32. In addition, different kernel types were used for the best separation of classes in SVM.

The experimental results gave varying accuracy in each cell size and kernel type of SVM. The best average accuracy was obtained in the model where the cell size was 128 x 128, and the kernel type was polynomial. The sensitivity was 0.938, specificity was 0.941, F-score was 0.930, G-mean was 0.939, accuracy was 0.940, and AUC was 0.978. Experimental results prove that the proposed approach has significant advantages in assessing pistachio species separation stability.

REFERENCES

- [1] Acar I, Eti S, Nut quality of 'Kirmizi', 'Siirt' and 'Ohadi' pistachio cultivars as affected by different pollinators. *V International Symposium on Pistachios and Almonds* 912, 81-86, (2009).
- [2] Ayhan S, Erdoğan Ş, Destek vektör makineleriyle sınıflandırma problemlerinin çözümü için çekirdek fonksiyonu seçimi. *Eskişehir Osmangazi Üniversitesi İktisadi ve İdari Bilimler Dergisi*, 9 (1): 175-201, (2014)
- [3] Balta F, Phenotypic differences of nut and yield characteristics in siirt pistachios ((*pistacia vera* L.) growth in siirt province. *Journal Of The American Pomological Society*, 56 (1): 50, (2002).
- [4] Başaran E, Image Wavelet Scattering and Densenet Based Pistachio Identification. *Uluslararası Anadolu Ziraat Mühendisliği Bilimleri Dergisi*, 4 (3): 81-87, (2022).
- [5] Bellomo M, Fallico B, Anthocyanins, chlorophylls and xanthophylls in pistachio nuts (*Pistacia vera*) of different geographic origin. *Journal of Food Composition and Analysis*, 20 (3-4): 352-359, (2007).
- [6] Christiansen RH, Hsu J, Gonzalez M, Wood SL, Monocular vehicle distance sensor using HOG and Kalman tracking. *2017 51st Asilomar Conference on Signals, Systems, and Computers*, 178-182, (2017).
- [7] Chu H, Zhang D, Shao Y, Chang Z, Guo Y, Zhang N, Using HOG descriptors and UAV for crop pest monitoring. *2018 Chinese Automation Congress (CAC)*, 1516-1519, (2018).
- [8] Ebrahimzadeh R, Jampour M, Efficient handwritten digit recognition based on histogram of oriented gradients and SVM. *International Journal of Computer Applications*, 104 (9), (2014).
- [9] Kumar SS, Sigappi A, Thomas GAS, Robinson YH, Raja S, Classification and Analysis of Pistachio Species Through Neural Embedding-Based Feature Extraction and Small-Scale Machine Learning Techniques. *International Journal of Image and Graphics*: 2450032, (2023).
- [10] Kusumo BS, Heryana A, Mahendra O, Pardede HF, Machine learning-based for automatic detection of corn-plant diseases using image processing. *2018 International conference on computer, control, informatics and its applications (IC3INA)*, 93-97, (2018).
- [11] Külekçi M, Aksoy A, Gaziantep ili dağ ve ova köylerinde antepfıstığı üretim maliyetlerinin karşılaştırılması. *Uludağ Üniversitesi Ziraat Fakültesi Dergisi*, 25 (1): 41-51, (2011).
- [12] Lisda L, Kusri K, Ariatmanto D, Classification of Pistachio Nut Using Convolutional Neural Network. *Inform: Jurnal Ilmiah Bidang Teknologi Informasi dan Komunikasi*, 8 (1): 71-77, (2023).

[13] Ozkan IA, Koklu M, Saraçoğlu R, Classification of pistachio species using improved k-NN classifier. *Health*, 23: e2021044, (2021).

[14] Özalın Ö, Köklü M, Yonar A, Yeniay Ö, Automatically Image Classification Based on a New CNN Architecture, (2022).

[15] Padmapriya J, Sasilatha T, Deep learning based multi-labelled soil classification and empirical estimation toward sustainable agriculture. *Engineering Applications of Artificial Intelligence*, 119: 105690, (2023).

[16] Pothen ME, Pai ML, Detection of rice leaf diseases using image processing. *2020 Fourth International Conference on Computing Methodologies and Communication (ICCMC)*, 424-430, (2020).

[17] Singh D, Taspınar YS, Kursun R, Cinar I, Koklu M, Ozkan IA, Lee H-N, Classification and analysis of pistachio species with pre-trained deep learning models. *Electronics*, 11 (7): 981, (2022).

[18] Tunalioglu R, Taskaya B, Antepfıstığı Tarımsal Ekonomi Araştırma Enstitüsü. *TEAE Bakış*, 5: 1-4, (2003).

[19] Yu P-S, Chen S-T, Chang I-F, Support vector regression for real-time flood stage forecasting. *Journal of hydrology*, 328 (3-4): 704-716, (2006).

¹ DEPARTMENT OF COMPUTER TECHNOLOGIES, ULUBORLU SELAHATTIN KARASOY VOCATIONAL SCHOOL,
ISPARTA UNIVERSITY OF APPLIED SCIENCES, ISPARTA, TURKEY
E-mail address: birkanbuyukarikan@isparta.edu.tr

A HYBRID DEEP REINFORCEMENT LEARNING ALGORITHM APPLICATION FOR VEHICLE ROUTING PROBLEM

M. ATMIŞ AND T. GÖÇKEN
0000-0003-3873-7545 and 0000-0003-4021-1374

ABSTRACT

Vehicle Routing Problem attempts to determine the optimal routes for a fleet of vehicles to deliver demanded needs to customers, considering the changing requirements and uncertainties in the transportation environment. In this study, developing a hybrid solution algorithm using deep reinforcement learning approaches and metaheuristic algorithms that are suitable for the problem is considered. At first, a constructive heuristic algorithm is used to generate an initial solution. Then, a double deep Q network-based deep reinforcement learning and a simulated annealing algorithm work collaboratively. The computational result shows that the proposed algorithm is promising in routing optimization.

1. INTRODUCTION

Vehicle Routing Problem (VRP) is a heavily studied NP-hard combinatorial optimization problem in the transportation and logistics field of research. The effective management of vehicle routing helps companies reduce operational costs and increases their competitiveness. VRP seeks to identify optimal routes for a fleet of vehicles to deliver goods to customers while simultaneously considering changing requirements and uncertainties in the transportation environment. Due to its combinatorial nature and complexity, conventional optimization approaches may not be practical to solve VRP.

VRP is a notable and highly studied research area that was first introduced in [1]. Many exact, approximate, heuristic, and metaheuristic methods have been proposed for solving VRP and its variants, however, providing fast and reliable solutions is still a challenge. With the development of reinforcement learning, deep neural networks, deep reinforcement learning-based methods, as a kind of heuristic method, have gained attention due to their enormous potential to efficiently generate high-quality solutions. Reinforcement learning (RL) refers to the training of machine-learning (ML) models to make sequential decisions. RL problems involve learning what actions are to be made and how to transform states into actions. The technique is to maximize a numerical reward signal for solving problems [2]. Deep Reinforcement Learning (DRL) enhances classic RL by employing deep neural networks (DNNs) as function approximators, which has been shown to be successful in a variety of control issues.

Date: July, 8, 2023.

Key words and phrases. Deep reinforcement learning, Simulated annealing, Vehicle routing problem, Optimization, Machine learning.

There has been an increase in the use of RL and DRL for VRP and its variants. In [3], the authors presented an end-to-end framework for solving capacitated VRP using RL. In [4], the authors propose a novel RL algorithm called the Multi-Agent Attention Model to solve VRP with soft time windows. They utilized an encoder-decoder framework with attention layers. In [5], the authors proposed a two-stage framework combining the DRL model with a local search method for VRP and VRP with time windows. The output of the DRL is given as the initial solution for the local search method, then the final solution is reached. In [6], the authors tackled heterogeneous capacitated VRP, they proposed a DRL method based on the attention mechanism with a vehicle selection decoder accounting for the heterogeneous fleet constraint and a node selection decoder accounting for the route construction. In [7], the authors proposed a heterogeneous attention mechanism for solving pickup and delivery VRP. In [8], the authors proposed a meta-learning-based DRL approach for multiobjective VRP. In [9], the authors proposed the formulation of a novel DRL framework to solve a dynamic and uncertain VRP. The partial observation Markov decision process is designed to frequently observe the changes in customers' demands in a real-time decision support system.

As far as we have seen from the literature review, RL/DRL and metaheuristic techniques were not used together in the VRP solution. We aim to contribute to vehicle routing optimization by developing a hybrid solution algorithm that combines DRL and Simulated Annealing (SA) algorithms.

2. PROBLEM DESCRIPTION

VRP is the problem of designing the most suitable delivery routes for the vehicles which will serve a group of customers. Each customer has a specified demand. They must be served with exactly one vehicle and in only one visit. The collection center of the products and the dispatching point of the vehicles is called the depot. All the vehicles must start the route from the depot and must return to the depot at the end of the route. There is a limited number of identical vehicles which have the same attributes such as capacity constraints. The total demand of customers delivered on the same route must not exceed the vehicle capacity. VRP with only one constraint, which is the vehicle capacity constraint, is referred to Capacitated Vehicle Routing Problem (CVRP). The objective is to minimize the total distance traveled by vehicles.

3. METHODOLOGY

The proposed approach, DRL-SA, consists of three parts: a constructive algorithm, a Deep Reinforcement Learning (DRL) algorithm, and a metaheuristic, Simulated Annealing (SA). These parts work collaboratively and iteratively to seek (near) optimal solutions.

In the implementation of the algorithm, both DRL and SA benefit from each other's feedback. The DRL starts with an initial state s_0 that is obtained from the Initial Algorithm and runs for a number of time steps and tries to learn which actions to take depending on the current state and passes the best state s_{best} it encounters to SA. The SA then uses s_{best} as its initial solution, runs for several iterations, passes back its best solution s_{best} to DRL, and thus one episode becomes completed. The combined algorithm runs for a number of episodes. As a result, the final s_{best} value and its corresponding total distance are reported as the final solution.

3.1. INITIAL ALGORITHM

To generate the initial feasible solution Sweep algorithm is utilized. The Sweep algorithm was proposed in 1974 [10].

In the Initial Algorithm, the polar angles of the customer nodes are calculated relative to the depot node. The calculated polar angles are ordered in an increasing scheme. Feasible clusters are created by rotating a ray beginning at a random angle and centered at the depot considering vehicle capacity. Then, feasible routes are obtained for each cluster.

3.2. DEEP REINFORCEMENT LEARNING STRATEGY

DRL is the combination of RL and deep learning. The term deep learning implies that an artificial neural network structure with more than one hidden layer is used while performing learning [11].

While designing the RL strategy, state, action, and reward attributes must be defined. The following parts will describe these attributes in detail. Also, the details of the deep learning algorithm are explained in the network structure.

3.2.1. State Space

The state space expresses the routes of all the vehicles in the problem. A one-dimensional array encoding scheme is used to represent the states. All the routes start and finish with the depot. That is, all the routes within the state representation start and end with 0's. Customer nodes are lined up in the order of visits of vehicles on the route.

3.2.2. Action Space

The finite action space A is composed of the following four actions.

- **Action 1:** Swap two random nodes within a random route.
- **Action 2:** Swap two random nodes between two different random routes.
- **Action 3:** Move a random node right next to another random node.
- **Action 4:** Inverse all the elements between two random nodes.
-

3.2.3. Reward Design

The reward value r_{t+1} is defined as the difference between the total distance of the current state $TD(s_t)$, and the total distance of the next state $TD(s_{t+1})$.

3.2.4. Network Structure

Q-Learning is a type of RL algorithm that learns how to associate action-state pairs with Q-values in a tabular environment. A Q-value, $Q(s_t, a_t)$ denotes how good it is to take the action a_t from state s_t . The goal is to maximize its expected discounted return of rewards. Mathematically, $Q(s_t, a_t)$ is defined as in Equation 1.

$$Q(s_t, a_t) = \mathbb{E} \left[\sum_{k=0}^{\tau} \gamma^k r_{t+k+1} \right] \quad (1)$$

where τ is the number of steps to take to reach the goal state from s_t and γ is the discount factor whose value is between [0, 1]. The discount factor indicates the rate of discounting future rewards and determines the present value of future rewards.

Q-learning algorithm iteratively updates the Q-values for each state-action pair using the Bellman optimality equation until the Q-function converges to the optimal Q-function, Q^* , as in Equation 2 [12].

$$Q^*(s_t, a_t) = \mathbb{E} \left[(r_{t+1} + \gamma \max_{a_{t+1} \in A} Q^*(s_{t+1}, a_{t+1}) | s_t, a_t) \right] \quad (2)$$

The equation states that for any state-action pair (s_t, a_t) , the expected return from starting in state s_t , selecting action a_t and following the Q^* -value thereafter will be the expected reward r_{t+1} , plus

the maximum expected discounted return that can be achieved from any possible next state-action pair (s_{t+1}, a_{t+1}) .

A Deep Q-Network (DQN) is a deep neural network that approximates the Q-function. It is first proposed in [13]. DQN accepts states from a given environment as input and then outputs estimated Q-values for each action. The objective of this network is to approximate the optimal Q-function that will satisfy the Bellman equation. This network is called the policy network. The predicted Q-value $Q^*(s_{t+1}, a_{t+1})$ in the Bellman equation is calculated in another network called target network. This type of architecture is called Double Deep Q-Network (DDQN) [11, 14, 15]. The target network is a clone of the policy network. The target network copies the weights from the policy network periodically while the policy network updates its weights at each iteration.

During learning training, the Experience Replay technique is incorporated. After each action is taken, the state, action, reward, and the next state value quadruple $(s_t, a_t, r_{t+1}, s_{t+1})$, called experience is stored. During each episode, both DRL and SA generate their experiences. At each iteration of the policy network to optimize parameters, if there are enough samples, experiences are uniformly sampled and are presented as input to the network.

Mean Squared Error (MSE) is used as the network's loss function. It finds the error between the approximated optimal Q-value, $Q^*(s_t, a_t)$, and the Q-value of the current state-action pair, $Q(s_t, a_t)$. After the loss is calculated, the weights within the network are updated. This process is done repeatedly for each state in the environment until the loss is sufficiently minimized and gets an approximate optimal Q-function.

While selecting an action Epsilon (ϵ)-greedy strategy is used. With this strategy, an exploration rate ϵ is defined and initially set to 1. This exploration rate is the probability that the agent will explore the environment rather than exploit it. As the agent learns more about the environment, ϵ gets decayed exponentially and the agent explores the environment with probability ϵ , and exploits it with probability $1 - \epsilon$. So, after the agent takes an action, it observes the next state and the reward gained from its action.

3.3. SIMULATED ANNEALING

Simulated annealing (SA) is a widely used metaheuristic that enables the search process to escape from a local optimum [16]. SA searches for possible neighborhood solutions allowing a move even if the moved neighbor's result is poorer than the current state. This action deteriorates the quality of the solution and thus expands the search space.

The algorithm starts with an initial feasible solution which is taken from DRL. At each iteration, SA generates a neighborhood solution and determines the objective function value based on this solution. If the resulting solution is better than the current solution, then the new solution is accepted unconditionally. Otherwise, the neighborhood solution is accepted with a probability. The probability of accepting a worse solution is getting smaller as the number of iterations increases. At the end of the iterations, SA forwards the best solution it reaches to DRL.

4. COMPUTATIONAL STUDY

The proposed algorithm is tested on a benchmark problem of CVRP. The data set named A-n32-k5 is available on CVRPLIB. It has 32 nodes, which include 1 depot and 31 customers, and 5 vehicles. Coordinates of all nodes are given, so Euclidean distance can be used to compute the distances. Customer demand quantities and capacity of the vehicles are available in the data set.

The proposed algorithm's code is written using Python programming language and is run on a virtual computer with Intel(R) Xeon(R) Gold 6130 processor technology, 2.1 GHz processor speed, and 8 GB RAM capacity. The appropriate values chosen for the parameters are demonstrated in Table 1.

Table 1. Algorithm parameters.

DRL Parameters	
Parameter Name	Value
Number of episodes	1000
No. of time steps	1000
Discount rate, γ	0.999
Exploration rate, ϵ	[0.01, 1]
Epsilon decay rate	0,001
Batch size	32
Memory size, K	100000
Learning rate, α	0,001
Target network update	10
No. of hidden layers	2
No. of output units	4
SA Parameters	
Parameter Name	Value
Initial temperature	100000
No. of iterations	1000
Temperature decay rate	0,9

The proposed algorithm reached the optimum solution with 5 vehicles and 784 units total distance in about 35 minutes. The graph of the initial solution (with 1331 units total distance) and optimum solution is given in Figure 1.

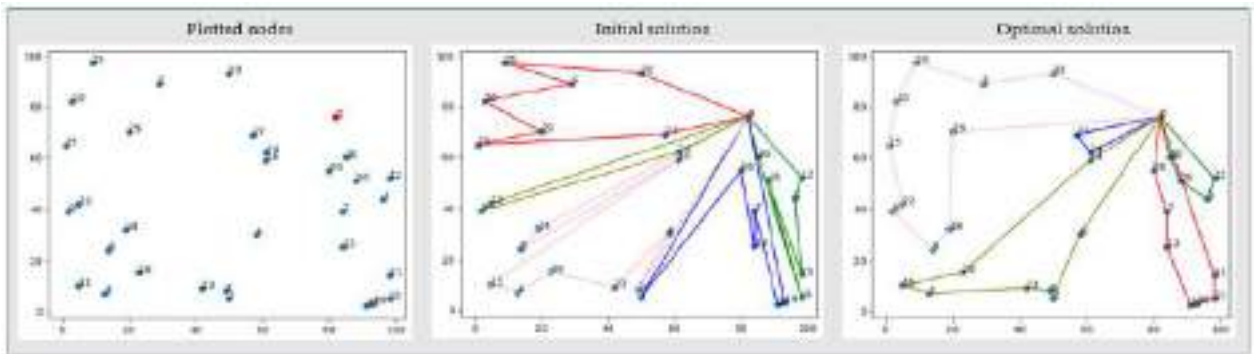


Figure 1. Routes of A-n32-k5.

5. CONCLUSIONS

In this study, we couple a Double Deep Q-Network-based DRL and an SA algorithm. In this coupling, different from the traditional SA algorithms where neighborhood structures are selected only randomly, DRL learns to choose the best neighborhood structure based on experience gained from previous episodes and delivers the selected neighborhood structure to SA to use in future iterations.

The computational result shows that the proposed solution algorithm is promising in solving the defined problem. It reveals that there exists a great potential in the application of machine learning

to routing optimization. Machine learning-enforced optimization algorithms may provide relatively better solutions.

In future work, we are working on implementing the proposed algorithm on bigger data sets. We will try to solve a different variant of VRP. Furthermore, parameter tuning can improve the efficiency of the algorithm. The effect of other metaheuristics that adopt sequential structures instead of SA will be investigated.

REFERENCES

- [1] G. B. Dantzig, J. H. Ramser, The truck dispatching problem, *Management science*, 6(1), 80-91, (1959).
- [2] R. S. Sutton, A. G. Bartow, *Reinforcement Learning: An Introduction*, MIT Press, Second Edition, (2020).
- [3] M. Nazari, A. Oroojlooy, L. Snyder, M. Takác, Reinforcement learning for solving the vehicle routing problem, *Advances in neural information processing systems*, 31, (2018).
- [4] K. Zhang, F. He, Z. Zhang, X. Lin, M. Li, Multi-vehicle routing problems with soft time windows: A multi-agent reinforcement learning approach, *Transportation Research Part C: Emerging Technologies*, 121, 102861, (2020).
- [5] J. Zhao, M. Mao, X. Zhao, J. Zou, A hybrid of deep reinforcement learning and local search for the vehicle routing problems, *IEEE Transactions on Intelligent Transportation Systems*, 22(11), 7208-7218, (2020).
- [6] J. Li, Y. Ma, R. Gao, Z. Cao, A. Lim, W. Song, J. Zhang, Deep reinforcement learning for solving the heterogeneous capacitated vehicle routing problem, *IEEE Transactions on Cybernetics*, 52(12), 13572-13585, (2021).
- [7] J. Li, L. Xin, Z. Cao, A. Lim, W. Song, J. Zhang, Heterogeneous attentions for solving pickup and delivery problem via deep reinforcement learning, *IEEE Transactions on Intelligent Transportation Systems*, 23(3), 2306-2315, (2021).
- [8] Z. Zhang, Z. Wu, H. Zhang, J. Wang, Meta-Learning-Based Deep Reinforcement Learning for Multiobjective Optimization Problems, *IEEE Transactions on Neural Networks and Learning Systems*, (2022).
- [9] W. Pan, S. Q. Liu, Deep reinforcement learning for the dynamic and uncertain vehicle routing problem, *Applied Intelligence*, 1-18, (2022).
- [10] B. E. Gillett, L. R. Miller, A heuristic algorithm for the vehicle-dispatch problem, *Operations research*, 22(2), 340-349, (1974).
- [11] F. Kosanoglu, M. Atmis, H. H. Turan, A deep reinforcement learning assisted simulated annealing algorithm for a maintenance planning problem, *Annals of Operations Research*, 1-32, (2022).
- [12] C. J. C. H. Watkins, P. Dayan, Q-learning. *Machine Learning*, 8, 279-292, (1992). <https://doi.org/10.1007/BF00992698>
- [13] V. Mnih, K. Kavukcuoglu, D. Silver, A. Graves, I. Antonoglou, D. Wierstra, M. Riedmiller, Playing Atari with deep reinforcement learning, *arXiv:1312.5602*, (2013).
- [14] H. van Hasselt, A. Guez, D. Silver, Deep reinforcement learning with double Q-learning, *Proceedings of the AAAI conference on artificial intelligence*, Vol. 30, No. 1, (2016).
- [15] J. Huang, Q. Chang, J. Arinez, Deep reinforcement learning based preventive maintenance policy for serial production lines, *Expert Systems with Applications*, 160, 113701, (2020).
- [16] S. Kirkpatrick, C. D. Gelatt, M. P. Vecchi, Optimization by simulated annealing, *Science*, 220, 671-680, (1983).

DEPARTMENT OF INDUSTRIAL ENGINEERING, ADANA ALPARSLAN TÜRKES SCIENCE AND TECHNOLOGY UNIVERSITY, ADANA, TURKEY.
Email address: myaktubay@atu.edu.tr

DEPARTMENT OF INDUSTRIAL ENGINEERING, ADANA ALPARSLAN TÜRKES SCIENCE AND TECHNOLOGY UNIVERSITY, ADANA, TURKEY.
Email address: tgoeken@atu.edu.tr

IFSCOM-E 2023
9TH IFS AND CONTEMPORARY MATHEMATICS AND ENGINEERING CONFERENCE
8-11 JULY 2023, TARSUS, MERSİN, TÜRKİYE
ISBN: 978-605-68670-8-8
pp: 153-159

FAULTS AND SUGGESTIONS DETECTED IN DISTRIBUTION PANEL AND TRANSFORMERS IN POWER PLANTS

HALE BAKIR*

0000-0001-5580-0505

ABSTRACT

The demand for the widespread use of solar power plants in Turkey with full efficiency is increasing day by day. Panel failures, transformer failures, such as panel failures, are among the failures that affect the efficiency. Maintenance and thermal imaging are often required if full efficiency in power generation from a solar power plant is desired. Thermal imaging methods are both fast and highly accurate in detecting faults. In this study, faults in distribution panels and transformers were detected in a power plant with thermal imaging technique and solution suggestions were presented.

INTRODUCTION

In order for the facilities not to experience instant stops and disruptions due to unexpected failures, each facility should be regularly maintained. At the beginning of these maintenance applications, maintenance works with a thermal camera are the main ones. All equipment that consumes or transmits power heats up and emits infrared energy (heat) before it fails. Thermal cameras, which are non-contact measurement devices, detect this invisible infrared energy emitted by objects and convert it into an electronic signal, and then display it as a thermal image on the camera screen.

Thermal cameras allow us to clearly see small problems that we cannot see with our eyes but can cause very serious problems. In addition, we think that some problems that we see with the eyes are not very urgent, but thermal cameras can also show us that the seriousness of the situation is high by giving us much deeper information. Industrial facilities that operate 24 hours a day, every day of the year, must be in continuous operation. In these non-stop working conditions, thermal cameras will be the best helper for power plant users. These devices, which produce results quickly, are much better, much more efficient and much cheaper, will also provide a much faster solution to the problems to be encountered.

Date: July, 8, 2023.

Key words and phrases. Thermal imaging, efficiency, transformer failures, panel failure

A challenging problem in the protection of power transformers is the fault detection and diagnosis (FDD). FDD has an essential role in the reliability and safety of modern power systems; thus, it has been recently the center of attention in both industrial and academic studies. Due to unpredictable nature of fault, it should be located and isolated fast so that its impact on transformers is minimized [1]. Some studies present methodologies for beginner fault detection in offline and online Power transformers. They are used to detect incipient faults and also to distinguish between incipient fault and short circuit fault [2]. A fault monitoring system is needed for practical remote control to identify faults and reduce their effects, thereby reducing economic losses. An effective fault monitoring system is useful for increasing the reliability of a protection system when faults develop [3]. Detection of these faults with thermal cameras provides fast and time saving [4].

Sometimes a small electrical problem can cause major fires. A cable with an undetected excess current may heat up and burn the cables. This can cause large fires. It should not be forgotten that about 35% of industrial fires are caused by electrical fires. This means a loss of approximately 300 billion Euros every year. In this study, the problems and solutions seen in transformers and panels in a solar power plant are presented with thermal imaging method.

MATERIAL AND METHOD

Thermal imaging

All objects have a certain heat and radiate that heat. An infrared camera (called a thermal imager) detects and measures the invisible infrared energy of objects. Unlike normal cameras, the thermal camera has a detector chip (sensor array) arranged to measure infrared energy into microblocks. These chipset blocks, designed differently from normal cameras, contain thousands of detectors. These detectors detect invisible infrared energy and generate an electronic signal. The special chipset in the camera processes the signals it receives from the pixels thanks to the algorithm in it and creates the heat map. Each temperature value is represented by a different color. The color characteristic resulting from this process is reflected on the camera screen as the temperature picture (thermal image) of the objects so that the error can be seen. Thanks to this technology, it combines the normal camera image with the infrared thermal image by pixel-by-pixel alignment. Contrast adjustment is made to see the heat more clearly in the thermal image. If the heating is high, it is detected that there is a fire, explosion or a malfunction due to overheating in the light yellow areas, if the heating is not high, it is purple and the system is operating normally [4].

Substation and distribution panels of solar power plant

In the study, fault or error detection was made by thermal heating in transformers and panels in the 6 MW Elmadağ power plant in Elmadağ, Ankara, which is shown in Figure 1. The thermal camera used in the plant is the latest generation DJI mavic brand. Thermal images were taken by DJI toolbox and temperature values were determined [5].



Fig. 1 Solar power plant

RESULTS AND DISCUSSION

Images taken from DJI toolbox as a result of thermal imaging are given in Figure 2-5. When the measurements were made by determining the temperature range of 20.7 minimum 52.1 max in Figure 2, 40.5 °C was detected in the bushing and it was determined that there was an oil leak at that point and it was confirmed by going to the power plant. In Figure 3 (a)-(b), overheating and 47.8 °C melting were detected at the connection poles of some thermal magnetic switches (tms). In Figure 4, 37.0 °C heating was detected at the connection points of the Main Distribution Panel (MDP). In Figure 5, it has been determined that 55.1°C current transformers are overheated and their bodies are cracked. Table 4 gives the order of importance according to temperature differences.

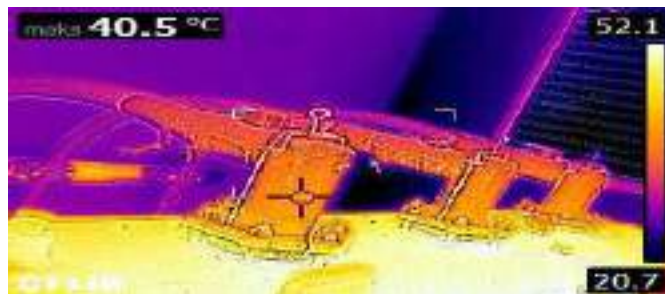
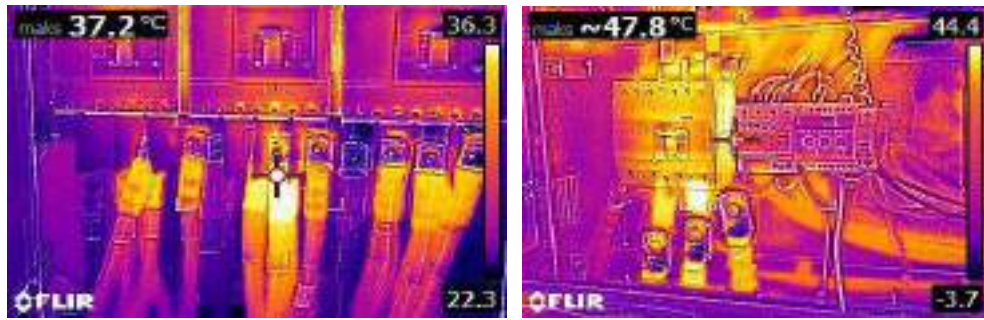


Fig. 2 Oil leak detected on bushing



(a)

(b)

Fig. 3 Overheating images of the connection poles of the thermal magnetic switches

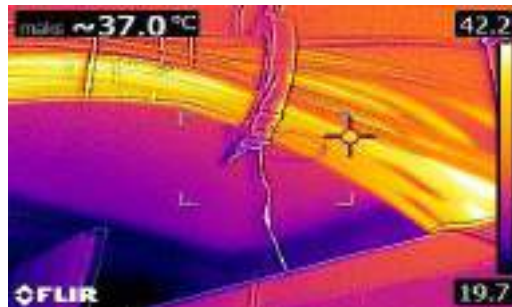


Fig. 4. Heating detection in MDP



Fig 5. Image of current transformers overheating and their bodies cracking

Table 4 Order of importance (By temperature differences)

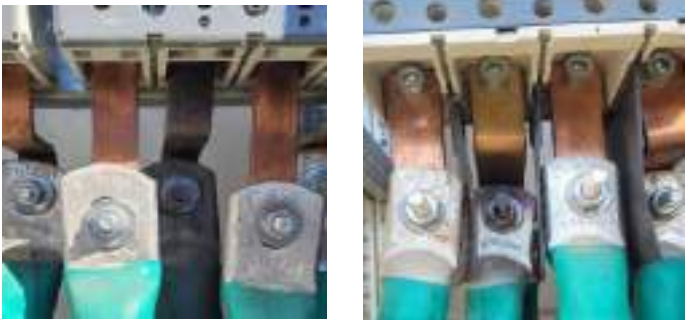
Normal	Should be examined	Should be repaired	Emergency response
<1.0 °C	1.0 -4.0 °C	4.0-15.0 °C	>15.0 °C

All distribution transformers have been inspected, overheating and gas formation have not been observed. There are some oil leaks in the bushings of the transformers shown in Figure 6. It has been determined that some of the bushing coatings are absent.



Fig. 6 Real image of bushings in transformers

As a result of the thermal examinations made in the field of the thermal magnetic switches (tms), the real image of which is given in Figure 7, some connection poles have overheated and melted. These connecting busbars should be insulated by tightness checks and replacement of busbars. In Main distribution panel (MDP), heating has generally been observed at the connection points, these warmings should be measured and marked with tightness control and torque wrench in the field. In addition, it was observed that general cleaning of MDPs was not done.



(a) (b)

Fig. 7 Thermal magnetic switch busbars

In Figure 8, it is seen that the current transformers in some MDPs are overheated and their bodies are cracked, they need to be changed in order to avoid situations such as explosion and fire.



Fig. 8 Current transformer image

Finally, it has been observed that general cleaning is not done in alternative current (AC) distribution boards, however, some switches have come off and overheating has occurred. Ges energy quality recorder (EQR) is faulty, it needs to be replaced.



Fig. 9 . Energy quality recorder (EQR)

CONCLUSION

In this study, faults in transformer and panels in a 6 MW power plant located in Ankara Elmadağ were determined. With the thermal camera, errors such as overheating and oil leakage were detected quickly. By detecting these faults in place and appropriately, the operation of the power plants at full efficiency and most importantly, the elements such as fire and explosion have been prevented. Today, fault detection continues in many places with thermal imaging method and continues to be preferred by switchboard users.

REFERENCES

- [1] A. R. Abbasi, Fault detection and diagnosis in power transformers: a comprehensive review and classification of publications and methods, *Electric Power Systems Research*, 209, 2022, 107990, <https://doi.org/10.1016/j.epsr.2022.107990>.
- [2] N. Yadaiah and N. Ravi, Fault Detection Techniques for Power Transformers, *IEEE/IAS Industrial & Commercial Power Systems Technical Conference*, Edmonton, AB, Canada, 2007, 1-9. <https://doi.org/10.1109/ICPS.2007.4292099>.
- [3] S.H. Asman, N.F. Ab Aziz, U.A. Ungku Amirulddin, M.Z.A. Ab Kadir, Transient Fault Detection and Location in Power Distribution Network: A Review of Current Practices and Challenges in Malaysia. *Energies*, 14, 2021, 2988. <https://doi.org/10.3390/en14112988>
- [4] H. Bakır, Detection of Faults in Photovoltaic Modules of SPPS in Turkey; Infrared Thermographic Diagnosis and Recommendations. *J. Electr. Eng. Technol.* 18, 2023, 1945–1957. <https://doi.org/10.1007/s42835-022-01245-6>
- [5] H. Bakır, A. Merabet, Evaluation and Solution Suggestions for Engineering and Workmanship Failures during Design and Installation of Solar Power Plants. *Energies*, 16(3), 2023, 1457. <https://doi.org/10.3390/en16031457>

DEPARTMENT OF ELECTRONICS AND AUTOMATION, SİVAS CUMHURİYET UNIVERSITY, SİVAS, TURKEY
E-mail address: halebakir@cumhuriyet.edu.tr

IFSCOM-E 2023
9TH IFS AND CONTEMPORARY MATHEMATICS AND ENGINEERING CONFERENCE
8-11 JULY 2023, TARSUS, MERSİN, TÜRKİYE
ISBN: 978-605-68670-8-8
pp: 160-169

MEASUREMENTS AND EVALUATION OF ELECTRIC FIELD EXPOSURE GENERATED BY MODEM IN HOME ENVIRONMENT

MUSTAFA MUTLU

0000-0001-6756-066

ABSTRACT

In the home environment, we have the opportunity to access the Internet, both with computers and mobile phones, thanks to the possibilities offered by the modem. Therefore, in this study, Spectran HF-60105 device was used to determine the electromagnetic field exposure values due to these modems and to find out where these values correspond to the limit values determined by the competent committees. The device is set to save 4236 power values in its memory in a 24-hour period. The Omnilog 90200 antenna (probe), which is in the working band (750-2500MHz), is attached to the device, especially when measuring the electromagnetic field values originating from GSM. The recorded power values were converted into electric field values and the variation of both power and electric field with the number of measurements was plotted using MATLAB. The curve that gives the smallest error in the MATLAB environment was fitted to the change of the electric field values, and the two of them were plotted on the same plane depending on the number of measurements, and the equation, coefficients and statistical values of the curve were obtained. In addition, the intensity and cumulative functions of the electric field values are plotted. The electric field values recorded during the measurement are 61 V/m 25 times the limit value determined by the International Commission on Non-Ionizing Radiation Protection (ICNIRP) for an environment, and 45.75 V/m determined by the Information and Communications Technologies Authority (ICTA), the limit value has been exceeded 66 times.

Date: July, 8, 2023.

Key words and phrases. Icnirp, Icta, Spectran HF 60105, Modem, Omnilog 90200

1. INTRODUCTION

It is a known fact that technology negatively affects our lives at the end of the rapid development of technology and the race in which societies use technology. The presence of electronic devices in all areas we live in causes us to be exposed to electromagnetic fields, some of which are 50 Hz sourced and some of which are GSM sourced. It is known that the energies of electromagnetic signals increase with frequency, so the harm they cause to humans grows in parallel with this. Every device we use in our house negatively affects our health proportional to the frequency it works with. In this study, it is aimed to determine the electromagnetic field that we are exposed to in environments where there are modems that allow us to connect to the internet via wi-fi in the home environment and to evaluate these values in terms of health. Knowing the value of electromagnetic exposure, both network-based and GSM (Global System for Mobile Communications), in the environments where people live, provides psychological relief. Below are some of the studies in which exposure measurements were made in a particular area.

Necessary recommendations have been made in order to create an environment where the measurements of electric fields in a school environment and in an open area are made and by evaluating these measurements, people in this environment can be less affected [1-6]. 6-minute GSM and network-based electric field values were measured at 32 points between 10:00 and 15:00 on weekdays in the Cumhuriyet campus of Ordu University. Then, the variation of these values with measurement, density and cumulative curves were plotted in MATLAB environment and all statistical values were extracted and the locations of the points exceeding the limit value were extracted [7]. Electric and magnetic field exposure limits to which people living in their living spaces are exposed in Turkey have been determined. There are studies conducted in parallel with the rumor that it triggers leukemia in children. The effects of domestic exposure, particularly in infants, on the health of these children have been investigated [8]. They measured the electromagnetic field values originating from transformers and high voltage lines in public areas in Konya and compared the field values with the limit values [9]. The average of the effective value of the electric field was measured for each point by using the electric field probe of the measuring instrument at 49 points where there is no direct view, provided that it remains within the scope of the base station named Ormeh on Mehmetçik Boulevard in Ordu Merkez Bahçelievler District, and the variation of the average depending on the distance from the base station antenna was calculated. [10]. The electric field effective value of the base station was measured at 500 points in the city center of Ordu, and the electric field map was drawn and modeled with 24-hour measurements made from the nearest places where the base stations are located, across the base stations [11]. He made and demonstrated various measurements to show the high frequency electromagnetic pollution on the digital map [12]. In the electromagnetic field measurements made between 12:00-17:59 at 152 points in the city center of Samsun in april, may and september, it was noted that all

measurement values were below the limit values determined by the authorized institutions [13]. ICNIRP, of which Turkey is a member, and ICTA in Turkey determine the public and occupational exposure limit values for both low frequency and GSM for inhabited areas. These values are shown in Table 1 [14].

Frequency range (MHz)	Electric Field (V/m)	
	ICNIRP	ICTA
0.010-0.15	87	65.25
0.15-1	87	65.25
1-10	$87/f^{0.5}$	$65.25/f^{0.5}$
10-400	28	21
400-2000	$1.375/f^{0.5}$	$1.03/f^{0.5}$
2000-60000	61	45.75

TABLE 1. Electric field limit values determined by ICNIRP and ICTA for humans

2. MATERIAL AND METHOD

In this study, it is aimed to measure, record and interpret the power exposure values around a modem in a house for a day. In order to measure these power values, Spectran HF-60105 and Omnilog 90200 antenna (probe) with working band (750-2500 MHz) are attached to this device. The device is set to record 4236 power data in dBm for 24 hours. In Table 2, the characteristics of the Spectran HF-60105 device used for the measurement are given.

	Spectran HF-60105 Electric and Magnetic Field Meter
Frequency range	1 MHz- 9.4 GHz
RBW(Resolution bandwidth)	200 Hz-50 MHz
Units	dBm, dB μ V, V/m, A/m, W/m ²
Introduction	50 Ohm SMA RF-input (f)
Demodulator	AM. FM. PM. GSM
Accuracy (typical)	+/- 1 dBi (typ.)
Interface	USB 2.0/1.1
Measuring range	-155dBm+20dBm

TABLE 2. Technical characteristics of the measuring device

Figure 1 shows the measuring device at the entrance of the house where the modem is located and the positioning of the measuring instrument.



FIGURE 1. Measuring device and measuring instrument

After the measurement was completed, the data in the memory of the measuring instrument were taken for evaluation.

3. RESEARCH FINDINGS AND DISCUSSION

In this study, after the power values in the environment where the modem is located, these power values are converted into electric field values. Statistical information of measured power and converted electric field values are given in Table 3. Table 3 shows that the electric field variation varies between 3.699 V/m and 75.974 V/m, the average value is 38.06 V/m and the standard deviation is 13.637 V/m.

	E (V/m)	Pr (dBm)
Minimum value	3.699	-44.4
Maximum value	75.974	-18.15
Average value	38.06	-36.891
Standard deviation	13.637	7.813

TABLE 3. Statistical values of measured power and converted electric field values

Figure 2 shows the variation of the power values in the environment where the modem is located, with the number of measurements. Looking at Figure 2, it is seen that the highest power value is -18.15 dBm, and when we convert this to mWatt, it is 0.01531mW, and the smallest value is -44.4 dBm, 0.0000363 mW.

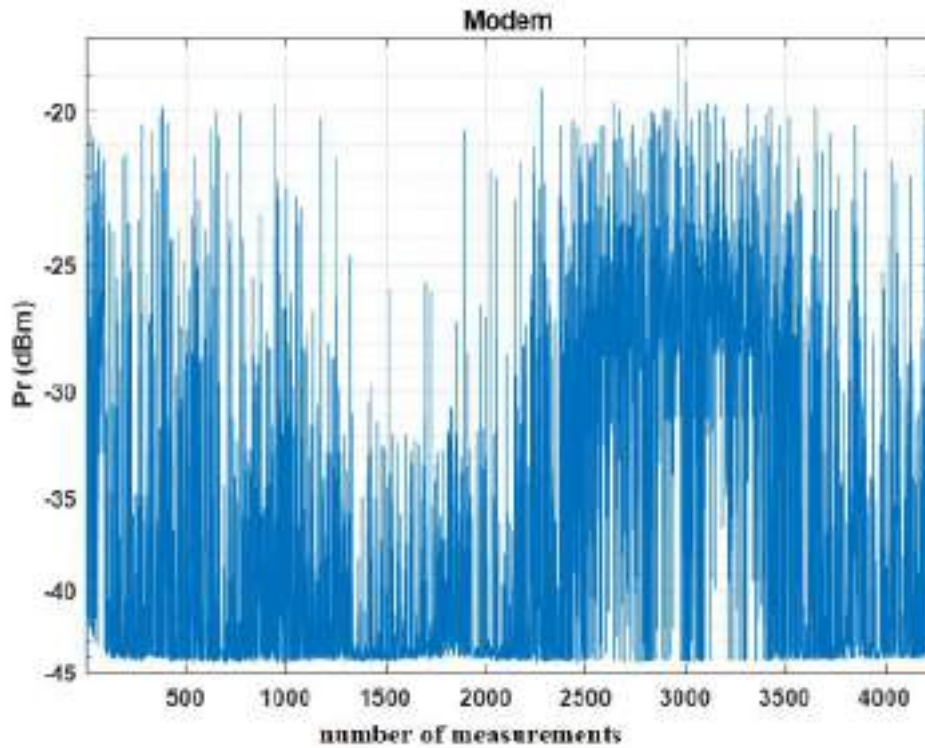


FIGURE 2. Variation of power depending on the number of measurements

In Figure 3, the number of measurements of the electric field effective values and the variation of the eighth order polynomial fitted to these field values are shown.

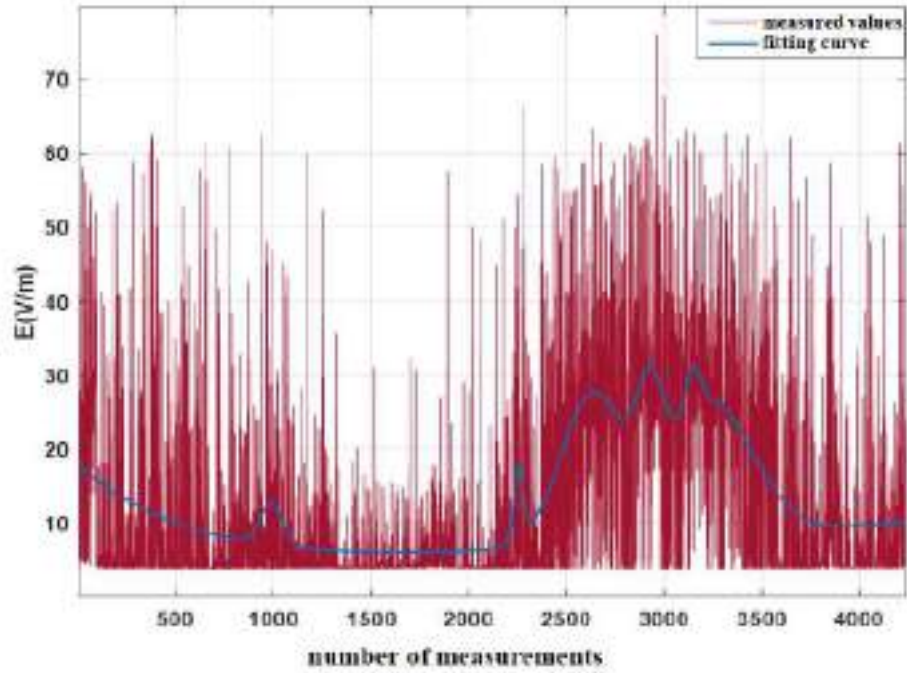


FIGURE 3. The measured electric field values and the change of the curve adapted to these values depending on the number of measurements

The equation, coefficients and some statistical values of the curve fitted to the measured electric field values are given in the table 4. Curve fitting multiple curves and polynomial degrees were tried in MATLAB, and as a result, the curve of the function with the lowest R-square value was decided.

Modem											
$f(x)=a_1\exp(-((x-b_1)/c_1)^2)+a_2\exp(-((x-b_2)/c_2)^2)+a_3\exp(-((x-b_3)/c_3)^2)+a_4\exp(-((x-b_4)/c_4)^2)+a_5\exp(-((x-b_5)/c_5)^2)+a_6\exp(-((x-b_6)/c_6)^2)+a_7\exp(-((x-b_7)/c_7)^2)+a_8\exp(-((x-b_8)/c_8)^2)$ (General model Gauss8) (Coefficients (with 95% confidence bounds))											
a₁	12.43	b₂	2254	c₃	229	a₅	5.692	b₆	- 3.191e ⁺⁰⁴	c₇	317.7
b₁	2924	c₂	37.37	a₄	5.74	b₅	988.9	c₆	6109	a₈	52.39
c₁	93.01	a₃	19.95	b₄	3148	c₅	80	a₇	18.57	b₈	1.849e ⁺⁰⁴
a₂	9.953	b₃	2630	c₄	49.36	a₆	1.033e ⁺¹³	b₇	3223	c₈	1.113e ⁺⁰⁴
SSE			5.422e ⁺⁰⁵								
R-square			0.3118								
Adjusted R-square			0.308								
RMSE			11.35								

TABLE 4. The coefficients of the polynomial fitted to the electric field measurement values, SSE (the sum of squared estimate of errors), Regression coefficient and RMSE (Root Mean Square Error) value are given

In Figure 4, the variation of the electric field values and the probability values of these values are shown. Considering the 4236 electric field values recorded in the measurement made from this graph, it is seen that

these values vary between 3.699-75.974 V/m. Again, it is seen from the graph that the electric field (average value) value with the highest probability is 4 V/m and the probability of level is 0.16666 (16.666%).

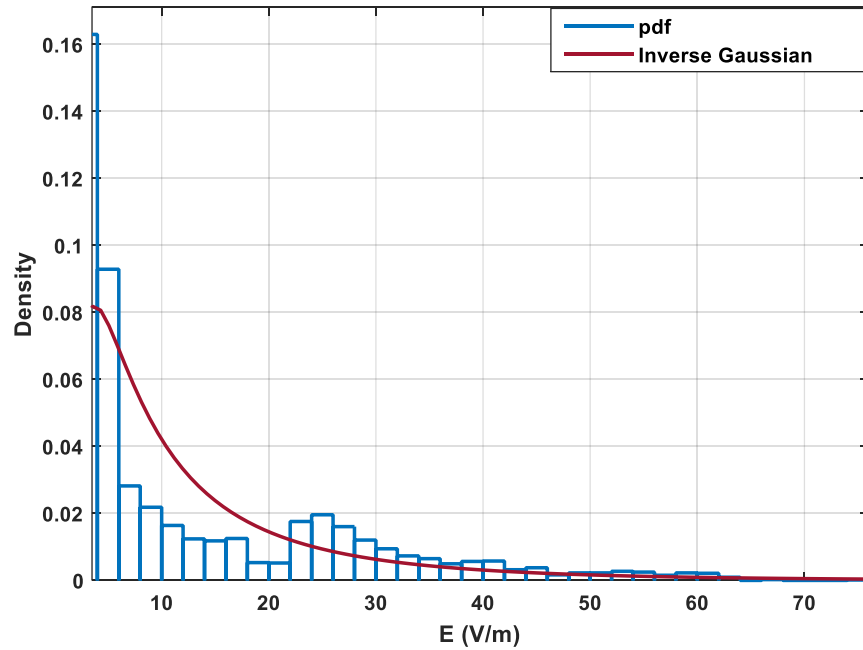


FIGURE 4. Electric field levels and variation of the probabilities of these levels

Figure 5 shows the performances of the electric field values.

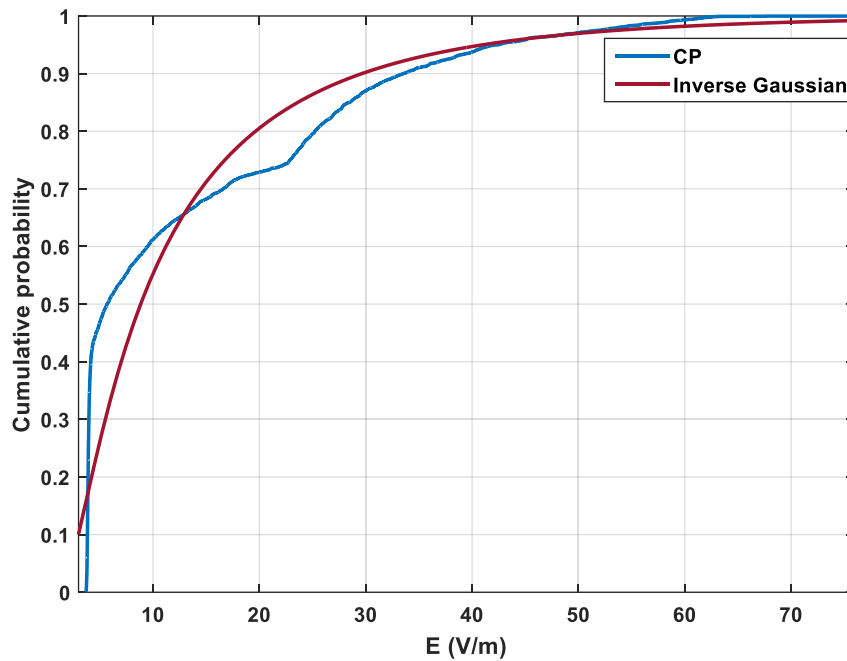


FIGURE 5. Measured electric field levels and the cumulative probability change of these levels

4. CONCLUSION

With the rapid change in technology and this trend, there will be sources that create electromagnetic fields in the areas we live, which will become a much bigger problem in the future. To measure the intensity of the electromagnetic field in the home environment, where there are modems that allow us to access the internet via Wi-fi, which is one of these sources, and to find out where these values correspond to the limit values determined by the competent institutions for these field values, to make arrangements and recommendations in a way that will not cause any health problems if these values are exceeded, will provide mental relaxation for people living in this environment. For this purpose, Spectran HF-60105 device to measure the power values in dBm at the entrance of the house where the modem is located, and the Omnilog 90200 antenna whose working band overlaps with the Modem's working band (750-2500 MHz) and which we generally use for GSM sourced electric field measurements. The power measurement was made by attaching the device to the device. The device is set to save 4236 power data in its memory in a 24-hour period. As a result of the measurement, the power data obtained from the device were converted into electric field values. The curve that best fits the electric field values (giving the lowest R-square value) was fitted. The variation of this electric field and the curve adapted to it with the number of measurements was plotted in the MATLAB environment. At the same time, statistical values of the fitted curve, power and electric field values were extracted. The change function and coefficients of the curve are given in the table.

It is seen that the electric field effective value varies between 3.699 V/m-75.974 V/m, its average is 38.06 V/m and its standard deviation is 13.637 V/m. In addition, electric field values and probability density and cumulative functions of these values are plotted in MATLAB. Looking at the density function, it is seen that the highest rate is 0.16666 (16.666%) with 4 V/m (mean value). ICNIRP is the institution that determines the electric field limit values all over the world, and ICTA is the authorized institution in Turkey. It is known that the total electric field (from GSM) limit value in an area is 61 V/m for ICNIRP and 45.75 V/m for ICTA. Of the 4236 electric field effective values measured, 25 of them are between 61 V/m 75.974 V/m, 66 of them are between 45-75.974, and in short, the limit value of ICNIRP in the measurement made is 25 times, the limit value determined by ICTA is 66 times, and the maximum value in this measurement (75.974 V/m), the limit value of ICNIRP is 124.54% and the limit value of ICTA is 166.06%. Considering that the power around the Modem will increase with the number of devices to be connected to it, it turns out that the Modem is not an innocent device at all. For this reason, keeping the modem away from bedrooms or environments where children are present is the simplest of the measures that can be taken. The most rational method is to use a cable modem, but unfortunately, it is no longer used due to the disadvantage that cable modem has a cable between the device and the modem, these connection cables are a shoestring and cause visual pollution. This study will shed light on the work to be done in this field and has shown that wireless modems are an electromagnetic field source that cannot be underestimated.

REFERENCES

- [1] G. Sarmaşık, R. Durusoy, A. Özkurt, Damages of electromagnetic fields we are exposed to in computer laboratories and solutions, XIV. Academic informatics conference papers 1-3 February Uşak University, (2012).
- [2] B. Korunur Engiz, Ç. Kurnaz, Measurement and evaluation of electric field strength in Samsun city center, International journal of applied mathematics, Electronics and computer, (2016).
- [3] B. K. Gül, Ç. Kurnaz, B. Korunur Engiz, Measurement and evaluation of electromagnetic pollution in Ondokuz mayıs university Kurupelit campus in Samsun, International journal of advances in electronics engineering, (2016).
- [4] Ç. Kurnaz, An Empirical modeling of electromagnetic pollution on a university campus (First Press), ACES Express journal, (2016).
- [5] B. Korunur Engiz, Ç. Kurnaz, Long term electromagnetic field measurement and assessment for a shopping mall, Radiation protection dosimetry, (2017).
- [6] Ç. Kurnaz, B. Korunur Engiz, U. Köse, An empirical study: the impact of the number of users on electric field strength of wireless communications, Radiation protection dosimetry, (2018).
- [7] M. Mutlu, M. Kara, Low and high frequency exposure electric field measurement in Ordu university main campus, 2nd International technological sciences and design symposium 2-5 June, Giresun/TURKIYE, (2022).
- [8] B.Y. Atikan, M.D. Bilgin, S. Akşit, Domestic electromagnetic field exposure in infants living in a city center in Turkey, Balıkesir Me2.130. October, (2018).
- [9] L. Seyfi, B. Akbal, Evaluation of magnetic field measurements made near some high voltage line and transformer buildings in Konya, 2nd International symposium on innovative approaches in scientific studies november 30-december 2, Samsun, Turkey, (2018).
- [10] M. Mutlu, Ç. Kurnaz, Evaluation of the electromagnetic field levels in Ordu city center for the selected base stations' coverage areas, 1.International technological design symposium. 27-29 june, page:657-665, Giresun/Turkey, (2018).

[11] Ç. Kurnaz, M. Mutlu, Comprehensive radiofrequency electromagnetic field measurements and assessments: a city center example, *Environ monit assess* 192. 334. <https://doi.org/10.1007/s10661-020-08312-3>, (2020).

[12] M. Cansız, Making a map of electromagnetic pollution with the Drive test method and evaluating the measurement results, *Diyarbakır*, (2012).

[13] B. Korunur Engiz, Electric field levels and evaluation in terms of public health: Samsun city center example, *Turkish journal of public health*,16 (2) 146, research paper (2018).

[14] International commission on non-ionizing radiation protection, exposure to static and low frequency electromagnetic fields, Biological effects and health consequences (0 Hz-100 kHz), International commission on non-ionizing radiation protection, Munich, Germany, 13, (2003).

ORDU UNIVERSITY VOCATIONAL SCHOOL OF TECHNICAL SCIENCES

Email address: mustafamutlu1071@gmail.com/mustafamutlu@odu.edu.tr/rhetoric_68@hotmail.com

IFSCOM-E 2023

9TH IFS AND CONTEMPORARY MATHEMATICS AND ENGINEERING CONFERENCE

8-11 JULY 2023, TARSUS, MERSİN, TÜRKİYE

ISBN: 978-605-68670-8-8

pp: 170-177

ELIMINATION OF ACTUATION SINGULARITIES OF KINEMATICALLY REDUNDANT RPR-RPRR PLANAR PARALLEL ROBOTS

MUSTAFA ÖZDEMİR and MUHAMMED YASİR ÇUBUK

0000-0002-4981-9573 and 0009-0007-4480-9118

ABSTRACT

Parallel robots are used in a wide range of applications in industry and medicine. This wide range of applications is due to their many advantages, such as high accuracy, high rigidity, and high load capacity. On the other hand, parallel robots have a complicated singularity problem as their main drawback. The most critical singularities are Type II or actuation singularities. This paper studies the elimination of actuation singularities of kinematically redundant RPR-RPRR planar parallel robots.

1. INTRODUCTION

Parallel robots are suitable for a wide range of applications because they offer significant advantages such as outstanding accuracy, remarkable rigidity, and high payload capacity [1]. On the other hand, parallel robots have one major disadvantage: they have different types of singularities.

In [2], three types of parallel robot singularities were defined based on the vanishing of the determinants of two Jacobian matrices. These are referred to as Type I (arising in the inverse kinematics solution), Type II (arising in the forward kinematics solution), and Type III (arising when Type I and Type II singularity conditions are satisfied simultaneously).

The most critical type of parallel robot singularities is Type II. This is because as the robot approaches Type II singularities, the magnitudes of the actuator torques and/or forces diverge to infinity and the control is lost [3]. It is for this reason that Type II singularities are also referred to in the literature as actuation singularities [4, 5]. Actuation singularities can occur in different orders depending on the task being performed [6–8].

Date: July, 8, 2023.

Key words and phrases. Parallel robot, planar parallel robot, kinematic redundancy, actuation singularity.

Redundancy is an efficient way to eliminate singularities in parallel robots [9]. There are four types of redundancy used in parallel robotics. These are as follows:

1. Actuation redundancy [10-14]
2. Kinematic redundancy [15-18]
3. Internal redundancy [19]
4. Artificial redundancy [20, 21]

The aim of this paper is to study the elimination of actuation singularities of a (3+1)-degree-of-freedom RPR-RPRR planar parallel robot with kinematic redundancy. Here R and P denote the revolute and prismatic joints, respectively. The actuated joints are underlined.

2. KINEMATIC ANALYSIS

The mechanism studied in the paper is shown in the figure below. It is a single-loop planar mechanism composed of seven links. The fixed Cartesian rectangular coordinate system xy has its origin at point A_1 .

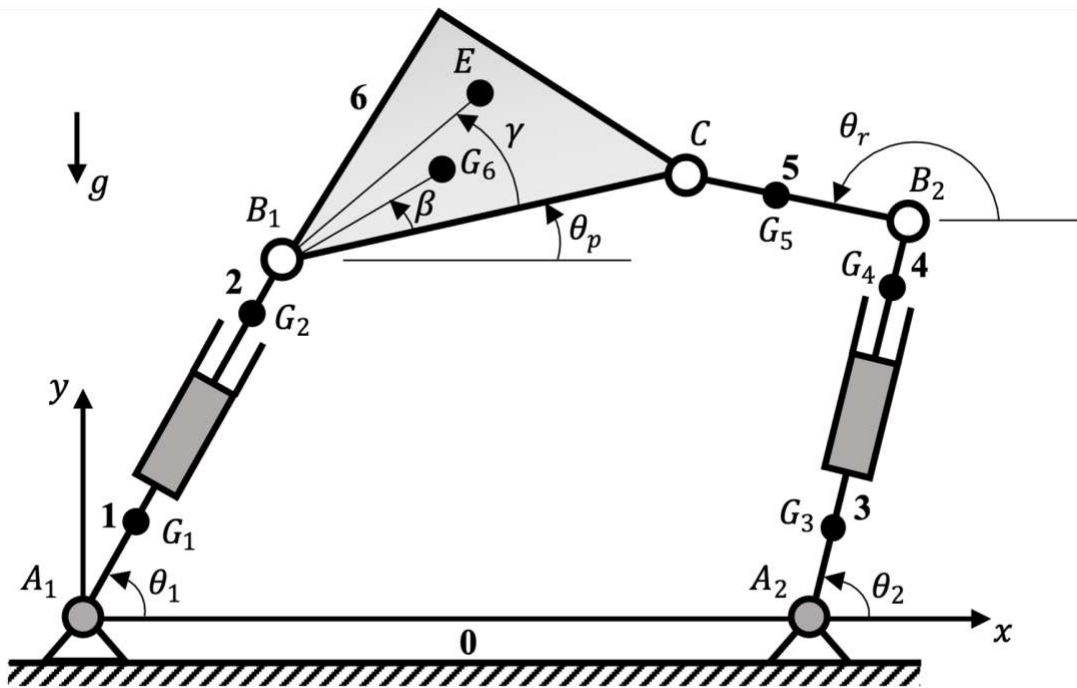


Figure 1. The seven-link RPR-RPRR planar parallel mechanism.

The link numbered 0 is the fixed link. Its length is given by $a_0 = |A_1A_2|$ (note that point A_2 is on the x -axis). There are two legs, the RPR and RPRR legs, which connect the moving platform to this fixed link. The

revolute joint variables $\theta_1, \theta_2, \theta_r$ and θ_p are shown in the figure. The prismatic joint variables are $s_1 = |A_1B_1|$ and $s_2 = |A_2B_2|$. Link 6 is the end-effector and point E is the endpoint.

The vector loop-closure equation for this mechanism can be written using complex numbers as follows:

$$s_1 e^{i\theta_1} + a_p e^{i\theta_p} = a_0 + s_2 e^{i\theta_2} + a_r e^{i\theta_r} \quad (1)$$

where $a_p = |B_1C|$, $a_r = |B_2C|$, and

$$e^{i\theta} = \cos(\theta) + i \sin(\theta) \quad (2)$$

with $i = \sqrt{-1}$. The real part and the imaginary part of equation (1) are written separately as

$$s_1 \cos(\theta_1) + a_p \cos(\theta_p) = a_0 + s_2 \cos(\theta_2) + a_r \cos(\theta_r) \quad (3)$$

$$s_1 \sin(\theta_1) + a_p \sin(\theta_p) = s_2 \sin(\theta_2) + a_r \sin(\theta_r) \quad (4)$$

The task variables are related to the joint variables by the following equations:

$$x_E(t) = s_1 \cos(\theta_1) + d \cos(\theta_p + \gamma) \quad (5)$$

$$y_E(t) = s_1 \sin(\theta_1) + d \sin(\theta_p + \gamma) \quad (6)$$

$$\theta_p(t) = \theta_p \quad (7)$$

$$\theta_r(t) = \theta_r \quad (8)$$

where $d = |B_1E|$ and $\gamma = \angle EB_1C$. By differentiating equations (3) to (8) with respect to time t and rearranging, we obtain

$$\dot{s}_1 \cos(\theta_1) - s_1 \dot{\theta}_1 \sin(\theta_1) - a_p \dot{\theta}_p \sin(\theta_p) - \dot{s}_2 \cos(\theta_2) + s_2 \dot{\theta}_2 \sin(\theta_2) + a_r \dot{\theta}_r \sin(\theta_r) = 0 \quad (9)$$

$$\dot{s}_1 \sin(\theta_1) + s_1 \dot{\theta}_1 \cos(\theta_1) + a_p \dot{\theta}_p \cos(\theta_p) - \dot{s}_2 \sin(\theta_2) - s_2 \dot{\theta}_2 \cos(\theta_2) - a_r \dot{\theta}_r \cos(\theta_r) = 0 \quad (10)$$

$$\dot{x}_E = \dot{s}_1 \cos(\theta_1) - s_1 \dot{\theta}_1 \sin(\theta_1) - d \dot{\theta}_p \sin(\gamma + \theta_p) \quad (11)$$

$$\dot{y}_E = \dot{s}_1 \sin(\theta_1) + s_1 \dot{\theta}_1 \cos(\theta_1) + d \dot{\theta}_p \cos(\gamma + \theta_p) \quad (12)$$

$$\dot{\theta}_p = \dot{\theta}_p \quad (13)$$

$$\dot{\theta}_r = \dot{\theta}_r \quad (14)$$

These velocity relations can be expressed in matrix-vector form as follows:

$$\mathbf{J}\dot{\mathbf{q}} = \dot{\boldsymbol{\eta}} \quad (15)$$

where

$$\mathbf{q} = [\theta_1 \quad s_1 \quad \theta_2 \quad s_2 \quad \theta_r \quad \theta_p]^T \quad (16)$$

$$\mathbf{J} = \begin{bmatrix} -s_1 \sin(\theta_1) & s_1 \cos(\theta_1) & -s_1 \sin(\theta_1) & s_1 \cos(\theta_1) & 0 & 0 \\ \cos(\theta_1) & \sin(\theta_1) & \cos(\theta_1) & \sin(\theta_1) & 0 & 0 \\ s_2 \sin(\theta_2) & -s_2 \cos(\theta_2) & 0 & 0 & 0 & 0 \\ -\cos(\theta_2) & -\sin(\theta_2) & 0 & 0 & 0 & 0 \\ a_r \sin(\theta_r) & -a_r \cos(\theta_r) & 0 & 0 & 0 & 1 \\ -a_p \sin(\theta_p) & a_p \cos(\theta_p) & -d \sin(\gamma + \theta_p) & d \cos(\gamma + \theta_p) & 1 & 0 \end{bmatrix}^T \quad (17)$$

$$\dot{\boldsymbol{\eta}} = [0 \quad 0 \quad \dot{x}_E \quad \dot{y}_E \quad \dot{\theta}_p \quad \dot{\theta}_r]^T \quad (18)$$

Equation (15) can be solved for $\dot{\mathbf{q}}$ as

$$\dot{\mathbf{q}} = \mathbf{J}^{-1}\dot{\boldsymbol{\eta}} \quad (19)$$

Thus, using the method of Ider [4], we can conclude that Type I singularities occur when $\det(\mathbf{J}) = -s_1 s_2 = 0$. However, in a real situation it is not possible for s_1 and s_2 to be zero [22, 23].

To study Type II singularities, we rewrite equations (9) and (10) in matrix-vector form as follows:

$$\mathbf{J}^c \dot{\mathbf{q}} = \mathbf{0} \quad (20)$$

where

$$\mathbf{J}^c = \begin{bmatrix} -s_1 \sin(\theta_1) & s_1 \cos(\theta_1) \\ \cos(\theta_1) & \sin(\theta_1) \\ s_2 \sin(\theta_2) & -s_2 \cos(\theta_2) \\ -\cos(\theta_2) & -\sin(\theta_2) \\ a_r \sin(\theta_r) & -a_r \cos(\theta_r) \\ -a_p \sin(\theta_p) & a_p \cos(\theta_p) \end{bmatrix}^T \quad (21)$$

The vectors of the actuated joint variables and of the unactuated joint variables are now written as follows, respectively:

$$\mathbf{q}^a = [\theta_1 \quad s_1 \quad \theta_2 \quad s_2]^T \quad (22)$$

$$\mathbf{q}^u = [\theta_r \quad \theta_p]^T \quad (23)$$

Using the above equations, equation (20) can be re-expressed as

$$\mathbf{J}^{ca} \dot{\mathbf{q}}^a + \mathbf{J}^{cu} \dot{\mathbf{q}}^u = \mathbf{0} \quad (24)$$

where

$$\mathbf{J}^{ca} = \begin{bmatrix} -s_1 \sin(\theta_1) & s_1 \cos(\theta_1) \\ \cos(\theta_1) & \sin(\theta_1) \\ s_2 \sin(\theta_2) & -s_2 \cos(\theta_2) \\ -\cos(\theta_2) & -\sin(\theta_2) \end{bmatrix}^T \quad (25)$$

$$\mathbf{J}^{cu} = \begin{bmatrix} a_r \sin(\theta_r) & -a_r \cos(\theta_r) \\ -a_p \sin(\theta_p) & a_p \cos(\theta_p) \end{bmatrix}^T \quad (26)$$

Solving equation (24) for $\dot{\mathbf{q}}^u$ gives

$$\dot{\mathbf{q}}^u = -(\mathbf{J}^{cu})^{-1} \mathbf{J}^{ca} \dot{\mathbf{q}}^a \quad (27)$$

Therefore, using the method of Ider [4], we can conclude that Type II singularities occur when $\det(\mathbf{J}^{cu}) = -a_p a_r \sin(\theta_p - \theta_r) = 0$. Note that a_p and a_r are non-zero lengths. So, Type II singularities occur when $\sin(\theta_p - \theta_r) = 0$.

3. DYNAMIC ANALYSIS

The vector of generalized coordinates can be chosen to be the vector of joint variables \mathbf{q} . Moving link j ($j = 1, 2, 3, 4, 5, 6$) has mass m_j , mass center G_j , and centroidal mass moment of inertia I_{G_j} . The locations of the mass centers are given by $r_1 = |A_1 G_1|$, $r_2 = |B_1 G_2|$, $r_3 = |A_2 G_3|$, $r_4 = |B_2 G_4|$, $r_5 = |B_2 G_5|$, $r_6 = |B_1 G_6|$, and $\beta = \angle G_6 B_1 C$. The gravitational acceleration g acts along the negative y -axis. The motor torques that are

associated with θ_1 and θ_2 are T_1 and T_2 , respectively. The linear actuator forces corresponding to s_1 and s_2 are F_1 and F_2 , respectively.

The equations of motion of the parallel robot can be expressed using the Lagrange multiplier method as follows:

$$\mathbf{M}\ddot{\mathbf{q}} + \mathbf{N} = \mathbf{Q} + (\mathbf{J}^c)^T \boldsymbol{\lambda} \quad (28)$$

Here, \mathbf{M} is the generalized mass matrix, \mathbf{N} is the vector of generalized nonlinear inertial and gravitational forces, \mathbf{Q} is the vector of generalized nonconservative external forces, and $\boldsymbol{\lambda}$ is the vector consisting of the Lagrange multipliers λ_1 and λ_2 . We have

$$\mathbf{M} = \begin{bmatrix} M_{1,1} & M_{1,2} & M_{1,3} & M_{1,4} & M_{1,5} & M_{1,6} \\ M_{2,1} & M_{2,2} & M_{2,3} & M_{2,4} & M_{2,5} & M_{2,6} \\ M_{3,1} & M_{3,2} & M_{3,3} & M_{3,4} & M_{3,5} & M_{3,6} \\ M_{4,1} & M_{4,2} & M_{4,3} & M_{4,4} & M_{4,5} & M_{4,6} \\ M_{5,1} & M_{5,2} & M_{5,3} & M_{5,4} & M_{5,5} & M_{5,6} \\ M_{6,1} & M_{6,2} & M_{6,3} & M_{6,4} & M_{6,5} & M_{6,6} \end{bmatrix} \quad (29)$$

$$\mathbf{N} = [N_1 \quad N_2 \quad N_3 \quad N_4 \quad N_5 \quad N_6]^T \quad (30)$$

$$\mathbf{Q} = [T_1 \quad F_1 \quad T_2 \quad F_2 \quad 0 \quad 0]^T \quad (31)$$

$$\boldsymbol{\lambda} = [\lambda_1 \quad \lambda_2]^T \quad (32)$$

where

$$M_{1,1} = I_{G_1} + m_1 r_1^2 + I_{G_2} + m_2 (s_1 - r_2)^2 + m_6 s_1^2 \quad (33)$$

$$M_{1,2} = M_{1,3} = M_{1,4} = M_{1,5} = 0 \quad (34)$$

$$M_{1,6} = m_6 r_6 s_1 \cos(\theta_p + \beta - \theta_1) \quad (35)$$

$$M_{2,1} = M_{2,3} = M_{2,4} = M_{2,5} = 0 \quad (36)$$

$$M_{2,2} = m_2 + m_6 \quad (37)$$

$$M_{2,6} = -m_6 r_6 \sin(\theta_p + \beta - \theta_1) \quad (38)$$

$$M_{3,1} = M_{3,2} = M_{3,4} = M_{3,6} = 0 \quad (39)$$

$$M_{3,3} = I_{G_3} + m_3 r_3^2 + I_{G_4} + m_4 (s_2 - r_4)^2 + m_5 s_2^2 \quad (40)$$

$$M_{3,5} = m_5 r_5 s_2 \cos(\theta_2 - \theta_r) \quad (41)$$

$$M_{4,1} = M_{4,2} = M_{4,3} = M_{4,6} = 0 \quad (42)$$

$$M_{4,4} = m_4 + m_5 \quad (43)$$

$$M_{4,5} = m_5 r_5 \sin(\theta_2 - \theta_r) \quad (44)$$

$$M_{5,1} = M_{5,2} = M_{5,6} = 0 \quad (45)$$

$$M_{5,3} = m_5 r_5 s_2 \cos(\theta_2 - \theta_r) \quad (46)$$

$$M_{5,4} = m_5 r_5 \sin(\theta_2 - \theta_r) \quad (47)$$

$$M_{5,5} = I_{G_5} + m_5 r_5^2 \quad (48)$$

$$M_{6,1} = m_6 r_6 s_1 \cos(\theta_p + \beta - \theta_1) \quad (49)$$

$$M_{6,2} = -m_6 r_6 \sin(\theta_p + \beta - \theta_1) \quad (50)$$

$$M_{6,3} = M_{6,4} = M_{6,5} = 0 \quad (51)$$

$$M_{6,6} = I_{G_6} + m_6 r_6^2 \quad (52)$$

$$N_1 = 2(m_2(s_1 - r_2) + m_6 s_1) \dot{s}_1 \dot{\theta}_1 - m_6 r_6 s_1 \dot{\theta}_p^2 \sin(\theta_p + \beta - \theta_1) \\ + (m_1 r_1 + m_2(s_1 - r_2) + m_6 s_1) g \cos(\theta_1) \quad (53)$$

$$N_2 = (m_2(r_2 - s_1) - m_6 s_1) \dot{\theta}_1^2 - m_6 r_6 \dot{\theta}_p^2 \cos(\theta_p + \beta - \theta_1) + (m_2 + m_6) g \sin(\theta_1) \quad (54)$$

$$N_3 = 2(m_4(s_2 - r_4) + m_5 s_2) \dot{s}_2 \dot{\theta}_2 + m_5 r_5 s_2 \dot{\theta}_r^2 \sin(\theta_2 - \theta_r) + (m_3 r_3 + m_4(s_2 - r_4) + m_5 s_2) g \cos(\theta_2) \quad (55)$$

$$N_4 = -(m_4(s_2 - r_4) + m_5 s_2) \dot{\theta}_2^2 - m_5 r_5 \dot{\theta}_r^2 \cos(\theta_2 - \theta_r) + (m_4 + m_5) g \sin(\theta_2) \quad (56)$$

$$N_5 = 2m_5 r_5 \dot{s}_2 \dot{\theta}_2 \cos(\theta_2 - \theta_r) - m_5 r_5 s_2 \dot{\theta}_2^2 \sin(\theta_2 - \theta_r) + m_5 g r_5 \cos(\theta_r) \quad (57)$$

$$N_6 = 2m_6 r_6 \dot{s}_1 \dot{\theta}_1 \cos(\theta_p + \beta - \theta_1) + m_6 r_6 s_1 \dot{\theta}_1^2 \sin(\theta_p + \beta - \theta_1) + m_6 g r_6 \cos(\theta_p + \beta) \quad (58)$$

Notice that \mathbf{M} is symmetric. Besides, two assumptions are worth noting. It is assumed that there are no external nonconservative forces or moments other than the actuator forces and torques. It is also assumed that there are no dissipative forces in the system. Equation (28) can be divided into two parts as follows:

$$\mathbf{M}^a \ddot{\mathbf{q}} + \mathbf{N}^a = \mathbf{Q}^a + (\mathbf{J}^{ca})^T \boldsymbol{\lambda} \quad (59)$$

$$\mathbf{M}^u \ddot{\mathbf{q}} + \mathbf{N}^u = \mathbf{Q}^u + (\mathbf{J}^{cu})^T \boldsymbol{\lambda} \quad (60)$$

where

$$\mathbf{M}^a = \begin{bmatrix} M_{1,1} & M_{1,2} & M_{1,3} & M_{1,4} & M_{1,5} & M_{1,6} \\ M_{2,1} & M_{2,2} & M_{2,3} & M_{2,4} & M_{2,5} & M_{2,6} \\ M_{3,1} & M_{3,2} & M_{3,3} & M_{3,4} & M_{3,5} & M_{3,6} \\ M_{4,1} & M_{4,2} & M_{4,3} & M_{4,4} & M_{4,5} & M_{4,6} \end{bmatrix} \quad (61)$$

$$\mathbf{M}^u = \begin{bmatrix} M_{5,1} & M_{5,2} & M_{5,3} & M_{5,4} & M_{5,5} & M_{5,6} \\ M_{6,1} & M_{6,2} & M_{6,3} & M_{6,4} & M_{6,5} & M_{6,6} \end{bmatrix} \quad (62)$$

$$\mathbf{N}^a = [N_1 \quad N_2 \quad N_3 \quad N_4]^T \quad (63)$$

$$\mathbf{N}^u = [N_5 \quad N_6]^T \quad (64)$$

$$\mathbf{Q}^a = [T_1 \quad F_1 \quad T_2 \quad F_2]^T \quad (65)$$

$$\mathbf{Q}^u = [0 \quad 0]^T \quad (66)$$

Therefore, the required actuator forces and torques can be calculated from

$$\mathbf{Q}^a = \mathbf{M}^a \ddot{\mathbf{q}} + \mathbf{N}^a - (\mathbf{J}^{ca})^T ((\mathbf{J}^{cu})^T)^{-1} (\mathbf{M}^u \ddot{\mathbf{q}} + \mathbf{N}^u) \quad (67)$$

It follows from equation (67) that the actuation singularity condition is $\det((\mathbf{J}^{cu})^T) = \det(\mathbf{J}^{cu}) = -a_p a_r \sin(\theta_p - \theta_r) = 0$, which is the same as the Type II singularity condition. See Ider [4] for more details on the equivalence of these two singularity conditions.

4. DISCUSSION AND CONCLUSIONS

In this paper we study the conditions for the occurrence of singularities in kinematically redundant RPR-RPRR planar parallel robots. We see that by replanning the motion of the degree of freedom $\theta_r(t)$ such that $\sin(\theta_p(t) - \theta_r(t)) \neq 0$ throughout the entire task, the trajectory of the moving platform, which originally

passes through actuation singularities, can be desingularized. In other words, actuation singularities can be eliminated by appropriate replanning of the motion of the redundant degree of freedom θ_r .

ACKNOWLEDGEMENTS

This paper is based on a part of the Master of Science Thesis of the second author (Muhammed Yasir ÇUBUK), which is in preparation in the Department of Mechanical Engineering (English) at Marmara University Institute of Pure and Applied Sciences under the supervision of the first author (Assoc. Prof. Dr. Mustafa ÖZDEMİR).

REFERENCES

- [1] Merlet, J.-P. *Parallel Robots*, 2nd edition, Springer, Dordrecht, (2006).
- [2] Gosselin, C., Angeles, J. Singularity analysis of closed-loop kinematic chains. *IEEE Transactions on Robotics and Automation*, 6(3), 281–290, (1990).
- [3] Choudhury, P., Ghosal, A. Singularity and controllability analysis of parallel manipulators and closed-loop mechanisms. *Mechanism and Machine Theory*, 35(10), 1455–1479, (2000).
- [4] Ider, S. K. Inverse dynamics of parallel manipulators in the presence of drive singularities. *Mechanism and Machine Theory*, 40(1), 33–44, (2005).
- [5] Ozgoren, M. K. Kinematic and kinetostatic analysis of parallel manipulators with emphasis on position, motion, and actuation singularities. *Robotica*, 37(4), 599–625, (2019).
- [6] Özdemir, M. Removal of singularities in the inverse dynamics of parallel robots. *Mechanism and Machine Theory*, 107, 71–86, (2017).
- [7] Özdemir, M. High-order singularities of 5R planar parallel robots. *Robotica*, 37(2), 233–245, (2019).
- [8] Özdemir, M. Hypersingularities of 3-RRR planar parallel robots. *Proceedings of the Romanian Academy Series A-Mathematics Physics Technical Sciences Information Science*, 22(4), 353–360, (2021).
- [9] Luces, M., Mills, J. K., Benhabib, B. A review of redundant parallel kinematic mechanisms. *Journal of Intelligent & Robotic Systems*, 86(2), 175–198, (2017).
- [10] Ganovski, L., Fisette, P., Samin, J. C. Piecewise overactuation of parallel mechanisms following singular trajectories: Modeling, simulation and control. *Multibody System Dynamics*, 12(4), 317–343, (2004).
- [11] Saglia, J. A., Dai, J. S., Caldwell, D. G. Geometry and kinematic analysis of a redundantly actuated parallel mechanism that eliminates singularities and improves dexterity. *Journal of Mechanical Design-Transactions of the ASME*, 130(12), 124501, (2008).
- [12] Shin, K., Yi, B.-J., Kim, W. Parallel singularity-free design with actuation redundancy: A case study of three different types of 3-degree-of-freedom parallel mechanisms with redundant actuation. *Proceedings of the Institution of Mechanical Engineers, Part C: Journal of Mechanical Engineering Science*, 228(11), 2018–2035, (2014).
- [13] Saafi, H., Laribi, M. A., Zegloul, S. Redundantly actuated 3-RRR spherical parallel manipulator used as a haptic device: improving dexterity and eliminating singularity. *Robotica*, 33(5), 1113–1130, (2015).
- [14] Li, S., Liu, Y., Cui, H., Niu, Y., Zhao, Y. Synthesis of branched chains with actuation redundancy for eliminating interior singularities of 3T1R parallel mechanisms. *Chinese Journal of Mechanical Engineering*, 29(2), 250–259, (2016).
- [15] Kotlarski, J., Heimann, B., Ortmaier, T. Influence of kinematic redundancy on the singularity-free workspace of parallel kinematic machines. *Frontiers of Mechanical Engineering*, 7(2), 120–134, (2012).
- [16] Gosselin, C., Laliberté, T., Veillette, A. Singularity-free kinematically redundant planar parallel mechanisms with unlimited rotational capability. *IEEE Transactions on Robotics*, 31(2), 457–467, (2015).

- [17] Gosselin, C., Schreiber, L.-T. Kinematically redundant spatial parallel mechanisms for singularity avoidance and large orientational workspace. *IEEE Transactions on Robotics*, 32(2), 286–300, (2016).
- [18] Isaksson, M. Kinematically redundant planar parallel mechanisms for optimal singularity avoidance. *Journal of Mechanical Design-Transactions of the ASME*, 139(4), 042302, (2017).
- [19] Parsa, S. S., Boudreau, R., Carretero, J. A. Reconfigurable mass parameters to cross direct kinematic singularities in parallel manipulators. *Mechanism and Machine Theory*, 85, 53–63, (2015).
- [20] Agarwal, A., Nasa, C., Bandyopadhyay, S. Dynamic singularity avoidance for parallel manipulators using a task-priority based control scheme. *Mechanism and Machine Theory*, 96, Part 1, 107–126, (2016).
- [21] Gao, Y., Chen, K., Gao, H., Xiao, P., Wang, L. Small-angle perturbation method for moving platform orientation to avoid singularity of asymmetrical 3-RRR planar parallel manipulator. *Journal of the Brazilian Society of Mechanical Sciences and Engineering*, 41(12), 538, (2019).
- [22] Sefrioui, J., Gosselin, C. M. On the quadratic nature of the singularity curves of planar three-degree-of-freedom parallel manipulators. *Mechanism and Machine Theory*, 30(4), 533–551, (1995).
- [23] Ider, S. K. Singularity robust inverse dynamics of planar 2-RPR parallel manipulators. *Proceedings of the Institution of Mechanical Engineers, Part C: Journal of Mechanical Engineering Science*, 218(7), 721–730, (2004).

DEPARTMENT OF MECHANICAL ENGINEERING, FACULTY OF ENGINEERING, MARMARA UNIVERSITY, RECEP TAYYİP ERDOĞAN CAMPUS, 34854 MALTEPE, İSTANBUL, TÜRKİYE

Email address: mustafa.ozdemir@marmara.edu.tr

DEPARTMENT OF MECHANICAL ENGINEERING (ENGLISH), INSTITUTE OF PURE AND APPLIED SCIENCES, MARMARA UNIVERSITY, GÖZTEPE CAMPUS, 34722 KADIKÖY, İSTANBUL, TÜRKİYE

Email address: yasircubuk97@gmail.com

INVESTIGATION OF CONVECTION HEAT TRANSFER COEFFICIENT EFFECTS ON THERMAL ENERGY STORAGE PERFORMANCE WITH PCM/GRAPHITE MATRIX COMPOSITE

Sare MITINCIK^{1*} and Mustafa Yusuf YAZICI¹

ABSTRACT

PCM-based thermal energy storage systems provide an effective means of capturing, storing, and releasing thermal energy. Their high energy storage density, temperature control capabilities, and contribution to sustainable energy practices make them a promising solution for optimizing energy utilization and reducing environmental impact. However, their low thermal conductivity values significantly limit their usability. Integration of PCMs with graphite matrix can significantly improve thermal conductivity, thereby enhancing energy storage efficiency. The main focus here is to ensure the effective maintenance of thermal energy and minimize energy losses by contributing to the development of more sustainable energy storage solutions. In this work, a numerical study has been conducted to predict the effect of environmental conditions on the thermal energy storage performance of graphite matrix saturated with PCM (paraffin) for solar thermal energy and waste heat recovery, including different convection heat transfer coefficient values of 0, 5, 10, and 50 W/m²K, which refer to adiabatic, natural convection/still air, forced convection with fans (air conditioning), and windy weather, respectively. The effect of the convection heat transfer coefficient is evaluated for different bulk density values of 100 kg/m³ and 143 kg/m³. Results indicated that uniform melting behavior was observed in the PCM/graphite matrix composite due to the high porosity of graphite, which allowed a dominant conduction heat transfer mechanism, and energy storage rates climbed with the increase in bulk density. Higher heat transfer coefficient values cause a higher total melting time and lower thermal energy storage rates. The effect of the convection heat transfer coefficient on total melting time is appreciable for 50 W/m²K compared to lower h values for each bulk density. The effect of the convection heat transfer coefficient is lower for a higher bulk density of 143 kg/m³. On the other hand, the effect of bulk density on the energy storage rate is maximum 9% for lower convection heat transfer coefficients (<50 W/m²K), while the impact level of bulk density increases to 15% at 50 W/m²K.

1. INTRODUCTION

A major increase in global energy consumption over time was brought about by the industrial revolution (Ahmed et al., 2022). In addition, according to the International Energy Agency (IEA) report, with the growing world economy and population, global energy demand is forecast to increase by a quarter by 2040. Also, more CO₂ is expected to be released, which negatively impacts efforts to combat climate change and sustainability (IEA, 2022). Currently, it has increased interest in research and boosted the development of new strategies for clean energy and energy sustainability. Within these strategies, thermal energy storage (TES) is seen as one of the key elements and research topics contributing to the goals of a green environment and low carbon emissions. At this point, PCMs with a

Date: July, 8, 2023.

Key words and phrases. Thermal energy storage, melting, composite PCMs, convection heat transfer coefficient, numerical

high amount of energy storage density, in addition to properties such as a wide melting range, chemical stability, and non-corrosiveness, have received much attention in TES systems. However, their poor thermal conductivity significantly limits the use of PCMs. Researchers have developed and implemented many techniques and arrangements to remedy the disadvantage of the low thermal conductivity of PCMs, such as nanoparticle (metal/carbon-based), fin, micro-capsulation, metal or graphite matrix etc (Venkateswarlu & Ramakrishna, 2022). One of these methods is graphite matrix with carbon derivative structures. Graphite matrices have high thermal conductivity and many other advantages (high adsorption capacity with high porosity rates (>80–85), stable chemical structure, low density, etc.), and these remarkable properties make them promising/effective materials for thermal energy storage applications. However, the use of graphite material for thermal energy storage is limited, and there is a gap in the literature for TES applications. Here are some studies from the literature for PCM/graphite matrix: (Mesalhy et al., 2005) was investigated the thermal performance of a few matrices with varied thermal conductivity and porosity ratios in shell-in-tube geometry, and results indicated that the best melting performance is provided by a matrix with high thermal conductivity and high pore size. In a study carried out by (Mills et al., 2006), the thermal conductivity of paraffin/graphite composite blocks with various bulk densities was experimentally investigated. They reported that the addition of graphite increased the heat conductivity of composite materials by 20–130 times. (Zhong et al., 2010) carried out an experimental study to enhance the thermal performance of paraffin with graphite by applying five composite blocks with different bulk densities and mass ratios in latent heat storage applications. They concluded that the thermal conductivity of the composite blocks increased 28–180 times when compared to the pure paraffin condition. Another study was performed by (Li et al., 2014) investigating the weight fraction of expanded graphite (EG) powder's impact on the thermal behavior of the paraffin/EG composite. They found that the paraffin/EG with 20% graphite weight fraction increased to 14 W/mK in comparison with pure paraffin's thermal conductivity of 0.32 W/mK, and melting performance increased by 43.8 times. (Xie et al., 2019) was experimentally studied the performance of PCM/expanded graphite (EG) slurry composites considering six cases with different bulk densities. In addition, they attempted to improve the storage performance of PCM/expanded graphite slurry composites by including carbon fiber and graphite sheets. It is seen that thermal conductivity and energy storage capacity were found to be higher in the graphite-sheet-containing blocks than in the carbon fiber-containing ones. (Yazici et al., 2021) focused on the melting capabilities of a paraffin/graphite matrix composite for use in thermal energy storage systems. They reported a 92% reduction in melting time and an increase in thermal conductivity of around 35 times when compared to pure paraffin. Furthermore, they observed a 31% reduction in the melting time of the PCM/graphite matrix as the inlet temperature of the heat transfer fluid increased. More recently, (Mitincik & Yazici, 2023) have numerically studied the effect of composite bulk densities and wall temperatures on storage performance in a paraffin/graphite matrix composite material with shell in tube geometry for solar energy and waste heat applications. They concluded that the storage performance increased up to 76 times with an increase in bulk density compared to the pure paraffin case. However, it was found that there is an ideal bulk density value (100 kg/m³), and only 8% change in storage performance was observed above 100 kg/m³. On the other hand, the effect of the increase in wall temperature on performance has been found to be greater at lower bulk densities due to decreased thermophysical properties. Similar studies were performed by (Zhang & Fang, 2006), (Liu et al., 2014), (Raza et al., 2016), and (Song et al., 2019).

Building on previous studies, it is clear that there is a lack of studies on TES applications using PCM/graphite matrix, and most of the studies focused just on the enhancement of thermal conductivity. This numerical study aims to investigate the effects of environmental conditions on the thermal energy storage performance of PCM/graphite matrix for solar thermal energy storage and waste heat recovery. Paraffin was used as a phase change material. Simulations was performed under two bulk density values of 100 kg/m³ and 143 kg/m³. The results from the numerical simulations are presented in the form of transient/time-dependent temperature profiles, liquid fractions, and energy storage rates for PCM/graphite matrix composites.

2. NUMERICAL APPROACH

In this section, the physical model, boundary conditions, assumptions, governing equations, and computational/ solution methodology are presented.

The numerical simulations was performed with the computational fluid dynamics (CFD) code of Ansys Fluent, which uses the finite volume method. In this package program, the mathematical equations used to solve the melting and solidification problems are based on the Enthalpy-Porosity technique, which eliminates the need for heat transfer characteristics in the mushy region during phase change period (Voller & Prakash, 1987). In Table 1, the properties of the PCM/graphite matrix composite used in numerical studies are given.

Table 1. Physical parameters of PCM/graphite matrix composite blocks of 100 kg/m³ and 143 kg/m³ (Mallow et al., 2016)

Parameters	100 kg/m ³	143 kg/m ³
Density (kg/m ³)	888.15	915.9
Specific heat (J/kg.K)	2381.45	2297.3
Thermal conductivity (W/m.K)	9.6	10.1
Latent heat (J/kg)	136 400	111 100
Melting Point (°C)	54.5	53.8

2.1. Physical model and boundary conditions

The physical model (indirectly numerical domain) for two-dimensional numerical analysis and local temperature points at different locations are displayed in Figure 1. CFD simulations were performed to be 2-D and symmetric by considering to reduce the computational cost (calculation time and mesh size). Shell-in-tube geometry is preferred as a thermal energy storage medium due to its high efficiency and compactness (A. K. Rai, 2012). The thermal energy storage medium consists of PCM/graphite matrix composite material. A calculation area is developed, neglecting the inner and outer wall thicknesses. Initial and boundary conditions are given both schematically and in text below:

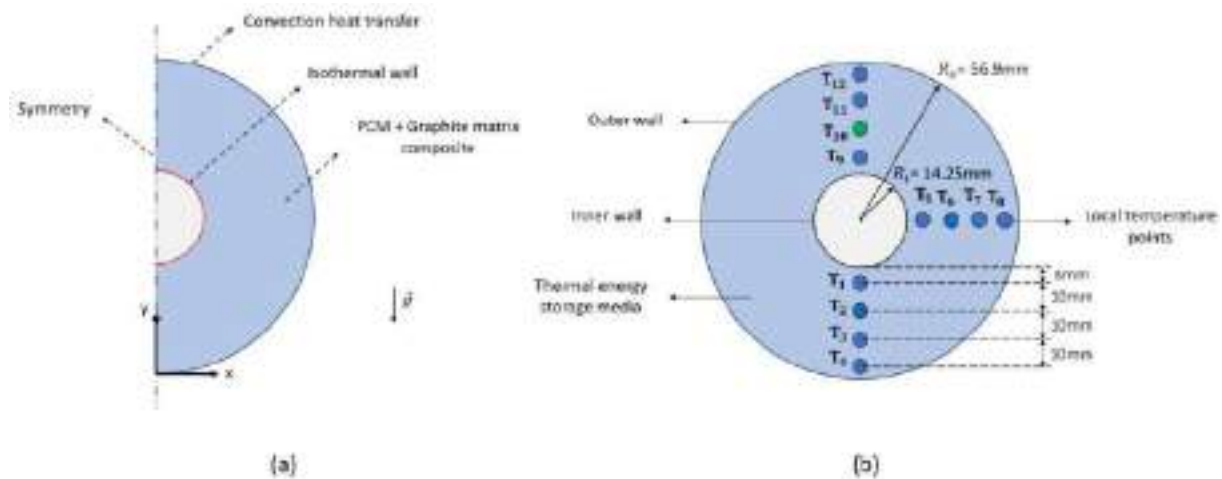


Figure 1. Physical model and boundary conditions (a), and local temperature points (b)

Composite PCM's initial temperature T_0 : 25°C

Isothermal wall boundary conditions T_{wall} : 85°C

For the symmetry axis; $\frac{\partial T}{\partial x} = 0$ (1)

For the outer wall, where there is convection heat transfer to the environment;

$$-k \frac{\partial T}{\partial x} = h (T_{wall} - T_{\infty}), -k \frac{\partial T}{\partial y} = h (T_{wall} - T_{\infty}), \quad (2)$$

$h = 0, 5, 10, 50 \text{ W/m}^2\text{K}$ and $T_{\infty} = 25^{\circ}\text{C}$

2.2. Assumptions and governing equations

The following assumptions were made during the numerical modeling:

- Composite PCM is homogeneous and isotropic.
- The viscosity of the PCM/graphite matrix composite is assumed to be infinity (10^5) (Song et al., 2019), (Ling et al., 2014), .
- Heat transfer occurs by conduction, neglecting the change in density during composite PCM's phase change period.
- There is no heat generation in the composite material.

Based on the assumptions, the governing equations of the model can be written as follows:

Energy:

For the composite PCM:

$$\rho \frac{\partial H}{\partial t} = k \left(\frac{\partial^2 T}{\partial x^2} + \frac{\partial^2 T}{\partial y^2} + \frac{\partial^2 T}{\partial z^2} \right) \quad (3)$$

Where ρ and k are density and thermal conductivity of the PCM/graphite matrix composite, respectively. H is the total enthalpy, which can be defined as the combination of sensible and latent heat:

$$H = h + \Delta H = h + \lambda L \quad (4)$$

$$h = h_0 + \int_{T_0}^T C_p \cdot dT \quad (5)$$

h_0 represents enthalpy at the initial temperature. Enthalpy changes caused by phase transitions can be calculated as:

$$\lambda = \begin{cases} 0 & T < T_{\text{solidus}} \\ \frac{T - T_{\text{solidus}}}{T_{\text{melting}} - T_{\text{solidus}}} & T_{\text{solidus}} < T < T_{\text{melting}} \\ 1 & T > T_{\text{melting}} \end{cases} \quad (6)$$

2.3. Computational/Solution methodology

After geometry is constrained as in Figure 1, fine structured meshes are generated by Ansys Meshing using quad elements, especially near the isothermal wall. The phase change period was simulated using the Fluent-Melting/Solidification model. Material properties are constant during the phase change (melting) period, and the PCM/graphite matrix was treated as a single composite material. Coupled algorithm was chosen for pressure-velocity coupling. Second Order Upwind discretization scheme was utilized for momentum and energy equations, and PRESTO! was used to calculate the pressure term. Convergence criteria were determined as 10^{-5} , 10^{-6} , and 10^{-6} for continuity, momentum, and energy equations, respectively.

3. RESULTS AND DISCUSSION

In the present study, a series of numerical calculations have been carried out with the CFD code ANSYS Fluent to analyze the effect of convection heat transfer coefficient and PCM/graphite matrix bulk

densities. In this section, model validation, solution independency and the numerical simulation results of the melting period are discussed.

3.1. Model validation

The validation was performed in two steps, including experimental work done by the authors (Mitincik & Yazici, 2023) and published data from the literature (Lv et al., 2016). Firstly, in the study performed by the authors, 75 kg/m³ paraffin/graphite matrix composite was used as a storage medium in shell-in-tube geometry (dimensions of D_{inner} : 28.5mm, D_{outer} : 113.8mm and L : 50mm). In order to achieve the isothermal wall boundary condition, it is assumed that the heat transfer fluid (water), which enters the copper pipe at 80°C, has an average pipe temperature of 76°C. It is not possible to obtain an entirely adiabatic wall even if an insulating layer is applied to the system; thus, the scenario was modeled with a convection heat transfer coefficient of 3 W/m²K to the surrounding medium. There are differences between numerical and experimental studies because the properties of composite materials are constant and isotropic. Another reason is that the wall thickness of the inner wall (isothermal wall) has been eliminated in the analysis. Thus, there is no thermal contact resistance between the isothermal wall and the composite material. The negative effects of the experimental study are reduced with the help of the numerical analysis. Secondly, from the literature, (Lv et al., 2016) performed an experimental and numerical study of polyethylene glycol (PEG)/expanded graphite (EG), investigating the effect of different mass fractions of expanded graphite in a rectangular prism. The numerical model was established for the case of the PEG/EG ratio is 92/8. It is seen that both validation studies provide excellent compatibility (Figure 2) and a suitable recipe for future calculations.

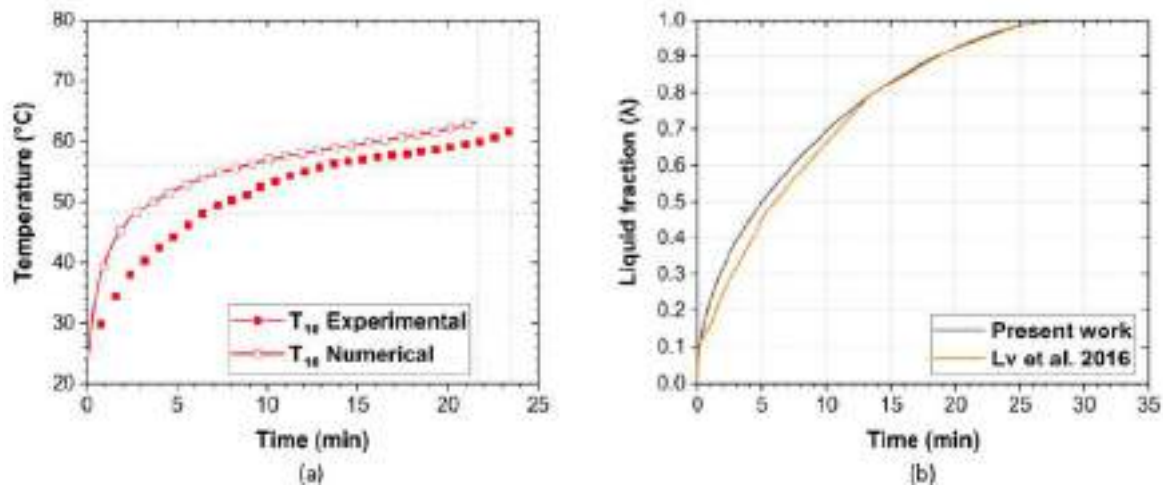


Figure 2. Validation of established numerical study: transient temperature profiles of work done by authors (a), liquid fraction variations from literature (b)

3.2. Solution independency

The realistic numerical solution should be independent of mesh and time step. Figure 3 illustrates the effects of the mesh size on the liquid fraction of the PCM/graphite matrix composite for 143 kg/m³ and adiabatic boundary condition. With a time step of 1s, the mesh independence study was carried out for the following mesh elements: 19000, 27000, and 39600. It was seen that the difference in liquid fractions of the composite was insignificant when the mesh elements increased from 27000 to 39000, and it was determined that 27000 elements are suitable for the reliability of the solution. It was also tested for the effect of time step by using four values of 2, 1, 0.5, and 0.2s under 27000 mesh elements, and 1s was found to be the best choice for numerical accuracy.

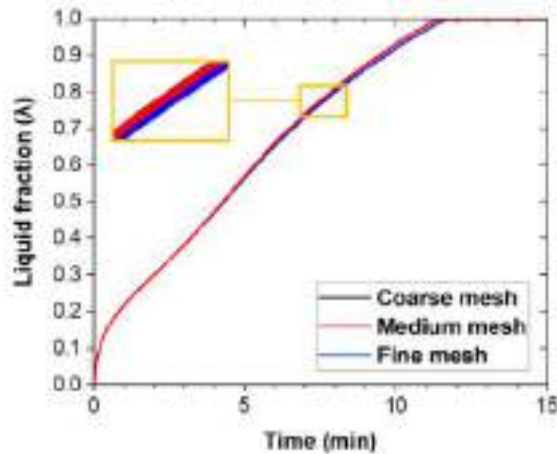


Figure 3. Mesh independency study

3.3. Numerical simulation results

Four convection heat transfer coefficients (0, 5, 10, and 50 W/m²K) are adopted for the thermal energy storage performance of PCM/graphite matrix composite materials. Convection heat transfer coefficients of 0, 5, 10, and 50 W/m²K refer to adiabatic, natural convection/still air, forced convection with fans (air conditioning) ($V = 1$ m/s), and windy weather ($V = 15$ m/s), respectively. For simplicity, temperature variations at local points are given just for 100 kg/m³. Similar temperature profiles with higher values are observed for 143 kg/m³. Figure 4 shows the temperature distributions of determined points (Figure 1-b) in PCM/graphite matrix thermal energy storage media for 100 kg/m³ bulk density and adiabatic boundary conditions. The dashed lines on the graphs indicate the melting temperature points (horizontal) and total melting times (vertical) of the PCM/graphite matrix composite. Although the geometrical dimensions are relatively large, the melting phenomenon occurs rapidly, and the storage/melting period is completed in 13.9 min. This is due to increased thermal pathways where the heat is transferred by increasing the internal surface area of the composite structure with the use of graphite material with a high porosity. Thus, by increasing the thermal conductivity value of the PCM/graphite matrix composite material (Table 1), the low thermal conductivity of the paraffin is eliminated. At the same time, the micron-sized pores suppress the natural convection encountered just in the paraffin melting mechanism, where no enhancement technique was used, creating flow resistance in the liquid paraffin during the melting period. As a result, the heat transfer in the porous material occurs through the conduction mechanism, and uniform melting behavior is observed in composite materials up to reaching the total melting condition. When the temperature profiles of the determined points are examined, it is seen that according to the region where the high temperature gradients are (near the isothermal wall), the temperatures fall towards the outer of thermal energy storage media. For example, the temperatures of T_1 , T_2 , T_3 and T_4 are 74°C, 66°C, 58°C and 54.5°C, respectively. The melting period in the shell in tube geometry is continued by transferring heat towards the entire PCM/graphite matrix composite. On the other hand, sensible heat storage is seen until the temperature of the system reaches the melting point, after that, latent heat storage is started, and transient/time-dependent temperature rises in local points are decreased. When temperatures go up, it means that sensible heat storage is started again in the system, as in the beginning of melting. It should be remembered that the sensible heat stored in the system accounts for almost half of the total stored thermal heat/energy because the local temperature points reach stable system temperatures.

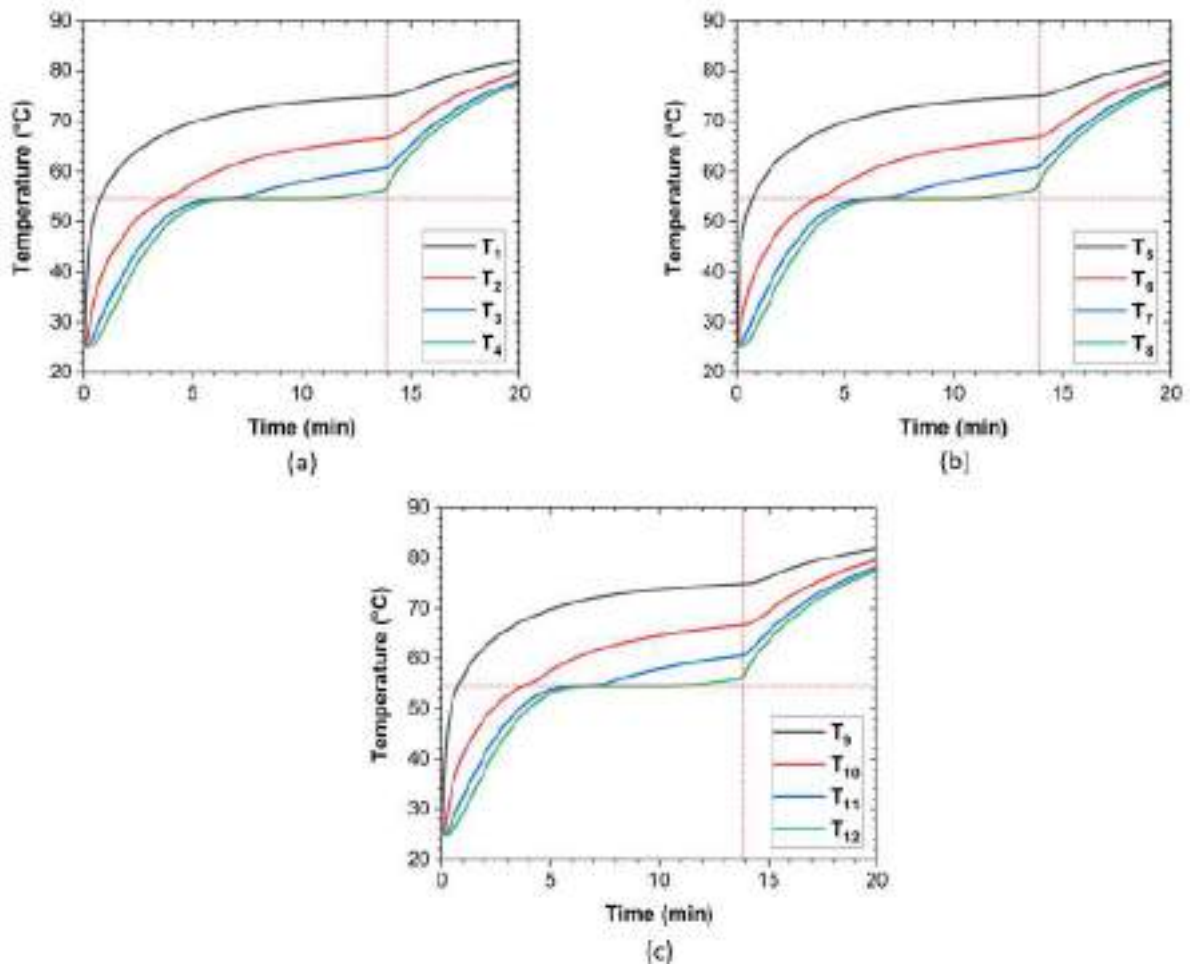


Figure 4. Transient temperature profiles under adiabatic boundary condition for 100 kg/m^3 bulk density

The transient liquid fractions of various convection heat transfer coefficients ($h = 0 \text{ W/m}^2\text{K}$; $h = 5 \text{ W/m}^2\text{K}$; $h = 10 \text{ W/m}^2\text{K}$; $h = 50 \text{ W/m}^2\text{K}$) for two different graphite matrix bulk densities (100 kg/m^3 and 143 kg/m^3) are given in Figure 5. It is shown that a higher convection heat transfer coefficient causes higher total melting times. The total melting times are 13.9 minutes ($h = 0 \text{ W/m}^2\text{K}$ / Adiabatic BC), 14.3 minutes ($h = 5 \text{ W/m}^2\text{K}$), 14.7 minutes ($h = 10 \text{ W/m}^2\text{K}$), and 19.2 minutes ($h = 50 \text{ W/m}^2\text{K}$) for 100 kg/m^3 bulk density, while they are 11.7 minutes ($h = 0 \text{ W/m}^2\text{K}$ / Adiabatic BC), 11.8 minutes ($h = 5 \text{ W/m}^2\text{K}$), 12 minutes ($h = 10 \text{ W/m}^2\text{K}$), and 15 minutes ($h = 50 \text{ W/m}^2\text{K}$) for 143 kg/m^3 bulk density. This is the result of higher heat losses with higher convection heat transfer coefficient values during the thermal energy storage period (or melting period). Moreover, the effect of the convection heat transfer coefficient on total melting time is appreciable for $50 \text{ W/m}^2\text{K}$ compared to lower h values for each bulk density. On the other side, the effect of the convection heat transfer coefficient is lower for a higher bulk density of 143 kg/m^3 compared to 100 kg/m^3 . The heat storage period (total melting time) considering $h = 50 \text{ W/m}^2\text{K}$ and $h = 0 \text{ W/m}^2\text{K}$ cases goes down by 27.6% and 22% for 100 kg/m^3 and 143 kg/m^3 , respectively. Higher bulk density provides more thermal bridges in graphite media, which ensure higher thermal conductance and, therefore, higher thermal diffusivity for TES medium (Table 1). It results in an enhanced thermal energy storage period, minimizing the possible heat losses to the environment.

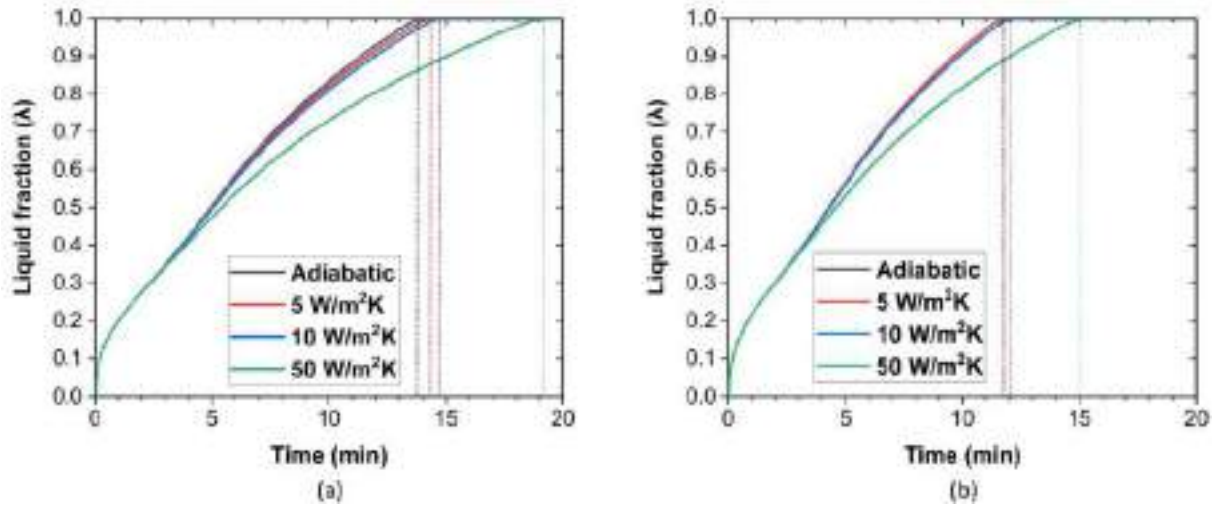


Figure 5. Liquid fraction variations of different convection heat transfer coefficient boundary conditions: for 100 kg/m³ bulk density (a), 143 kg/m³ bulk density (b)

The transient temperature profiles are given in Figure 6. Temperature variations support the liquid fraction curves. Higher temperature values are obtained with higher bulk density for each h value. This is the result of the enhanced heat diffusivity in the storage medium, which contributes to the total melting period. The highest convection heat transfer coefficient value of 50 W/m²K presents lower temperature readings in terms of higher heat losses.

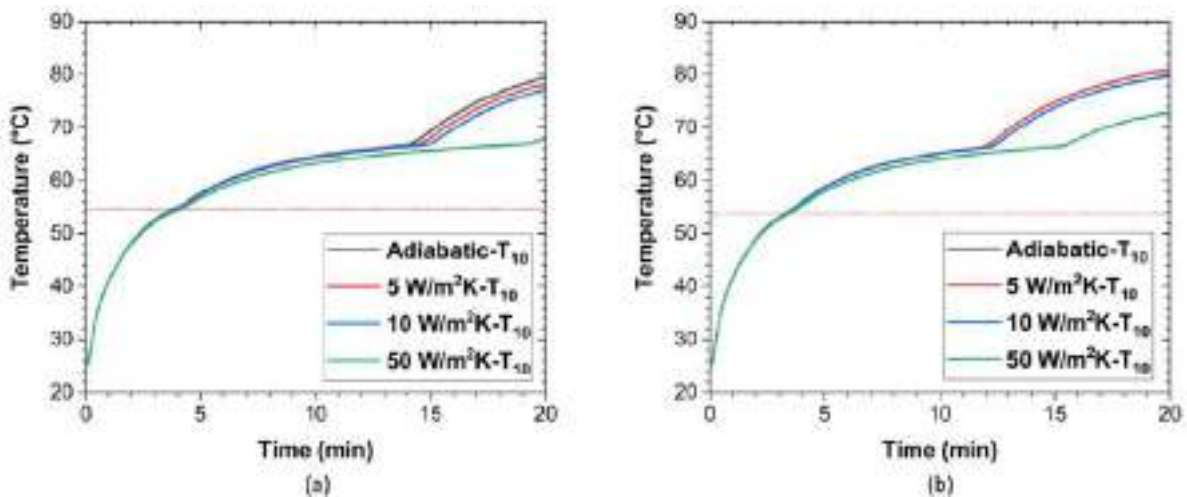


Figure 6. Transient temperature profiles of different boundary conditions and T_{10} points: for 100 kg/m³ bulk density (a), 143 kg/m³ bulk density (b)

The energy storage rate (S) in the thermal energy storage system is formulated as follows:

$$S = \frac{Q}{m \times t} \quad (7)$$

Q , m , and t correspond to stored energy, mass, and total melting time. Figure 7 shows the energy storage rate of the PCM/graphite matrix composite with a bulk density of 100 kg/m³ and 143 kg/m³ under different convection heat transfer coefficient values. The heat storage rate decreases with an increase in convection heat transfer coefficient values for all cases. A higher bulk density case, which ensures higher thermal diffusivity in the medium, shows superior performance. The total thermal energy storage rates considering 50 W/m²K and adiabatic BCs deteriorate by 29% and 23% for 100 kg/m³ and 143 kg/m³, respectively. The effect of bulk density on the energy storage rate is at a level of 6–9% for lower convection heat transfer coefficients (<50 W/m²K), while the impact level of bulk density increases to

15% at 50 W/m²K. It clearly demonstrates the negative impact of operating conditions on storage rates and the importance of thermal insulation in these types of systems.

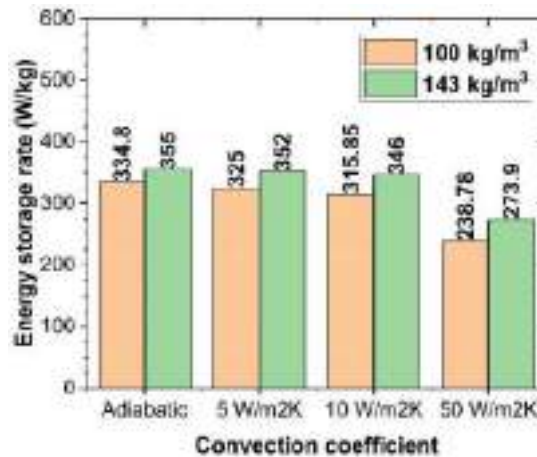


Figure 7. Energy storage rates of PCM/graphite matrix composites under various convection heat transfer coefficients for 100 kg/m³ and 143 kg/m³ bulk densities

4. CONCLUSIONS

This study provides insight on the effect of convection heat transfer coefficient due to forced convection such as air conditioners, fans, and windy weather with different bulk densities (100 and 143 kg/m³) of PCM/graphite matrix and in shell-in-tube geometry. A number of numerical studies are conducted to observe the effects of heat transfer/loss coefficients. The key findings of this investigation can be summarized as follows:

- The main heat transfer mechanism is conduction, and a uniform temperature distribution has been observed in PCM/graphite matrix composites.
- Higher heat transfer coefficient values cause higher total melting times and lower energy storage rates.
- The effect of the convection heat transfer coefficient on total melting time is appreciable for 50 W/m²K compared to lower h values for each bulk density.
- The effect of the convection heat transfer coefficient is lower for a higher bulk density of 143 kg/m³ compared to 100 kg/m³.
- A higher bulk density case, which ensures higher thermal diffusivity, shows superior energy storage rates.
- The effect of bulk density on the energy storage rate is maximum at 9% for lower convection heat transfer coefficients (<50 W/m²K), while the impact level of bulk density increases to 15% at 50 W/m²K.

NOMENCLATURE

BC	: Boundary Condition
CFD	: Computational Fluid Dynamics
EG	: Expanded Graphite
IEA	: International Energy Agency
PCM	: Phase Change Material
TES	: Thermal Energy Storage

REFERENCES

- [1] A. K. Rai, M. M. A *practical approach to design and optimization of single phase liquid to liquid shell and tube heat exchanger*. 1985, 429-437. (2012).
- [2] Ahmed, S. F., Rafa, N., Mehnaz, T., Ahmed, B., Islam, N., Mofijur, M., Hoang, A. T., & Shafiullah, G. M. Integration of phase change materials in improving the performance of heating, cooling, and clean energy storage systems: An overview. *Journal of Cleaner Production*, 364(March), 132639. <https://doi.org/10.1016/j.jclepro.2022.132639>, (2022).
- [3] *International Energy Agency (IEA) World Energy Outlook 2022*. <https://www.iea.org/reports/world-energy-outlook-2022/executive-summary>. (2022).
- [4] Li, Z., Sun, W. G., Wang, G., & Wu, Z. G. Experimental and numerical study on the effective thermal conductivity of paraffin/expanded graphite composite. *Solar Energy Materials and Solar Cells*, 128, 447-455. <https://doi.org/10.1016/J.SOLMAT.2014.06.023>, (2014).
- [5] Ling, Z., Chen, J., Fang, X., Zhang, Z., Xu, T., Gao, X., & Wang, S. Experimental and numerical investigation of the application of phase change materials in a simulative power batteries thermal management system. *Applied Energy*, 121, 104-113. <https://doi.org/10.1016/J.APENERGY.2014.01.075>, (2014).
- [6] Liu, X. H., Ling, Z. Y., Sun, P., Fang, X. M., Xu, T., & Zhang, Z. G. Experimental study and numerical simulation on thermal energy storage characteristics of composite phase change materials in annular space of vertical double-pipe heat exchanger. *Advanced Materials Research*, 1053, 143-149. <https://doi.org/10.4028/WWW.SCIENTIFIC.NET/AMR.1053.143>, (2014).
- [7] Lv, Y., Zhou, W., & Jin, W. Experimental and numerical study on thermal energy storage of polyethylene glycol/expanded graphite composite phase change material. *Energy and Buildings*, 111, 242-252. <https://doi.org/10.1016/J.ENBUILD.2015.11.042>, (2016).
- [8] Mallow, A., Abdelaziz, O., & Graham, S. Thermal charging study of compressed expanded natural graphite/phase change material composites. *Carbon*, 109, 495-504. <https://doi.org/10.1016/J.CARBON.2016.08.030>, (2016).
- [9] Mesalhy, O., Lafdi, K., Elgafy, A., & Bowman, K. Numerical study for enhancing the thermal conductivity of phase change material (PCM) storage using high thermal conductivity porous matrix. *Energy Conversion and Management*, 46(6), 847-867. <https://doi.org/10.1016/J.ENCONMAN.2004.06.010>, (2005).
- [10] Mills, A., Farid, M., Selman, J. R., & Al-Hallaj, S. Thermal conductivity enhancement of phase change materials using a graphite matrix. *Applied Thermal Engineering*, 26(14-15), 1652-1661. <https://doi.org/10.1016/J.APPLTHERMALENG.2005.11.022>, (2006).
- [11] Mitincik, S., & Yazici, M. Y. Numerical study on the thermal energy storage performance of graphite matrix composite with phase change in shell-in-tube: Effects of bulk density and wall temperature. *Journal of Energy Storage*, 72(PA), 108304. <https://doi.org/10.1016/j.est.2023.108304>, (2023).
- [12] Raza, G., Shi, Y., & Deng, Y. Expanded graphite as thermal conductivity enhancer for paraffin wax being used in thermal energy storage systems. *Proceedings of 2016 13th International Bhurban Conference on Applied Sciences and Technology, IBCAST 2016*, 1-12. <https://doi.org/10.1109/IBCAST.2016.7429846>, (2016).
- [13] Song, Y., Zhang, N., Jing, Y., Cao, X., Yuan, Y., & Haghghat, F. Experimental and numerical investigation on dodecane/expanded graphite shape-stabilized phase change material for cold energy storage. *Energy*, 189. <https://doi.org/10.1016/J.ENERGY.2019.116175>, (2019).
- [14] Venkateswarlu, K., & Ramakrishna, K. Recent advances in phase change materials for thermal energy storage-a review. *Journal of the Brazilian Society of Mechanical Sciences and Engineering*, 44(1), 1-17. <https://doi.org/10.1007/s40430-021-03308-7>, (2022).
- [15] Voller, V. R., & Prakash, C. A fixed grid numerical modelling methodology for convection-diffusion mushy region phase-change problems. *International Journal of Heat and Mass Transfer*, 30(8), 1709-1719. [https://doi.org/10.1016/0017-9310\(87\)90317-6](https://doi.org/10.1016/0017-9310(87)90317-6), (1987).
- [16] Xie, M., Huang, J., Ling, Z., Fang, X., & Zhang, Z. Improving the heat storage/release rate and photo-thermal conversion performance of an organic PCM/expanded graphite composite block. *Solar Energy Materials and Solar Cells*, 201. <https://doi.org/10.1016/J.SOLMAT.2019.110081>, (2019).

[17] Yazici, M. Y., Saglam, M., Aydin, O., & Avci, M. Thermal energy storage performance of PCM/graphite matrix composite in a tube-in-shell geometry. *Thermal Science and Engineering Progress*, 23.(2021). <https://doi.org/10.1016/J.TSEP.2021.100915>

[18] Zhang, Z., & Fang, X. (2006). Study on paraffin/expanded graphite composite phase change thermal energy storage material. *Energy Conversion and Management*, 47(3), 303–310. <https://doi.org/10.1016/J.ENCONMAN.2005.03.004>

[19] Zhong, Y., Li, S., Wei, X., Liu, Z., Guo, Q., Shi, J., & Liu, L. (2010). Heat transfer enhancement of paraffin wax using compressed expanded natural graphite for thermal energy storage. *Carbon*, 48(1), 300–304. <https://doi.org/10.1016/J.CARBON.2009.09.03>

¹SAMSUN UNIVERSITY, SAMSUN, 55420, TURKEY

E-mail address: sare.mitincik@samsun.edu.tr

MULTI-OBJECTIVE OPTIMIZATIONS OF CIRCULAR AND SQUARE DUCTS UNDER LAMINAR FLOW AND CONSTANT WALL TEMPERATURE CONDITIONS

MUHAMMET NASIF KURU

0000-0002-5941-1221

ABSTRACT

Optimum parameters of ducts having different cross-sections (circular and square) are explored using multi-objective optimization algorithms in this study. Heat transfer and fluid flow analysis of ducts are done with finite volume method. The flow is assumed as steady, incompressible and laminar. Three different multi-objective problems are investigated for each cross-section, i.e. (1) maximization of heat transfer (\dot{Q}) and minimization of pressure drop (ΔP), (2) maximization of heat transfer (\dot{Q}) and minimization of entropy generation (\dot{S}_{gen}), (3) minimizations of volume (V) and pumping power (\dot{W}_{pump}). Air is used as a working fluid, inlet and wall temperatures are given and constant. Three optimization variables are used which are hydraulic diameter (D_h), duct length (L) and inlet velocity (V_{in}). Optimum parameters of different multi-objective optimization problems are obtained and comparisons are done in detail. The effect of optimization variables on the objective functions are also discussed. It can be inferred that optimum parameters of ducts (circular and square) can be determined according to the design objectives. Moreover, optimum parameters differ from each other.

1. INTRODUCTION

Yilmaz [1] studied entropy generation for developing hydrodynamically and thermally flow in circular duct where laminar flow and constant wall temperature are assumed. He derived analytical formulations that gave minimum entropy generation value which was used to obtain optimum dimensions of circular duct for the given inlet and wall temperature.

Jarungthammachote [2] investigated the entropy generation in the hexagonal duct for fully developed laminar flow and constant heat flux. It was found that hexagonal duct has lower and higher dimensionless entropy generation values as compared to rectangular and circular ones, respectively for the same cross-sectional area and hydraulic diameter assumptions.

Kucuk [3] carried out a numerical study in the concentric curved annular ducts with square cross-sectional area where the flow is laminar, incompressible, hydrodynamically and thermally fully developed under constant wall temperature.

Leong and Ong [4] used circular, square and equilateral triangle ducts to enhance the thermal performance under constant heat flux condition. The working fluids are Al_2O_3 and MWCNT based nanofluids. It was found that circular duct has lower total entropy generation as compared to other

Date: July, 8, 2023.

Key words and phrases. Multi-objective optimization, circular and square ducts, laminar flow.

studied cross-sections. They also reported that MWCNT based water nanofluids have lower total entropy generation with respect to Al_2O_3 one, this was attributed to the higher thermal conductivity of MWCNT.

Demirel [5] optimized the convective heat transfer in a packed duct using the first and second laws of thermodynamics where the wall temperature was taken constant. He concluded that convective heat transfer may be enhanced using suitable operating conditions and design parameters.

Oztop [6] obtained entropy generation using analytically for semi-circular ducts where the flow is laminar and constant heat flux is assumed at the duct surface. It was stated that increasing the cross-sectional area led to increase in total entropy generation for the same Reynolds number.

Sahin [7] studied analytically the entropy generation in a smooth duct at constant wall temperature where the flow is turbulent and fully developed. If the viscosity was taken constant, entropy generation values were inconsequentially for viscous fluids. However, constant viscosity assumption gave reasonable values.

Tokgoz et al. [8] determined the characteristics of flow and thermal efficiency for corrugated ducts using numerical and experimental methods. Reynolds number were in the range of 3000 to 6000. Aspect ratios (S/H) were 0.1, 0.2 and 0.3. It was found that heat transfer increases with the increment in aspect ratio and the turbulence intensity get higher for the increasing of corrugation height.

Yilmaz et al. [9] obtained optimum shape and dimensions of ducts for the prescribed pressure loss that gave maximum heat transfer in laminar flow regime. They derived analytical formulations in order to calculate optimum values.

In this work, optimum geometrical dimensions and working condition of circular and square ducts were investigated using multi-objective optimization algorithms. Parametric model of ducts and numerical solutions were obtained using Ansys Workbench software. For the optimization studies, genetic algorithm tool of Modefrontier commercial optimization driver was used in order to obtain optimum values. Optimum parameters of different multi-objective optimization problems are obtained and comparisons are done in detail.

2. MATHEMATICAL MODEL, SOLUTION PROCEDURE, DATA ANALYSIS

The flow is laminar, steady and incompressible. Based on the assumptions, governing equations for continuity, momentum and energy are expressed below [10] :

Continuity Equation:

$$\frac{\partial u_i}{\partial x_i} = 0 \quad (1)$$

Momentum Equation:

$$\rho \frac{\partial}{\partial x_j} (u_i u_j) = -\frac{\partial p}{\partial x_i} + \frac{\partial}{\partial x_j} \left(\mu \frac{\partial u_i}{\partial x_j} \right) \quad (2)$$

Conservation of Energy:

$$\rho u_j \frac{\partial T}{\partial x_j} = \frac{\partial}{\partial x_j} \left[\frac{\mu}{Pr} \frac{\partial T}{\partial x_j} \right] \quad (3)$$

Air is used as a working fluid, inlet and wall temperatures are given as $T_{in} = 22 \text{ }^\circ\text{C}$ and $T_{wall} = 28 \text{ }^\circ\text{C}$, respectively. Isometric view and dimensions of circular and square ducts are given in Figure 1.

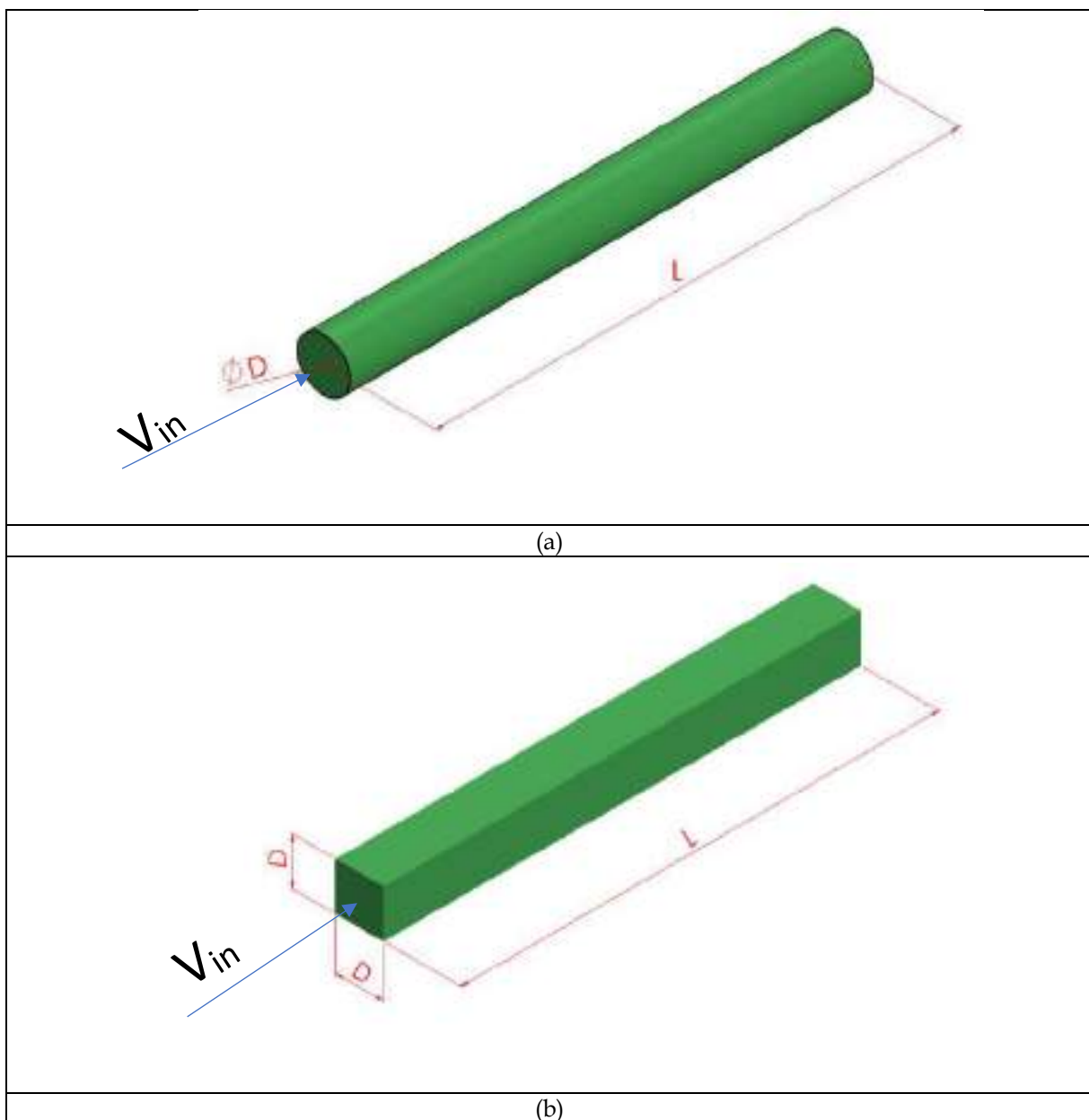


Figure 1. Isometric view and dimensions of (a) circular (b) square ducts

Three-dimensional mesh and front view of mesh are shown in Figure 2a and 2b, respectively. Mesh independence studies were also carried out for four mesh structures for both ducts and appropriate mesh size was chosen for numerical analysis. Boundaries of ducts are illustrated in Figure 2c where uniform inlet is chosen for inlet boundary, constant wall temperature is assigned to wall boundary, pressure outlet is given for outlet boundary condition.

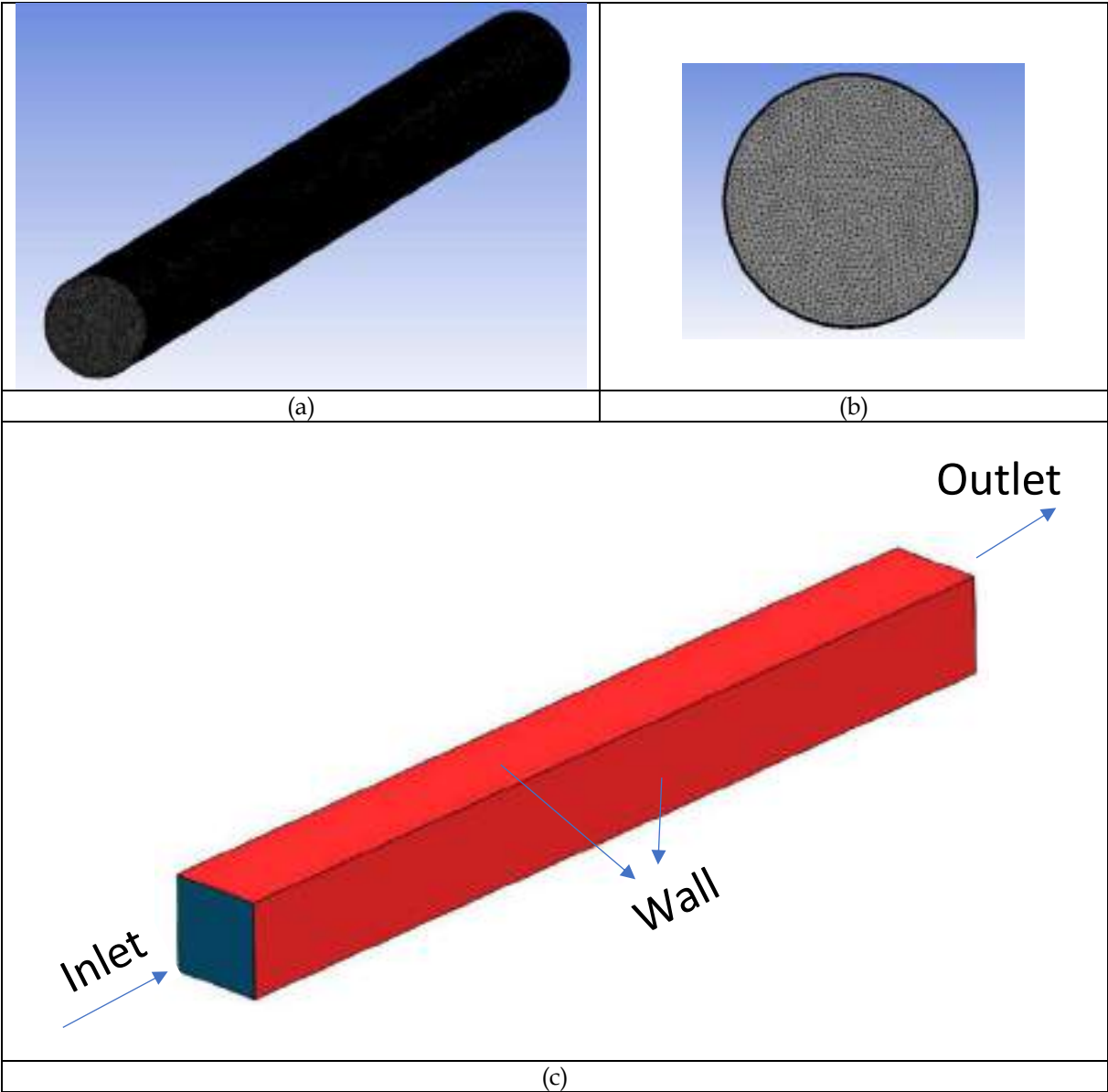


Figure 2. (a) Three-dimensional mesh (b) front view of mesh (c) boundaries of square duct

Reynolds number (Re)

Reynolds number is given as

$$Re = \frac{\rho V_{in} D_h}{\mu} \quad (4)$$

where D_h is the square duct's hydraulic diameter calculated from

$$D_h = \frac{4 H_{duct} W_{duct}}{2 (H_{duct} + W_{duct})} \quad (5)$$

Pressure Drop (ΔP)

Pressure drop is obtained from the difference of inlet, P_{in} and outlet, P_{out} pressure values

$$\Delta P = P_{in} - P_{out} \quad (6)$$

Entropy Generation (\dot{S}_{gen})

The entropy generation is calculated with Bejan's formula [11]

$$\dot{S}_{gen} = \frac{\dot{Q} (T_{wall} - T_{in})}{T_{in}^2} + \frac{\Delta P V_{in} A_{ch}}{T_{in}} \quad (7)$$

Pumping Power (\dot{W}_{pump})

The pumping power is computed using cross-sectional area of the duct A_{ch} as follows:

$$\dot{W}_{pump} = V_{in} A_{ch} \Delta P \quad (8)$$

Volume ($Volume$)







The volume of duct is calculated as follows:

$$Volume = A_{ch} L \quad (9)$$

3. OPTIMIZATION PROBLEMS

Three different multi-objective problems are investigated for each cross-section, i.e. (1) maximization of heat transfer (\dot{Q}) and minimization of pressure drop (ΔP), (2) maximization of heat transfer (\dot{Q}) and minimization of entropy generation (\dot{S}_{gen}), (3) minimizations of volume (V) and pumping power (\dot{W}_{pump}). Three optimization variables are used which are hydraulic diameter (D_h), duct length (L) and

inlet velocity (V_{in}). Each optimization variable is bounded with lower and upper values and step sizes are also given. The multi-objective optimization problems for three cases are formulated as follows:

Case-1		Case-2		Case-3	
					
Objective Functions					
Maximize \dot{Q} Minimize ΔP		Maximize \dot{Q} Minimize \dot{S}_{gen}		Minimize $Volume$ Minimize \dot{W}_{pump}	
Optimization Variables					
$1\text{ m/s} \leq V_{in} \leq 6\text{ m/s}, step = 0.5\text{ m/s}$					
$3\text{ mm} \leq D \leq 7\text{ mm}, step = 1\text{ mm}$					
$50\text{ mm} \leq L \leq 100\text{ mm}, step = 5\text{ mm}$					

The optimization flowchart is shown in Figure 3. The optimization process is started with the definition of the design of experiments. In this study, multi-objective genetic algorithm (MOGA) is used for optimization runs. MOGA is coupled with Ansys Workbench program which is used for geometry and mesh creation, numerical computation. Python scripting language is utilized for post-processing of the results. The optimization workflow is drawn with Modefrontier which is shown in Figure 4.

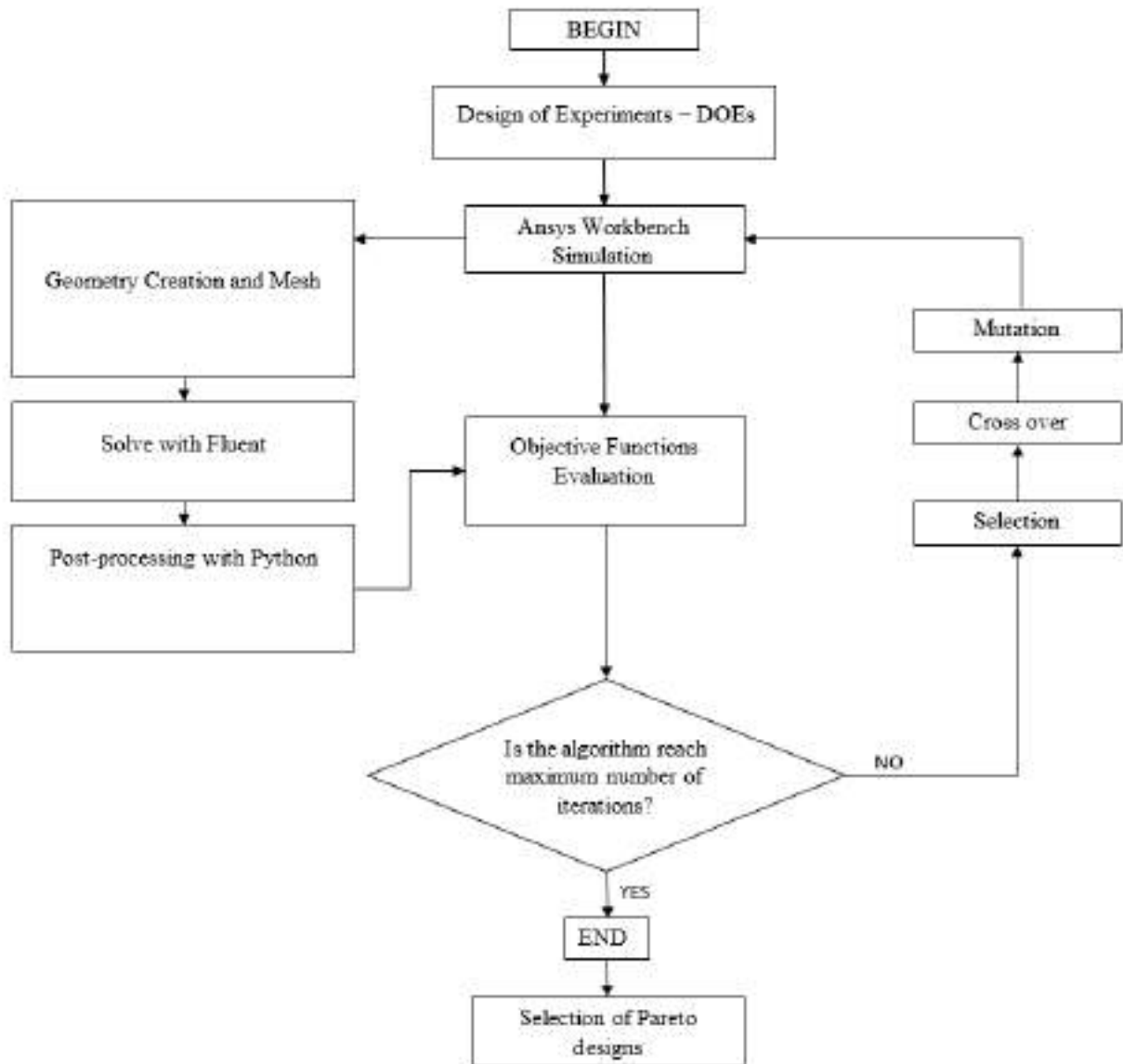


Figure 3. Optimization flowchart

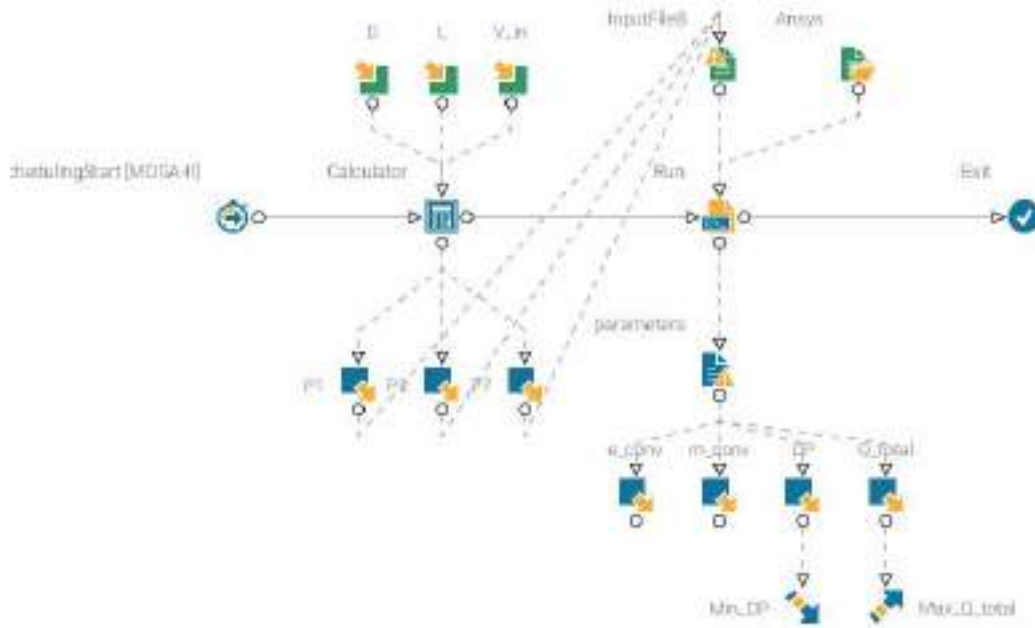
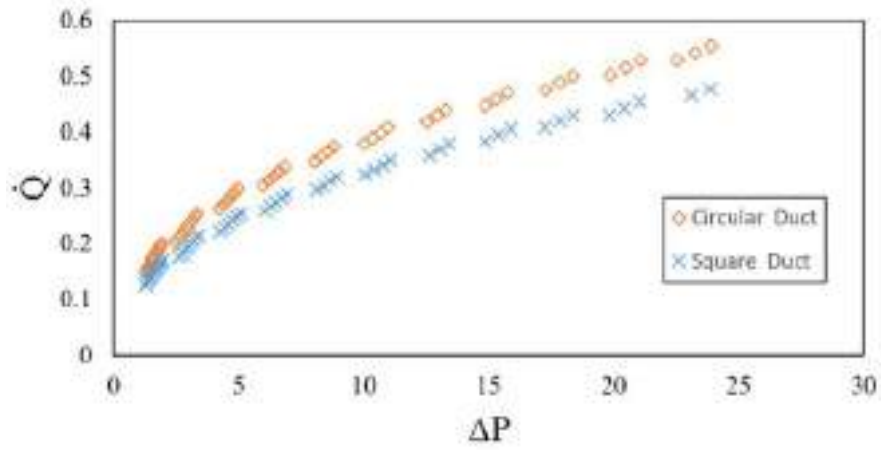


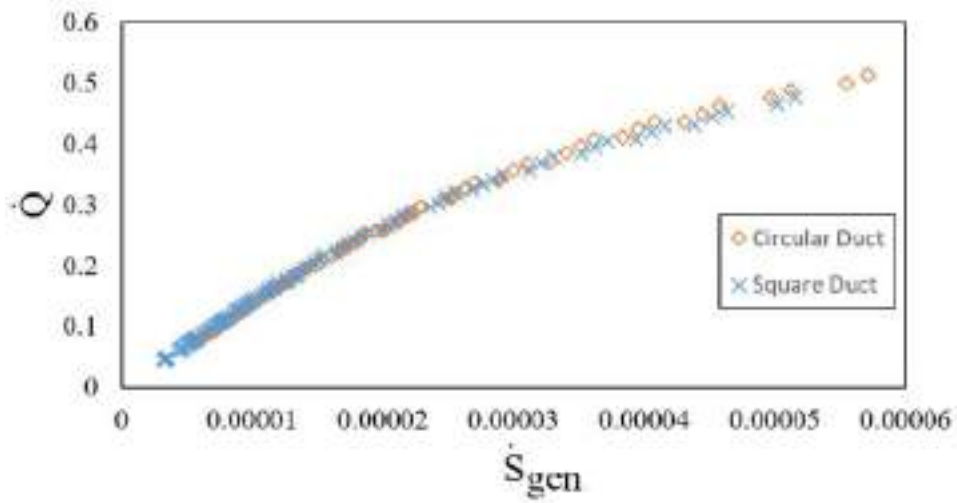
Figure 4. Optimization workflow

4. RESULTS

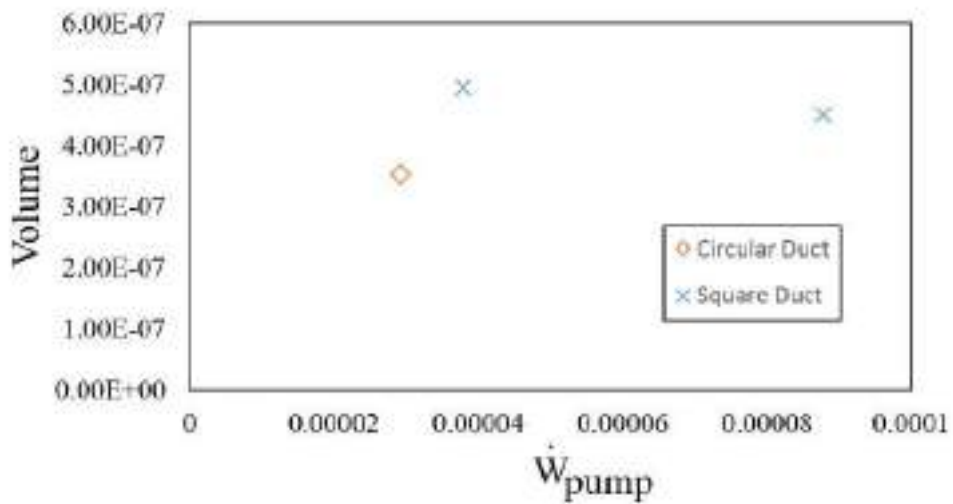
Discussions of the results of multi-objective optimization studies for three cases are done in this section. Comparisons of pareto designs for \dot{Q} vs. ΔP , \dot{Q} vs. \dot{S}_{gen} and $Volume$ vs. \dot{W}_{pump} are given in Figure 5. For the higher heat transfer values \dot{Q} , pressure drop ΔP is also high. It can be seen that higher heat transfer values are obtained for circular ducts as compared to square ducts. Moreover, entropy generation values are nearly same for both duct geometries. For case-3, square duct optimization study has two pareto designs and circular duct has one pareto design.



(a)



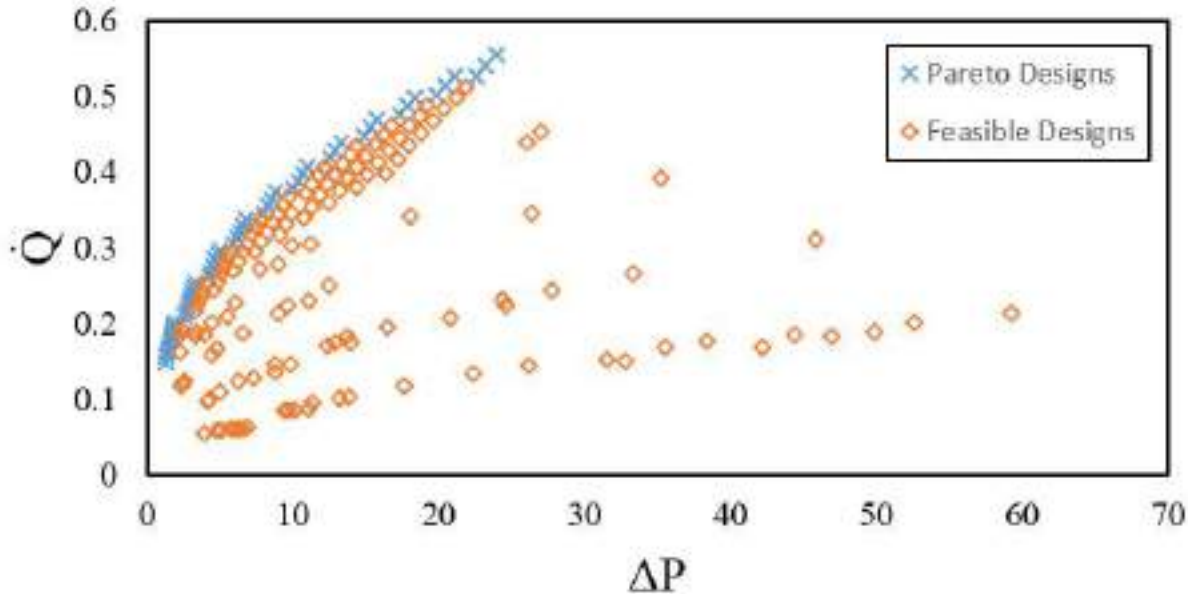
(b)



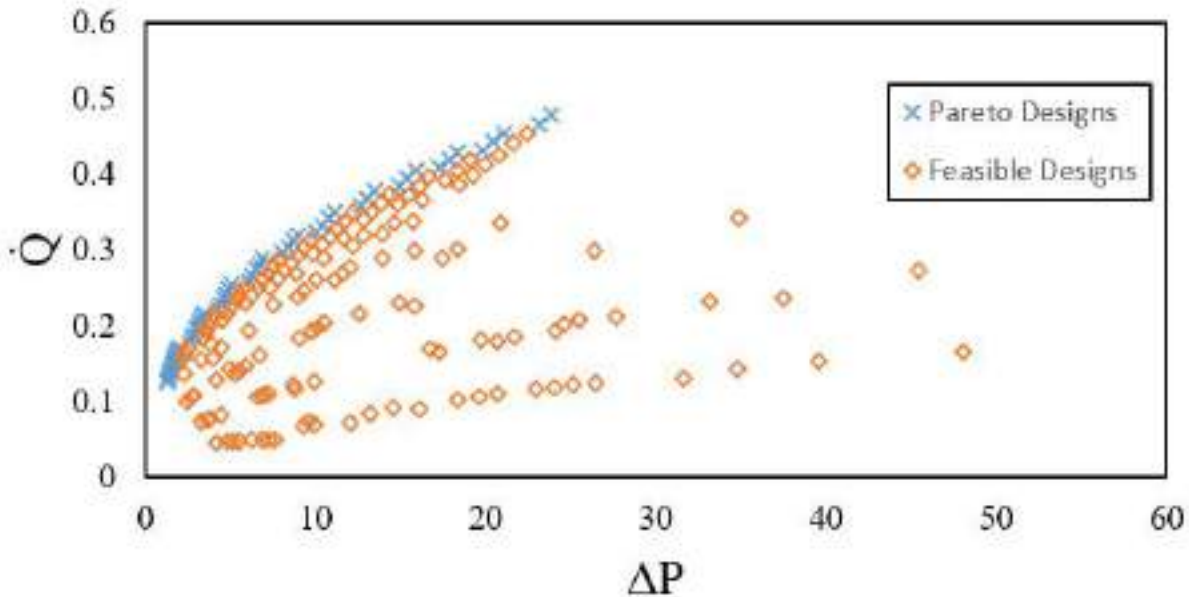
(c)

Figure 5. Pareto designs comparisons of (a) \dot{Q} vs. ΔP (b) \dot{Q} vs. \dot{S}_{gen} (c) *Volume* vs. \dot{W}_{pump} , (units are given in nomenclature)

\dot{Q} vs. ΔP of pareto and feasible designs for circular and square duct optimization studies are presented in Figure 6. Optimization algorithm reaches nearly maximum ΔP of 60 Pa for circular duct and 48 Pa for square duct. The design numbers for both duct studies are closely same. For the studied optimization variables maximum heat transfer is obtained as 0.55 W for circular duct where the optimization variables have the maximum values ($V_{in} = 6 \text{ m/s}$, $D = 7 \text{ mm}$, $L = 100 \text{ mm}$).



(a)



(b)

Figure 6. \dot{Q} vs. ΔP of pareto and feasible designs for (a) circular (b) square duct optimization studies, (units are given in nomenclature)

Nomenclature

D : diameter, m

D_h : hydraulic diameter, m

ΔP : pressure drop, Pa

L : duct length, m

Re : Reynolds number

\dot{Q} : heat transfer, W

\dot{S}_{gen} : entropy generation, W/K

T_{in} : inlet temperature, °C, K

V_{in} : inlet velocity, m/s

\dot{W}_{pump} : pumping power, W

REFERENCES

- [1] A. Yilmaz, Minimum entropy generation for laminar flow at constant wall temperature in a circular duct for optimum design, *Heat Mass Transf.* 45 1415–1421. <https://doi.org/10.1007/s00231-009-0519-4>, (2009).
- [2] S. Jarunthammachote, Entropy generation analysis for fully developed laminar convection in hexagonal duct subjected to constant heat flux, *Energy*. 35 5374–5379. <https://doi.org/10.1016/j.energy.2010.07.020>, (2010).
- [3] H. Kucuk, Numerical analysis of entropy generation in concentric curved annular ducts, *J. Mech. Sci. Technol.* 24 1927–1937. <https://doi.org/10.1007/s12206-010-0629-4>, (2010).
- [4] K.Y. Leong, H.C. Ong, Entropy generation analysis of nanofluids flow in various shapes of cross section ducts, *Int. Commun. Heat Mass Transf.* 57 72–78. <https://doi.org/10.1016/j.icheatmasstransfer.2014.07.017>, (2014).
- [5] Y. Demirel, S. Arabm, Pergamon o~,o-s,m(gs)ooo~.x, 20 959–967, (1995).
- [6] H.F. Oztop, Effective parameters on second law analysis for semicircular ducts in laminar flow and constant wall heat flux, *Int. Commun. Heat Mass Transf.* 32 266–274. <https://doi.org/10.1016/j.icheatmasstransfer.2004.05.018>, (2005).
- [7] A.Z. Şahin, A second law comparison for optimum shape of duct subjected to constant wall temperature and laminar flow, *Heat Mass Transf.* 33 425–430. <https://doi.org/10.1007/s002310050210>, (1998).
- [8] N. Tokgoz, M.M. Aksoy, B. Sahin, Investigation of flow characteristics and heat transfer enhancement of corrugated duct geometries, *Appl. Therm. Eng.* 118 518–530. <https://doi.org/10.1016/j.applthermaleng.2017.03.013>, (2017).
- [9] A. Yilmaz, M.T. Erdinç, T. Yilmaz, Optimization of crossflow staggered tube banks for prescribed pressure loss and effectiveness, *J. Thermophys. Heat Transf.* 31 878–888. <https://doi.org/10.2514/1.T5033>, (2017).
- [10] W. FM, *Viscous Fluid Flow*, Second Edition, McGraw-Hill, New York, 1991.
- [11] A. Bejan, *Entropy generation minimization*, CRC press Boca Raton, FL, 1995. <http://www.crcpress.com/product/isbn/9780849396519>.

TARSUS UNIVERSITY, VOCATIONAL SCHOOL OF TECHNICAL SCIENCES AT MERSIN TARSUS ORGANIZED
INDUSTRIAL ZONE, MACHINERY PROGRAM, 33400, TARSUS/MERSIN, TURKEY
Email address: mnasifkuru@tarsus.edu.tr

IFSCOM-E 2023
9TH IFS AND CONTEMPORARY MATHEMATICS AND ENGINEERING CONFERENCE
8-11 JULY 2023, TARSUS, MERSİN, TÜRKİYE
ISBN: 978-605-68670-8-8
pp: 200-204

CONTRA CONTINUITY FOR λ -STRONG β -I-CLOSED SETS

SEYFETTİN FIDAN and AYNUR KESKİN KAYMAKCI

0009-0009-2680-7420 and 0000-0001-5909-8477

ABSTRACT

In this paper we investigate the notion of λ -strong β -I-open sets which are complement of λ -strong β -I-closed sets. Then, defining types of contra continuity for λ -strong β -I-closed sets we will give properties and characterizations of them. We investigate the relationships among the other functions with it.

1.INTRODUCTION

Kuratowski[6] defined the concept of local function of a set via ideal and topology. It is known that this notion is a generalization of the closure of a set. Let (X, τ) be a topological space and I is an ideal on X . Then, the local function of a subset of X with respect to I and τ is denoted by $A^*(I, \tau)$ (briefly A^*) and defined as the following. $A^* = \{x \in X \mid \forall U \in \tau(x), (U \cap A) \notin I\}$ ($\exists \tau(x) = \{U \in \tau \mid x \in U\}$). Jankovic and Hamlett[5] introduced a new Kuratowski closure operator cl^* using local function and obtained a new topology was denoted by τ^* after then τ . They called ideal topological space for (X, τ, I) . Obvious that they used the notions ideal and topology to obtain a new topology. Hatir, Keskin and Noiri[4] defined the concept of strong β -I-open set and used it to establish some decompositions of generalized continuity. Arenas[1] focused on λ -sets. Recently, Tekin and Kaymakci[6] used the class of strong β -I-open sets to define and study the notions $\lambda_{s\beta I}$ -sets and $\lambda_{s\beta I}$ -closed sets. In particular using these notions they characterized the $s\beta$ -I- T_1 spaces and strong β -I- $T_{1/2}$ -spaces. Besides, they used the (strong β -I- T_1) class of $\lambda_{s\beta I}$ -closed sets to define and characterize new types of continuity called $\lambda_{s\beta I}$ -continuous, quasi $\lambda_{s\beta I}$ -continuous and λ_I -irresolute functions. On the other hand; Arenas, Dontchev and Ganster[1] studied on λ -closed sets and obtain a dual of continuity. Caldas, Ekici, Jafari and Noiri[2] introduced contra continuity for λ -closed sets. Besides; Granadas, Sanabria, Rosas and Carpintero[3] defined contra $\lambda_{s\beta I}$ -continuous functions.

In this work, we investigate the notion of λ -strong β -I-open sets which are complement of λ -strong β -I-closed sets. Then, defining types of contra continuity for λ -strong β -I-closed sets we will give properties and characterizations of them. We investigate the relationships among the other functions with it.

Date: July, 8, 2023.

2000 Mathematics Subject Classification. Primary 54 C08; Secondary 54 D10.

Key words and phrases. strong β -I-open, λ -strong β -I-closed set, λ -strong β -I-open set, λ -strong β -I-contra continuous functions.

2. PRELIMINARIES

Throughout this paper, $\text{Int}(A)$ and $\text{Cl}(A)$ denote the interior and the closure of a subset A of a topological space (X, τ) , respectively. Also $\wp(X)$ denote the power set of X . An ideal I on X is a nonempty subfamily of $\wp(X)$ which satisfies the following conditions:

If $A \subset B$ and $B \in I$, then $A \in I$.

If $A, B \in I$ then $(A \cup B) \in I$.

Some well-known types of ideals on topological space (X, τ) , are the family of all nowhere dense subsets of X , the family of all closed and discrete subsets of X and the family of all meager subsets of X . In the sequel, (X, τ, I) (or simply X) denote a topological space (X, τ) with an ideal I on X , which is simply called an ideal space. Given an ideal space (X, τ, I) and a subset A of X , the local function of A with respect to I and τ is defined as $A^* = \{x \in X \mid \forall U \in \tau(x), (U \cap A) \notin I\}$ ($\exists \tau(x) = \{U \in \tau \mid x \in U\}$). When there is no chance for confusion, we will simply write A^* instead of a $A^*(I, \tau)$. It is a well known fact that $\text{Cl}^*(A) = A \cup A^*$ is a Kuratowski closure operator and hence, $\tau^*(I, \tau) = \{U \subset X : \text{Cl}^*(X - U) = X - U\}$ is a topology on X , which is finer than τ . If there is no chance to confusion, we will write τ^* instead $\tau^*(I, \tau)$.

The members of τ^* are called τ^* -open sets and their complements are called τ^* -closed sets. It is easy to see that a subset A of X is τ^* -closed if and only if $A^* \subset A$. According to [4], $A \subset X$ is strong β - I -open if $A \subset \text{Cl}^*(\text{Int}(\text{Cl}^*(A)))$. The family of all strong β - I -open sets of X is denoted by $s\beta\mathcal{O}(X, \tau)$ and the complement of a strong β - I -open set is called strong β - I -closed set. As in [7], we say that $A \subset X$ is a $\lambda^{s\beta}_I$ -set if $A = \lambda^{s\beta}_I(A)$, where $\lambda^{s\beta}_I(A)$ is the intersection of all strong β - I -open subsets of X containing A . Besides, according to [7], we say that $A \subset X$ is $\lambda^{s\beta}_I$ -closed if $A = L \cap F$, where L is a $\lambda^{s\beta}_I$ -set and F is a τ^* -closed set.

The complement of a $\lambda^{s\beta}_I$ -closed set is called $\lambda^{s\beta}_I$ -open. We have the following results.

Lemma 2.1. ([7]) Every τ^* -open set is $\lambda^{s\beta}_I$ -open.

Lemma 2.2. ([7]) Let $\{A_\alpha : \alpha \in \Delta\}$ be a collection of a subsets of a space (X, τ, I) . If A_α is a $\lambda^{s\beta}_I$ -open set for each $\alpha \in \Delta$, then $\bigcup \{A_\alpha : \alpha \in \Delta\}$ is $\lambda^{s\beta}_I$ -open set.

Definition 1.1. ([3]) A function $f: (X, \tau, I) \rightarrow (Y, \sigma, J)$ is called

- 1) Contra Λ s I -continuous, if $f^{-1}(V)$ is a Λ s I -closed subset of X for each open set V of Y .
- 2) Contra quasi- Λ s I -continuous, if $f^{-1}(V)$ is a Λ s I -closed subset of X for σ^* -open subset V of Y .
- 3) Contra Λ s I -irresolute if $f^{-1}(V)$ is a Λ s I -closed subset of X for each Λ s J -open subset V of Y .

Definition 2.2. ([7]) A function $f: (X, \tau, I) \rightarrow (Y, \sigma, J)$ is called:

- 1) $\lambda^{s\beta}_I$ -continuous, if $f^{-1}(V)$ is a $\lambda^{s\beta}_I$ -open subset of X for each open subset V of Y .
- 2) Quasi- $\lambda^{s\beta}_I$ -continuous, if $f^{-1}(V)$ is a $\lambda^{s\beta}_I$ -open subset of X for each σ^* -open set V of Y .
- 3) $\lambda^{s\beta}_I$ -irresolute, if $f^{-1}(V)$ is a $\lambda^{s\beta}_I$ -open subset of X for each $\lambda^{s\beta}_I$ -open subset V of Y .

Definition 3.1. A function $f: (X, \tau, I) \rightarrow (Y, \sigma, J)$ is called:

- 1) Contra $\lambda^{s\beta}_I$ -continuous, if $f^{-1}(V)$ is a $\lambda^{s\beta}_I$ -closed subset of X for each open set V of Y .
- 2) Contra quasi- $\lambda^{s\beta}_I$ -continuous, if $f^{-1}(V)$ is a $\lambda^{s\beta}_I$ -closed subset of X for σ^* -open subset V of Y .
- 3) Contra $\lambda^{s\beta}_I$ -irresolute, if $f^{-1}(V)$ is a $\lambda^{s\beta}_I$ -closed subset of X for each $\lambda^{s\beta}_I$ -open subset V of Y .

3. CONTRA CONTINUOUS FUNCTIONS FOR Λ -STRONG B - I -CLOSED SETS

In this section, we introduce and study certain types of contra continuity in terms of Λ s I -closed sets. We establish some relationships and characterizations for these new classes for functions. Next we consider a function f defined from an ideal space (X, τ, I) to an ideal space (Y, σ, J) . First, we present the definitions and characterizations of some variants of continuity due to Sanabria at all [7].

Definition 3.1. A function $f:(X,\tau,I)\rightarrow(Y,\sigma,J)$ is called:

- 1) Contra $\lambda^{s\beta}_I$ -continuous, if $f^{-1}(V)$ is a $\lambda^{s\beta}_I$ -closed subset of X for each open set V of Y .
- 2) Contra quasi- $\lambda^{s\beta}_I$ -continuous, if $f^{-1}(V)$ is a $\lambda^{s\beta}_I$ -closed subset of X for σ^* - open subset V of Y .
- 3) Contra $\lambda^{s\beta}_I$ -irresolute, if $f^{-1}(V)$ is a $\lambda^{s\beta}_I$ -closed subset of X for each $\lambda_{s\beta J}$ -open subset V of Y .

Theorem 3.1. Let $f:(X,\tau,I)\rightarrow(Y,\sigma,J)$ be a function. The following statements hold:

- 1) If f is contra $\lambda^{s\beta}_I$ -irresolute, then it is contra quasi- $\lambda^{s\beta}_I$ -continuous.
- 2) If f is contra quasi- $\lambda^{s\beta}_I$ -continuous, then it is contra $\lambda^{s\beta}_I$ -continuous.

Proof. (1) Let V be any σ^* - open subset of Y . We have V is a $\lambda_{s\beta J}$ -open subset of Y and since f is contra $\lambda^{s\beta}_I$ -irresolute, it follows that $f^{-1}(V)$ is a $\lambda^{s\beta}_I$ -closed subset of X . Therefore, f is contra quasi- $\lambda^{s\beta}_I$ -continuous.

(2) Let V be any open subset of Y . Then, we have V is σ^* - open subset of Y . Since f is contra quasi- $\lambda^{s\beta}_I$ -continuous, it follows that $f^{-1}(V)$ is a $\lambda^{s\beta}_I$ -closed subset of X . This shows that f is $\lambda^{s\beta}_I$ -continuous.

Corollary 3.1. Let $f:(X,\tau,I)\rightarrow(Y,\sigma,J)$ be a function. If f is contra $\lambda^{s\beta}_I$ -irresolute, then it is contra $\lambda^{s\beta}_I$ -continuous.

Proof. The proof obtaine from Theorem 3.1.

According to Theorem 3.1, we have the following diagram.

contra $\lambda^{s\beta}_I$ -irresolute \rightarrow contra quasi- $\lambda^{s\beta}_I$ -continuous \rightarrow contra $\lambda^{s\beta}_I$ -continuous

Remark 3.1. The converses of implications of Diagram I are not true in generally as shown the next examples.

Example 3.1. Let (X,τ,I) and (Y,σ,J) be two ideal topological spaces such that $X=Y= \{a,b,c\}$, $\tau= \{\emptyset,X,\{a,c\}\}$, $\sigma=\{\emptyset,X,\{a,c\},\{b\}\}$, $I=\{\emptyset,\{b\}\}$ and $J=\{\emptyset,\{a\}\}$. Then, we have the identity function and $f:(X,\tau,I)\rightarrow(Y,\sigma,J)$ is contra $\lambda_{s\beta I}$ - continuous. Since $f^{-1}(\{c\})$ and $f^{-1}(\{b,c\})$ are not $\lambda_{s\beta I}$ -closed subsets of X , but is not contra quasi $\lambda_{s\beta I}$ -continuous.

Example 3.2. Let (X,τ,I) and (Y,σ,J) be two ideal topological spaces such that $X=Y= \{a,b,c\}$, $\tau= \{\emptyset,X,\{b,c\}\}$, $\sigma=\{\emptyset,X,\{a,c\},\{b\}\}$, $I=\{\emptyset,\{a\}\}$ and $J=\{\emptyset,\{a\}, \{a,c\}\}$. Then we have the identity function and $f:(X,\tau,I)\rightarrow(Y,\sigma,J)$ is contra $\lambda_{s\beta I}$ - continuous, but is not contra quasi $\lambda_{s\beta I}$ -continuous because $f^{-1}(\{c\})$ and $f^{-1}(\{b,c\})$ are not $\lambda_{s\beta I}$ -closed subsets of X .

Theorem 3.2. Let (Y,σ) be any T_0 -space and $f:(X,\tau,I)\rightarrow(Y,\sigma)$ be a function. If contra $\lambda_{s\beta I}$ -continuous function f is constant, then (X,τ,I) is a $\lambda_{s\beta I}$ -connected space.

Proof. Suppose that (X,τ,I) does not is a $\lambda_{s\beta I}$ -connected space and contra $\lambda_{s\beta I}$ -continuous function $f:(X,\tau,I)\rightarrow(Y,\sigma)$ is constant. By [7, Theorem 3.4], there exists a proper nonempty subset A of X which is both $\lambda_{s\beta I}$ -open and $\lambda_{s\beta I}$ -closed. Let $Y=\{a,b\}$ endowed with the topology $\sigma=\{Y, \emptyset,\{a\},\{b\}\}$. If $f:(X,\tau,I)\rightarrow(Y,\sigma)$ is a function such that $f(A)=\{a\}$ and $f(X-A)=\{b\}$, then f is non constant contra $\lambda_{s\beta I}$ -continuous function and (Y,σ) is T_0 -space, which contradicts the hypothesis. Therefore, (X,τ,I) is a $\lambda_{s\beta I}$ -connected space.

Theorem 3.3. If $f:(X,\tau,I)\rightarrow(Y,\sigma)$ is a closed injective contra $\lambda_{s\beta I}$ -continuous function and (Y,σ) is an ultra normal space, then (X,τ,I) is a $\lambda_{s\beta I}$ -normal space.

Proof. Let A and B be two disjoint closed subsets of X . Since f is closed injective, $f(A)$ and $f(B)$ are disjoint closed subsets of Y . Besides as (Y, σ) is an ultra normal space, there exists two disjoint closed subsets U and V of Y such that $f(A) \subset U$ and $f(B) \subset V$. Moreover according to hypothesis since f is contra $\lambda_{\sigma\beta\Gamma}$ -continuous it follows that $f^{-1}(U)$ and $f^{-1}(V)$ are disjoint $\lambda_{\sigma\beta\Gamma}$ -closed subsets of X such that $A \subset f^{-1}(U)$ and $B \subset f^{-1}(V)$. This shows that (X, τ, I) is a $\lambda_{\sigma\beta\Gamma}$ -normal space.

In the next three theorems, we give some characterizations of contra $\lambda^{\sigma\beta\Gamma}$ -continuous, contra quasi- $\lambda^{\sigma\beta\Gamma}$ -continuous and contra $\lambda^{\sigma\beta\Gamma}$ -irresolute functions, respectively.

Theorem 3.4. For a function $f:(X, \tau, I) \rightarrow (Y, \sigma, J)$, the following statements are equivalent:

- 1) f is contra $\lambda^{\sigma\beta\Gamma}$ -continuous.
- 2) $f^{-1}(B)$ is a $\lambda^{\sigma\beta\Gamma}$ -open subset of X for each closed subset B of Y .
- 3) For each $x \in X$ and each closed subset B of Y containing $f(x)$, there exists a $\lambda^{\sigma\beta\Gamma}$ -open subset U of X such that $x \in U$ and $f(U) \subset B$.

Proof. (1) \Rightarrow (2) Let B any closed subset of Y . Then $V = Y - B$ is an open subset of Y and, as f is contra $\lambda^{\sigma\beta\Gamma}$ -continuous, $f^{-1}(V)$ is a $\lambda^{\sigma\beta\Gamma}$ -closed subset of X . Since $f^{-1}(V) = f^{-1}(Y - B) = f^{-1}(Y) - f^{-1}(B) = X - f^{-1}(B)$, we conclude that $f^{-1}(B)$ is a $\lambda^{\sigma\beta\Gamma}$ -open subset of X .

(2) \Rightarrow (1) Let V any open subset of Y . Then $B = Y - V$ is a closed subset of Y and, by hypothesis, $f^{-1}(B)$ is a $\lambda^{\sigma\beta\Gamma}$ -open subset of X . Since $f^{-1}(B) = f^{-1}(Y - V) = f^{-1}(Y) - f^{-1}(V) = X - f^{-1}(V)$, we obtain that $f^{-1}(V)$ is a $\lambda^{\sigma\beta\Gamma}$ -closed subset of X . This shows that f is contra $\lambda^{\sigma\beta\Gamma}$ -continuous.

(1) \Rightarrow (3) Let $x \in X$ and B be any closed subset of Y such that $f(x) \in B$. Then $x \in f^{-1}(B)$ and because f is contra $\lambda^{\sigma\beta\Gamma}$ -continuous, $f^{-1}(B)$ is a $\lambda^{\sigma\beta\Gamma}$ -open subset of X . If $U = f^{-1}(B)$, then U is a $\lambda^{\sigma\beta\Gamma}$ -open subset of X such that $x \in U$ and $f(U) = f(f^{-1}(B)) \subset B$.

(3) \Rightarrow (1) Let B any closed subset of Y and let $x \in f^{-1}(B)$. Then $f(x) \in B$ and, by hypothesis, there exists a $\lambda^{\sigma\beta\Gamma}$ -open subset U_x of X such that $x \in U_x$ and $f(U_x) \subset B$. Thus, $x \in U_x \subset f^{-1}(f(U_x)) \subset f^{-1}(B)$ and hence we obtain that $f^{-1}(B) = \bigcup \{U_x : x \in f^{-1}(B)\}$.

Theorem 3.5. For a function $f:(X, \tau, I) \rightarrow (Y, \sigma, J)$, the following statements are equivalent:

- 1) f is contra quasi- $\lambda^{\sigma\beta\Gamma}$ -continuous.
- 2) $f^{-1}(B)$ is a $\lambda^{\sigma\beta\Gamma}$ -open subset of X for each σ^* -closed subset B of Y .
- 3) For each $x \in X$ and each σ^* -closed subset B of Y containing $f(x)$, there exists a $\lambda^{\sigma\beta\Gamma}$ -open subset U of X such that $x \in U$ and $f(U) \subset B$.

Proof. It is proven in a similar way to the Theorem 3.4.

Theorem 3.5. For a function $f:(X, \tau, I) \rightarrow (Y, \sigma, J)$, the following statements are equivalent:

- 1) f is contra $\lambda^{\sigma\beta\Gamma}$ -irresolute.
- 2) $f^{-1}(B)$ is a $\lambda^{\sigma\beta\Gamma}$ -open subset of X for each $\lambda^{\sigma\beta\Gamma}$ -closed subset B of Y .
- 3) For each $x \in X$ and each $\lambda^{\sigma\beta\Gamma}$ -closed subset B of Y containing $f(x)$, there exists a $\lambda^{\sigma\beta\Gamma}$ -open subset U of X such that $x \in U$ and $f(U) \subset B$.

Proof. It is proven in a similar way to the Theorem 3.4.

REFERENCES

- [1] Arenas F. G., Dontchev J., Ganster M., On λ -sets and dual of generalized continuity, Questions Answers Gen. Topology, 15, 3-13, (1997).
- [2] M. Caldas, E. Ekici, S. Jafari and T. Noiri, On the class of contra λ -continuous functions, Annales Univ. Sci. Budapest., 49, 75-86, (2006).
- [3] C. Granados, J. Sanabria, E. Rosas and C. Carpintero, On contra λ^s -continuous functions and their applications, J. Math. Comput. Sci., 3(11), 2834-2846, (2021).
- [4] E. Hatır, A. Keskin and T. Noiri, On a New Decomposition of Continuity via Idealization, JP Jour. Geometry and Topology, 3(1), 53-64, (2003).
- [5] D. Jankovic and T. R. Hamlett, New topologies from old via ideals, Amer. Math. Monthly, 97, 295-310, (1990).
- [6] K. Kuratowski, Topologie I, Monografie Matematyczne, tom 3, PWN-Polish Scientific Publishers, Warszawa, 1933.
- [7] Tekin(Akkoyun) and A. Keskin Kaymakci, On Maki's λ -sets via strong β -I-open set, 4th International Conference on Pure and Applied Mathematics (ICPAM-VAN 2022), VAN(2022).

SELÇUK UNIVERSITY, FACULTY OF SCIENCE, DEPARTMENT OF MATHEMATICS, CAMPUS, 42031,
KONYA/TÜRKİYE
Email address: 1seyfettinfidan1@gmail.com

SELÇUK UNIVERSITY, FACULTY OF SCIENCE, DEPARTMENT OF MATHEMATICS, CAMPUS, 42031,
KONYA/TÜRKİYE
Email address, author two: akeskin@selcuk.edu.tr

IFSCOM-E 2023

9TH IFS AND CONTEMPORARY MATHEMATICS AND ENGINEERING CONFERENCE

08-11 JULY 2023 TARSUS, MERSIN, TÜRKİYE

ISBN: 978-605-68670-8-8

pp: 205-212

FIXED-POINT THEOREMS VIA FUZZY-INTERPOLATIVE KANNAN TYPE CONTRACTION

MERYEM ŞENOCAK

0000-0002-2988-9419

ABSTRACT. In this article, fuzzy-interpolative Kannan-type contraction is defined and then a theorem is proved that provides the existence of a fixed point for this contraction in both fuzzy metric spaces and extended fuzzy metric spaces. With new concepts and new theorems, a generalization of the existing ones in the literature has been obtained.

1. INTRODUCTION

The attraction of the fuzzy concept, which was first defined by Zadeh [16], in 1965, is increasing day by day. This concept is used not only in mathematical analysis and general topology, but also in many fields.

The metric concept can be considered as one of the most important components regarding fixed point field. The metric in its most general form; it can be expressed as associating a positive real number with pairs of points in space.

In the last fifty years, many generalizations of this concept have been obtained. The fuzzy metric is one of them. But unlike metric spaces; in fuzzy metric spaces, the distance between two objects is not expressed as an exact real number.

The concept first defined by Kramosil and Michalek [11], aroused great repercussions with the transfer of contraction mappings to fuzzy metric spaces. George Veeramani [2], who made a change in this definition, redefined the fuzzy metric space with a slight modification. A lot of work has been done on contraction mappings, which are the cornerstone of fixed point area in both spaces ([3], [4], [7], [12]).

After famous Banach [1] contraction principle, many mathematicians defined many contraction mapping and proved theorems to prove the existence of a fixed point. In 1968 Kannan [9] defined a new contraction. There have been many researchers working in different spaces using this contraction.

In this article; a contraction redefined by Karapınar [10] with an interpolative approach and extended fuzzy metric spaces defined by Gregori et al.[5] are two

Date: July, 8, 2023.

2000 Mathematics Subject Classification. 47H10, 03E72, 54E50, 54H25.

Key words and phrases. Fixed-point, Fuzzy metric space, Interpolative contraction.

very important points. First it is defined the interpolative-fuzzy Kannan type contraction in fuzzy metric spaces and then it is modified this contraction to the extended fuzzy metric spaces. In addition it has been used the new contraction to prove a fixed point theorem in both fuzzy metric spaces. While doing all these operations, it has been used the methods in ([13], [14]). So, it have been obtained another generalization of an interpolative contraction existing in the literature.

2. PRELIMINARIES

Now in this section, we present some definitions and theorems that will be used later in the article.

We present the definition of t -norm accepted as the basic operator of fuzzy logic;

Definition 1. [15] *A binary operation $*$: $[0, 1] \times [0, 1] \rightarrow [0, 1]$ is called a continuous triangular norm (t -norm) if the conditions hold; associative and commutative, continuous, for all $a, b, c, d \in [0, 1]$ $a * 1 = a$ and $a * b < c * d$, whenever $a < c$ and $b < d$.*

Kramosil and Michalek [11] generalized probabilistic metric space via fuzzy metric. After then George and Veeramani [2] made slight modification in this concept. Many authors have studied in these metrics. A lot of authors introduced different fuzzy structures and studied in them.

Definition 2. [2], *A fuzzy metric space (FMS) is a triple $(X, \hat{W}, *)$, $X (\neq \emptyset)$, $*$ is a continuous t -norm and \hat{W} is a fuzzy set on $X^2 \times (0, \infty)$, providing the conditions, $\forall \zeta, \xi, \eta \in X$ and $t, s > 0$;*

$$(FMS_1) \quad \hat{W}(\zeta, \xi, t) > 0;$$

$$(FMS_2) \quad \hat{W}(\zeta, \xi, t) = 1 \iff \zeta = \xi;$$

$$(FMS_3) \quad \hat{W}(\zeta, \xi, t) = \hat{W}(\xi, \zeta, t);$$

$$(FMS_4) \quad \hat{W}(\zeta, \xi, t) * \hat{W}(\xi, \eta, s) \leq \hat{W}(\zeta, \eta, t + s);$$

$$(FMS_5) \quad \hat{W}(\zeta, \xi, \cdot) : (0, \infty) \rightarrow [0, 1] \text{ is continuous.}$$

$\hat{W}(\zeta, \xi, t)$ can also be thought of as grading the closeness between ζ and ξ with t .

(FMS₄) by (NA)

$$(NA) = \hat{W}(\zeta, \xi, t) * \hat{W}(\xi, \eta, s) \leq \hat{W}(\zeta, \eta, \max\{t, s\})$$

or

$$\hat{W}(\zeta, \xi, t) * \hat{W}(\xi, \eta, t) \leq \hat{W}(\zeta, \eta, t)$$

for $\forall \zeta, \xi, \eta \in X$ and $t, s > 0$; then the triple $(X, \hat{W}, *)$ is said to be non-Archimedean FMS [8].

The closest metrics to classical metrics are stationary fuzzy metrics that do not depend on "t".

Definition 3. [6] *A stationary fuzzy metric space (SFMS) is a triple $(X, \hat{W}, *)$, $X (\neq \emptyset)$, $*$ is a continuous t -norm and \hat{W} is a fuzzy set on X^2 providing the conditions, $\forall \zeta, \xi \in X$;*

$$(S_1) \quad \hat{W}(\zeta, \xi) > 0;$$

$$(S_2) \quad \hat{W}(\zeta, \xi) = 1 \iff \zeta = \xi;$$

$$(S_3) \quad \hat{W}(\zeta, \xi) = \hat{W}(\xi, \zeta);$$

$$(S_4) \quad \hat{W}(\zeta, \xi) * \hat{W}(\xi, y) \leq \hat{W}(\zeta, y).$$

$(\zeta_i)_{i \in \mathbb{N}}$ in a SFMS, (X, \hat{W}) is said to be Cauchy if $\lim_{i,j \rightarrow \infty} \hat{W}(\zeta_i, \zeta_j) = 1$;
 $(\zeta_i)_{i \in \mathbb{N}} \rightarrow \zeta \in X$ if $\lim_{i \rightarrow \infty} \hat{W}(\zeta_i, \zeta) = 1$.

We now give the definition of a space defined by Gregori et al, which is actually a kind of generalization of FMS. With the GV approach, they examine the \hat{W} fuzzy metrics that satisfy the $\wedge_{t>0} \hat{W}(\zeta, \xi, t) > 0$ on X.

Definition 4. [5] An extended fuzzy metric space (EFMS) is a triple $(X, \hat{W}^0, *)$, $X (\neq \emptyset)$, $*$ is a continuous t-norm and \hat{W}^0 is a fuzzy set on $X^2 \times [0, \infty)$ providing the conditions, $\forall \zeta, \xi, \eta \in X$ and $t, s \geq 0$;

- (EFM₁) $\hat{W}^0(\zeta, \xi, t) > 0$;
- (EFM₂) $\hat{W}^0(\zeta, \xi, t) = 1 \iff \zeta = \xi$;
- (EFM₃) $\hat{W}^0(\zeta, \xi, t) = \hat{W}^0(\xi, \zeta, t)$;
- (EFM₄) $\hat{W}^0(\zeta, \xi, t) * \hat{W}^0(\xi, \eta, s) \leq \hat{W}^0(\zeta, \eta, t + s)$;
- (EFM₅) $\hat{W}^0_{\zeta, \xi} : [0, \infty) \rightarrow (0, 1]$ is continuous.

Similarly (EFM₄) by (NA)* = $\hat{W}^0(\zeta, \xi, t) * \hat{W}^0(\xi, \eta, s) \leq \hat{W}^0(\zeta, \eta, \max\{t, s\})$ or $\hat{W}^0(\zeta, \xi, t) * \hat{W}^0(\xi, \eta, t) \leq \hat{W}^0(\zeta, \eta, t)$ for $\forall \zeta, \xi, \eta \in X$ and $t, s > 0$; then the triple $(X, \hat{W}, *)$ is said to be non-Archimedean EFMS.

Theorem 1. [5] Let M be a fuzzy set on $X^2 \times (0, \infty)$, and denote by \hat{W}^0 its extension to $X^2 \times [0, \infty)$ given by

$$\hat{W}^0(\zeta, \xi, t) = \hat{W}(\zeta, \xi, t)$$

for all $\zeta, \xi \in X, t > 0$ and

$$\hat{W}^0(\zeta, \xi, 0) = \wedge_{t>0} \hat{W}(\zeta, \xi, t).$$

Then, $(X, \hat{W}^0, *)$ is an EFMS $\iff (X, \hat{W}, *)$ is a FMS satisfying for each $\zeta, \xi \in X$ the condition $\wedge_{t>0} \hat{W}(\zeta, \xi, t) > 0$.

Proposition 1. [5] $(N_{\hat{W}}, *)$ is a stationary fuzzy metric on X $\iff \wedge_{t>0} \hat{W}(\zeta, \xi, t) > 0$ for all $\zeta, \xi \in X$. It is clear that

$$(1) \quad \hat{W}^0(\zeta, \xi, 0) = \wedge_{t>0} \hat{W}(\zeta, \xi, t) = N_{\hat{W}}(\zeta, \xi).$$

Proposition 2. [5] Let $(X, \hat{W}^0, *)$ is complete $\iff (X, N_{\hat{W}}, *)$ is complete.

There are different completeness and Cauchy sequence definitions in FMS ([2], [4]). The authors [5] have adapted one of these from FMS to EFMS. As follows;

Definition 5. [5] $\{\zeta_n\}$ in X is named Cauchy sequence if given $\delta \in (0, 1)$, it can be find $n_\delta \in \mathbb{N}$ such that $\hat{W}^0(\zeta_n, \zeta_m, 0) > 1 - \delta$ for all $n, m \geq n_\delta$.

$$\{\zeta_n\} \text{ is Cauchy } \iff \lim_{m,n} \hat{W}^0(\zeta_n, \zeta_m, 0) = 1.$$

An EFMS is called complete if every Cauchy sequence is convergent.

With the help of interpolation, Karapınar [10] modified a mapping that has an important place in the literature, and obtained a kind of generalization. This resounding study has inspired many researchers.

Now we remember the interpolative Kannan type contraction defined in metric spaces [10]:

Definition 6. [10] Let (X, d) be a metric space. The self-mapping $\mathfrak{S} : X \rightarrow X$ is an interpolative Kannan type contraction, if there exist a constant $\lambda \in [0, 1)$ and $\alpha \in (0, 1)$ such that

$$d(\mathfrak{S}\zeta, \mathfrak{S}\xi) \leq \lambda [d(\zeta, \mathfrak{S}\zeta)]^\alpha \cdot [d(\xi, \mathfrak{S}\xi)]^{1-\alpha}$$

for all $\zeta, \xi \in X$ with $\zeta \neq \mathfrak{S}\zeta$.

Theorem 2. [10] Let (X, d) be a complete metric space. A self mapping $\mathfrak{S} : X \rightarrow X$ possesses a fixed point in and \mathfrak{S} , if there exist constants $\lambda \in [0, 1)$ and $\alpha \in (0, 1)$ such that

$$d(\mathfrak{S}\zeta, \mathfrak{S}\xi) \leq \lambda [d(\zeta, \mathfrak{S}\zeta)]^\alpha \cdot [d(\xi, \mathfrak{S}\xi)]^{1-\alpha}$$

for all $\zeta, \xi \in X/\text{Fix}(\mathfrak{S})$.

In this article, we adapt the interpolative Kannan type contraction to various fuzzy metric spaces, making use of this work, which has also inspired us.

So, we have obtained another generalization of an interpolative contraction existing in the literature.

3. MAIN RESULT

We are ready to introduce new definition of fuzzy-interpolative Kannan type contraction modifying the definition to fuzzy metrics.

Definition 7. Let $(X, \hat{W}, *)$ be a FMS. $\mathfrak{S} : X \rightarrow X$ is a fuzzy-interpolative Kannan type contraction, if there exist a constant $\lambda \in (0, 1)$ and $\alpha \in (0, 1)$ such that

$$(3.1) \quad \left[1 - \hat{W}(\mathfrak{S}\zeta, \mathfrak{S}\xi, t)\right] \geq \lambda \left[1 - \hat{W}(\zeta, \mathfrak{S}\zeta, t)\right]^\alpha \cdot \left[1 - \hat{W}(\xi, \mathfrak{S}\xi, t)\right]^{1-\alpha}$$

for all $\zeta, \xi \in X$ and $t > 0$; with $\zeta \neq \mathfrak{S}\zeta$.

Theorem 3. Let $(X, \hat{W}, *)$ be a complete non-Archimedean FMS and \mathfrak{S} be a fuzzy-interpolative Kannan type contraction. Then \mathfrak{S} has a fixed point in X , for all $\zeta, y \in X/\text{Fix}(\mathfrak{S})$.

Proof. Let $\zeta_0 \in X$. Define the sequence $\{\zeta_n\}$ in X with $\zeta_{n+1} = \mathfrak{S}\zeta_n, \forall n \in \mathbb{N}$.

Provided that $\zeta_{n+1} = \zeta_n$ for some $n \in \mathbb{N}$, then $\zeta^* = \zeta_n$ is a fixed point of \mathfrak{S} .

Presume that $\zeta_n \neq \zeta_{n+1}, \forall n \in \mathbb{N}$.

Implementing (3.1) with $\zeta = \zeta_n, \xi = \zeta_{n-1}$, we obtain

$$\begin{aligned} \left[1 - \hat{W}(\zeta_{n+1}, \zeta_n, t)\right] &= \left[1 - \hat{W}(\mathfrak{S}\zeta_n, \mathfrak{S}\zeta_{n-1}, t)\right] \\ &\geq \lambda \left[1 - \hat{W}(\zeta_n, \mathfrak{S}\zeta_n, t)\right]^\alpha \cdot \left[1 - \hat{W}(\zeta_{n-1}, \mathfrak{S}\zeta_{n-1}, t)\right]^{1-\alpha} \\ &= \lambda \left[1 - \hat{W}(\zeta_{n-1}, \zeta_n, t)\right]^{1-\alpha} \cdot \left[1 - \hat{W}(\zeta_n, \zeta_{n+1}, t)\right]^\alpha \end{aligned}$$

and we have,

$$\left[1 - \hat{W}(\zeta_n, \zeta_{n+1}, t)\right]^{1-\alpha} \geq \lambda \left[1 - \hat{W}(\zeta_{n-1}, \zeta_n, t)\right]^{1-\alpha}.$$

and so, we obtain that $\{\hat{W}(\zeta_n, \zeta_{n+1}, t)\}$ is non-increasing and;

$$\begin{aligned} [1 - \hat{W}(\zeta_n, \zeta_{n+1}, t)] &\geq \lambda [1 - \hat{W}(\zeta_{n-1}, \zeta_n, t)] \\ &\geq \lambda^2 [1 - \hat{W}(\zeta_{n-2}, \zeta_{n-1}, t)]^{1-\alpha} \\ &\quad \dots \\ &\geq \lambda^n [1 - \hat{W}(\zeta_0, \zeta_1, t)]^{1-\alpha} \end{aligned}$$

as $n \rightarrow \infty$,

$$\lim_{n \rightarrow \infty} [1 - \hat{W}(\zeta_n, \zeta_{n+1}, t)] \geq \lim_{n \rightarrow \infty} \lambda^n [1 - \hat{W}(\zeta_0, \zeta_1, t)]$$

$\lambda^n \rightarrow 0$ we obtain,

$$\lim_{n \rightarrow \infty} [1 - (\hat{W}\zeta_n, \zeta_{n+1}, t)] = 0 \implies \hat{W}(\zeta_n, \zeta_{n+1}, t) = 1.$$

Using (NA), for $n < m$;

$$\hat{W}(\zeta_n, \zeta_m, t) \geq \hat{W}(\zeta_n, \zeta_{n+1}, t) * \hat{W}(\zeta_{n+1}, \zeta_{n+2}, t) * \dots * \hat{W}(\zeta_{m-1}, \zeta_m, t)$$

and as $n, m \rightarrow \infty$,

$$\begin{aligned} \lim_{n, m \rightarrow \infty} \hat{W}(\zeta_n, \zeta_m, t) &\geq \lim_{n \rightarrow \infty} \hat{W}(\zeta_n, \zeta_{n+1}, t) * \lim_{n \rightarrow \infty} \hat{W}(\zeta_{n+1}, \zeta_{n+2}, t) * \dots * \lim_{n \rightarrow \infty} \hat{W}(\zeta_{m-1}, \zeta_m, t) \\ &\geq 1 * 1 * \dots * 1 \\ &\geq 1 \end{aligned}$$

We obtain,

$$\lim_{n \rightarrow \infty} \hat{W}(\zeta_n, \zeta_m, t) = 1$$

And so, we solve an important point of the proof that $\{\zeta_n\}$ is a Cauchy sequence. Since X is complete,

$$\exists \zeta^* \in \mathcal{X} : \text{as } n \rightarrow \infty \text{ and } \zeta_n \rightarrow \zeta^*$$

Implementing (3.1) with $\zeta = \zeta_n$, $\xi = \zeta^*$, we obtain

$$[1 - \hat{W}(\mathfrak{S}\zeta_n, \mathfrak{S}\zeta^*, t)] \geq \lambda [1 - \hat{W}(\zeta_n, \mathfrak{S}\zeta_n, t)]^\alpha \cdot [1 - \hat{W}(\zeta^*, \mathfrak{S}\zeta^*, t)]^{1-\alpha}$$

as $n \rightarrow \infty$ and using $\lim_{n \rightarrow \infty} [\hat{W}(\zeta_n, \zeta_{n+1}, t) - 1] = 0$;

$$[1 - \hat{W}(\mathfrak{S}\zeta_n, \mathfrak{S}\zeta^*, t)] = 0 \implies \hat{W}(\mathfrak{S}\zeta_n, \mathfrak{S}\zeta^*, t) = 1$$

By the uniqueness of the limit, we get $\zeta^* = \mathfrak{S}\zeta^*$, that is, ζ^* is a fixed point of \mathfrak{S} . □

Now we transfer the definitions and the theorem to EFMS.

Definition 8. Let $(X, \hat{W}^0, *)$ be an EFMS. $\mathfrak{S} : X \rightarrow X$ is a fuzzy - \hat{W}^0 -interpolative Kannan type contraction, if equation (3.1) is satisfied for all $t \geq 0$. Particularly, \mathfrak{S} is called fuzzy-0- interpolative Kannan type contraction, if equation (3.1) is satisfied for all $t = 0$.

Theorem 4. Let $(X, \hat{W}^0, *)$ be a complete non-Archimedean EFMS and \mathfrak{S} be a fuzzy – \hat{W}^0 – interpolative Kannan type contraction. Then \mathfrak{S} has a fixed point in X , for all $\zeta, \xi \in X/\text{Fix}(\mathfrak{S})$.

Proof. We will examine the proof in two cases.

Case 1. $t > 0$;

In this case, since $\hat{W}^0(\zeta, \xi, t) = \hat{W}(\zeta, \xi, t) \forall \zeta, \xi \in X$, it is same situation in fuzzy metric spaces and introduced above in the proof of Theorem 3.

Case 2. $t = 0$;

Let $\zeta_0 \in X$. Define the squence $\{\zeta_n\}$ in X with $\zeta_{n+1} = \mathfrak{S}\zeta_n, \forall n \in \mathbb{N}$.

Provided that $\zeta_{n+1} = \zeta_n$ for some $n \in \mathbb{N}$, then $\zeta^* = \zeta_n$ is a fixed point of \mathfrak{S} .

Presume that $\zeta_n \neq \zeta_{n+1}, \forall n \in \mathbb{N}$.

Using (2.1), implementing (3.1) with $\zeta = \zeta_n, \xi = \zeta_{n-1}, t = 0$ and using similar way above the proof we obtain;

$$\begin{aligned} [1 - \hat{W}^0(\mathfrak{S}\zeta_n, \mathfrak{S}\zeta_{n-1}, 0)] &= [1 - N_{\hat{W}}(\mathfrak{S}\zeta_n, \mathfrak{S}\zeta_{n-1})] \\ &\geq \lambda \cdot [1 - N_{\hat{W}}(\zeta_n, \mathfrak{S}\zeta_n)]^\alpha \cdot [1 - N_{\hat{W}}(\zeta_{n-1}, \mathfrak{S}\zeta_{n-1})]^{1-\alpha} \end{aligned}$$

and we have

$$[1 - N_{\hat{W}}(\zeta_n, \zeta_{n+1})]^{1-\alpha} \geq \lambda \cdot [1 - N_{\hat{W}}(\zeta_{n-1}, \zeta_n)]^{1-\alpha}$$

we obtain that $\{N_{\hat{W}}(\zeta_n, \zeta_{n+1})\}$ is non- increasing and so we have,

$$[1 - N_{\hat{W}}(\zeta_n, \zeta_{n+1})] \geq \lambda^n [1 - N_{\hat{W}}(\zeta_0, \zeta_1)].$$

Since, as $n \rightarrow \infty$ and $\lambda^n \rightarrow 0$,

$$\lim_{n \rightarrow \infty} N_{\hat{W}}(\zeta_n, \zeta_{n+1}) = 1.$$

which implies that for $n < m$, using (3.1) with $\zeta = \zeta_n, \xi = \zeta_m, t = 0$ and using Definition 3, and as $n \rightarrow \infty$,

$$\begin{aligned} \lim_{n \rightarrow \infty} N_{\hat{W}}(\zeta_n, \zeta_m) &\geq \lim_{n \rightarrow \infty} N_{\hat{W}}(\zeta_n, \zeta_{n+1}) * \lim_{n \rightarrow \infty} N_{\hat{W}}(\zeta_{n+1}, \zeta_{n+2}) * \dots * \lim_{n \rightarrow \infty} N_{\hat{W}}(\zeta_{m-1}, \zeta_m) \\ &\geq 1 * 1 * \dots * 1 = 1 \end{aligned}$$

We obtain that $\lim_{n \rightarrow \infty} N_{\hat{W}}(\zeta_n, \zeta_m) = 1$ And so, we solve an important point of the proof that $\{\zeta_n\}$ is a Cauchy sequence. Since X is complete, $\exists \zeta^* \in X$: as $n \rightarrow \infty$ and $\zeta_n \rightarrow \zeta^*$

Since \mathfrak{S} is continuous, as $\zeta_n \rightarrow \zeta^*$ we have $\mathfrak{S}\zeta_n \rightarrow \mathfrak{S}\zeta^*$ and using (2.1), we obtain,

$$\lim_{n \rightarrow \infty} N_{\hat{W}}(\mathfrak{S}\zeta_n, \mathfrak{S}\zeta^*) = 1.$$

By the uniqueness of the limit, we get $\zeta^* = \mathfrak{S}\zeta^*$, that is, ζ^* is a fixed point of \mathfrak{S} . \square

Example 1. Let the EFMS $(X, \hat{W}^0, *)$, where $X = \{1, 2, 3, 4\}$, $*$ is product t -norm and \hat{W}^0 is given by

$$\hat{W}^0(\zeta, \xi, t) = \frac{\min\{\zeta, \xi\} + t}{\max\{\zeta, \xi\} + t}$$

for $\forall \zeta, \xi \in X$ and $t \geq 0$. We define a self mapping

$$\mathfrak{S} = \begin{pmatrix} 1 & 2 & 3 & 4 \\ 3 & 1 & 2 & 4 \end{pmatrix}$$

on X . Then, \mathfrak{S} is a fuzzy- \hat{W}^0 - interpolative Kannan type contraction for $\lambda = \frac{1}{2}$ and $\alpha = \frac{1}{2}$ such that;

$$\begin{aligned} \hat{W}^0(1, 1, t) &= \hat{W}^0(2, 2, t) = \hat{W}^0(3, 3, t) = \hat{W}^0(4, 4, t) = 1 \\ \hat{W}^0(1, 2, t) &= \hat{W}^0(2, 1, t) = \frac{1+t}{2+t} \\ \hat{W}^0(1, 3, t) &= \hat{W}^0(3, 1, t) = \frac{1+t}{3+t} \\ \hat{W}^0(2, 3, t) &= \hat{W}^0(3, 2, t) = \frac{2+t}{3+t} \end{aligned}$$

for $\zeta = 1, \xi = 2$ and $\forall t \geq 0$,

$$\begin{aligned} \frac{2+t}{3+t} &> \frac{1}{8} \\ \frac{2}{3+t} &> \frac{1}{4} \frac{1}{2+t} \\ \sqrt{\frac{2}{3+t}} &> \frac{1}{2} \sqrt{\frac{1}{2+t}} \\ \frac{2}{3+t} &> \frac{1}{2} \sqrt{\frac{1}{2+t}} \sqrt{\frac{2}{3+t}} \\ [1 - \hat{W}^0(\mathfrak{S}(1), \mathfrak{S}(2), t)] &> \frac{1}{2} [1 - \hat{W}^0(1, \mathfrak{S}(1), t)]^{\frac{1}{2}} [1 - \hat{W}^0(2, \mathfrak{S}(2), t)]^{\frac{1}{2}}. \end{aligned}$$

for $\zeta = 1, \xi = 3$ and $\forall t \geq 0$,

$$\begin{aligned} 4 &> 2 \\ \frac{4}{3+t} &> \frac{2}{3+t} \\ \sqrt{\frac{1}{3+t}} &> \frac{1}{2} \sqrt{\frac{2}{3+t}} \\ \frac{1}{3+t} &> \frac{1}{2} \sqrt{\frac{1}{3+t}} \sqrt{\frac{2}{3+t}} \\ [1 - \hat{W}^0(\mathfrak{S}(1), \mathfrak{S}(3), t)] &> \frac{1}{2} [1 - \hat{W}^0(1, \mathfrak{S}(1), t)]^{\frac{1}{2}} [1 - \hat{W}^0(3, \mathfrak{S}(3), t)]^{\frac{1}{2}}. \end{aligned}$$

for $\zeta = 3, \xi = 2$ and $\forall t \geq 0$,

$$\begin{aligned} \frac{3+t}{2+t} &> \frac{1}{16} \\ \sqrt{\frac{1}{2+t}} &> \frac{1}{4} \sqrt{\frac{1}{3+t}} \\ \frac{1}{2+t} &> \frac{1}{2} \sqrt{\frac{1}{2+t}} \sqrt{\frac{1}{3+t}} \\ [1 - \hat{W}^0(\mathfrak{S}(3), \mathfrak{S}(2), t)] &> \frac{1}{2} [1 - \hat{W}^0(3, \mathfrak{S}(3), t)]^{\frac{1}{2}} [1 - \hat{W}^0(2, \mathfrak{S}(2), t)]^{\frac{1}{2}}. \end{aligned}$$

That is \mathfrak{S} is a fuzzy- \hat{W}^0 - interpolative Kannan type contraction and "4" is unique fixed point of \mathfrak{S} .

4. CONCLUSION

In this article; first it is defined the interpolative-fuzzy Kannan type contraction in fuzzy metric spaces and then it is modified this contraction to extended fuzzy metric spaces. And then, this new contraction has been used to prove a fixed point theorem in some fuzzy metric spaces. So, it has been obtained another generalization of an interpolative contraction existing in the literature. While creating these fixed point theorems in some fuzzy metric spaces; it is aimed to give an idea to new researchers who want to study on interpolative contractions in fuzzy metric spaces and extended fuzzy metric spaces.

REFERENCES

- [1] S., Banach, Sur les oprations dans les ensembles abstrails et leur application aux quations intgraes, Fund Math., 3; 133-181, (1922).
- [2] A., George, P., Veeramani, On some results in fuzzy metric spaces, Fuzzy Sets and Systems, 64;395-399, [http://dx.doi.org/10.1016/0165-0114\(94\)90162-7](http://dx.doi.org/10.1016/0165-0114(94)90162-7), (1994).
- [3] D., Gopal, C., Vetro, Some new fixed point theorems in fuzzy metric spaces, Iranian Journal of Fuzzy Systems, 11(3); 95-107, (2014).
- [4] M., Grabiec, Fixed points in fuzzy metric spaces, Fuzzy Sets and Systems, 27;385-389, [https://doi.org/10.1016/0165-0114\(88\)90064-4](https://doi.org/10.1016/0165-0114(88)90064-4), (1988).
- [5] V., Gregori, J. J. Minana, D., Miravet, Extended fuzzy metrics and fixed point theorems, Mathematics Journal, 7,303, <https://doi.org/10.3390/math7030303>, (2019).
- [6] V., Gregori, S., Romaguera, Characterizing completable fuzzy metric spaces, Fuzzy Sets and Systems, 144;411-420, DOI:10.1016/S0165-0114(03)00161-1, (2014).
- [7] V., Gregori, A., Sapena, On fixed point theorems in fuzzy metric spaces, Fuzzy Sets and Systems, 125;245-252, [https://doi.org/10.1016/S0165-0114\(00\)00088-9](https://doi.org/10.1016/S0165-0114(00)00088-9), (2002).
- [8] V., Istratescu, An introduction to theory of probabilistic metric spaces with applications, Ed Tehnica, Bucureşti, Romanian, (1974).
- [9] R., Kannan, Some results on fixed points. Bull Calcutta Math. Soc. 60;71-76, (1968).
- [10] E., Karapınar, Adv. Theory Nonlinear Anal. Appl. 2;85-87, (2018).
- [11] I., Kramosil, J., Michalek, Fuzzy metrics and statistical metric spaces, Kybernetika, 11;336-344, (1975).
- [12] D., Mihet, Fuzzy ψ - contractive mappings in non-Archimedean fuzzy metric space, Fuzzy Sets and Systems, 159;739-744. 10, <https://doi.org/10.1016/j.fss.2007.07.006>, (2008).
- [13] M., Senocak, E., Güner, Fixed-point theorems in extended fuzzy metric spaces via α - ϕ - M^0 - and β - ψ - M^0 - fuzzy contractive mappings, Communications Faculty of Sciences University of Ankara Series A1: Mathematics and Statistics, DOI:10.31801/cfsuasmas.1038245, (2023).
- [14] M., Senocak, E., Güner, Some Fixed Point Theorems in Extended Fuzzy Metric Spaces, Erzincan University Journal of Science Technology, DOI:10.18185/erzifbed.1146294, (2023).
- [15] B., Schwizer, A., Sklar, Statistical metric spaces, Pacific Journal of Mathematics 10;315-367, (1960).
- [16] L.A., Zadeh, Fuzzy sets, Inform. Control, 8;338-353, (1965).

ANKARA UNIVERSITY, ANKARA, TURKEY
 Email address: meryemsnc@gmail.com

IFSCOM-E 2023
9TH IFS AND CONTEMPORARY MATHEMATICS AND ENGINEERING CONFERENCE
8-11 JULY 2023, TARSUS, MERSİN TÜRKİYE
ISBN: 978-605-68670-8-8
pp: 213-220

INVESTIGATION OF THE CAPACITY FACTOR OF THE EGE REGION WIND POWER PLANTS ACCORDING TO THE REAL GENERATIONS

İSRAFİL KARADÖL

0000-0002-9239-0565

ABSTRACT

With the developing industry and technology, the need for energy has also increased. Meeting the increasing energy demand from renewable energy sources is encouraged by the states. In the last 10 years, Turkey has prepared many incentive packages in this field by turning to domestic and national resources in the energy sector. Before the installation of renewable energy power plants, some criteria of the facility should be investigated and analyzed. The feasibility studies carried out before the investment in wind power plants allows optimum operation of existing resources and maximum benefit from these resources. In addition, financial and technical issues (depreciation period, turbine selection, etc.) can be predicted according to the feasibility study. This study aims to obtain information about the capacity factor of the region and the provinces in the region by using the real generation of 86 facilities in the Ege region. For this purpose, the provinces' annual mean, maximum, and minimum capacity factors were calculated according to the facilities' generation in the Ege region in 2022. According to the calculations, the annual mean capacity factor of the Ege Region is 34.4%. The mean annual capacity factors of İzmir, Manisa, Aydın, Muğla, Uşak, Denizli, and Afyonkarahisar provinces were calculated as 39.9%, 38.6%, 32.8%, 33.9%, 29.3%, 34.5%, and 31.8%, respectively. According to all these results, it is predicted that it will be beneficial for the investor to give priority to İzmir in site selection for the new facilities to be established in the Ege Region.

1. INTRODUCTION

The need for energy is constantly increasing due to reasons such as increasing population, developing industry, and a lifestyle compatible with technology. The constantly growing energy demand poses great challenges for the energy sector. Countries have turned to traditional energy sources such as coal, oil, and natural gas in order to meet their energy demand. However, in the early 2000s, they encountered many problems (global warming, greenhouse gas, environmental pollution, etc.) depending on the use of these resources. In addition, researchers have predicted that if traditional energy sources continue with their current use potential, they can be used for a maximum of 160 years[1]. For all these reasons, states have turned to renewable energy sources as an alternative to traditional energy sources in recent years in order to meet the increasing energy demand. Renewable energy; is an energy type that has continuity, continues natural processes, does not end with secondary energy conversion, and continues by being renewed. Renewable energy sources; wind, solar, hydroelectric, biomass, wave, tidal, geothermal, and current energy. These resources have less negative impact on the environment than traditional energy resources and there is no problem of depletion. In addition, other advantages of these resources are that there is no risk of price increase, they are produced where they can be consumed, they support local development, and reduce foreign dependency, especially in energy[2].

Date: July, 8, 2023.

Key words and phrases. Wind Energy, Capacity Factor, Ege Region

The total renewable energy installed power of the world is 3064 GW by the end of 2021 [3]. With this installed power, 28% of the electrical energy produced in the world in 2021 was met from renewable energy sources[4]. When we evaluate Turkey, the cumulative installed power of electricity in March 2023 is 104348 MW. Renewable energy sources constitute 54.8% of this installed power. 45.2% of Turkey's energy needs are met by coal and natural gas. In order to reduce foreign dependency on electricity generation from traditional energy sources, the use of coal has been given priority as a country policy due to its domestic and national characteristics. However, the use of this resource causes many problems for the environment and natural life. When we analyze renewable energy and electricity generation in Turkey according to resource types, hydraulic energy ranks first with an installed power of 30.3%. This energy source is followed by wind 11%, solar 9.4%, geothermal 1.6%, and other energy sources 2.5%[5].

Turkey has a high wind energy potential, especially in coastal areas due to its mathematical and special position[6]. It is predicted that Turkey's offshore wind energy potential is 11000MW, while its onshore wind energy potential is 37000MW[6]-[8]. Türkiye currently uses 23.9% of its total potential in wind energy. In other words, Türkiye does not use 76.1% of its wind potential. This situation shows that Turkey is inclined to grow and develop in the field of wind energy. In this context; When we examine the wind potential in Turkey regionally, the Aegean Region attracts the attention of national and international investors in terms of wind energy potential. In addition, large investments have been made in this region in recent years[9]-[11]. These investments were also emphasized on many platforms under the name of national and domestic energy moves.

One of the important factors in the efficient operation of wind power plants is to investigate the capacity factors of the facilities and the potential of the region. When we examine the studies in this field; Geçgel and Tarhan examined the capacity factors, turbine turning ratios, and the reasons for the change in the capacity factor of the wind farms established in Çanakkale[12]. Yıldız and Akgül; compared the wind and solar energy potential in these areas by taking specific points in the Mediterranean region as reference[13]. Dong et al. proposed a hybrid method aiming to optimally determine the factors to be considered when deciding on wind energy investments[14]. Zhang et al. proposed a two-module wind farm utility management system with wind speed estimation and wind power simulation[14]. There has not been much study in the literature on the evaluation of the potential of wind energy regionally or spatially. The studies carried out are mostly on the evaluation of wind energy at the scale of Türkiye [15]-[19].

The basic raw material used for electricity generation in wind power plants is wind energy. Wind energy is not constantly variable due to its structure and turbine installation costs of these facilities are high. Therefore, before installing wind farms, it plays an important role in the dominance of the technical characteristics of the region, capacity factor changes, wind direction, and length. The purpose of determining the turbine type according to the wind turbine regime and the generation characteristics of the area, the calculation, and examination of the turbine rotation capacity in the provinces where the wind power plant will be established are of great importance.

In this study; The annual mean, maximum, and minimum wind capacity factors of all provinces were examined by using the 2022 electricity generation data of the wind power plants in all provinces in the Aegean region. It is anticipated that this study will guide the newly established wind power plants in the Aegean region in terms of determining the potential of the provinces.

2. MATERIAL METHOD

2.1. Study Area

In the study, when evaluated in terms of wind potential, the Aegean Region, which has a high capacity, was examined. There are eight provinces in total in the Aegean region (Afyon, Aydın, Denizli, İzmir, Kütahya, Manisa, Muğla, and Uşak). The mean annual wind speed distributions of the provinces in this region at an altitude of 100 meters are given in the yellow area on the left in Figure 1. In the figure given, it is seen that the wind speed of the provinces, especially in the coastal areas, is 7 and above. Winds with a speed of 7.5 and above are observed in İzmir and its surroundings. In the inner parts of the Aegean, the mean annual wind speed varies according to location. If we evaluate the inner parts of the Aegean in general, it is seen that the annual mean wind speed of these provinces is approximately 6-6.5 m/s. In addition, the annual mean power density of the Aegean region at an altitude of 100 meters is given on the right side of Figure 1. In this area, which is determined by the orange line, the province with the highest power density is İzmir. In this area, İzmir is followed by Aydın and Muğla. In the inner parts of the Aegean region, the province with the highest power density is Afyon. In other provinces, it is seen that the wind migration density reaches up to 300 W/m² in some special locations.

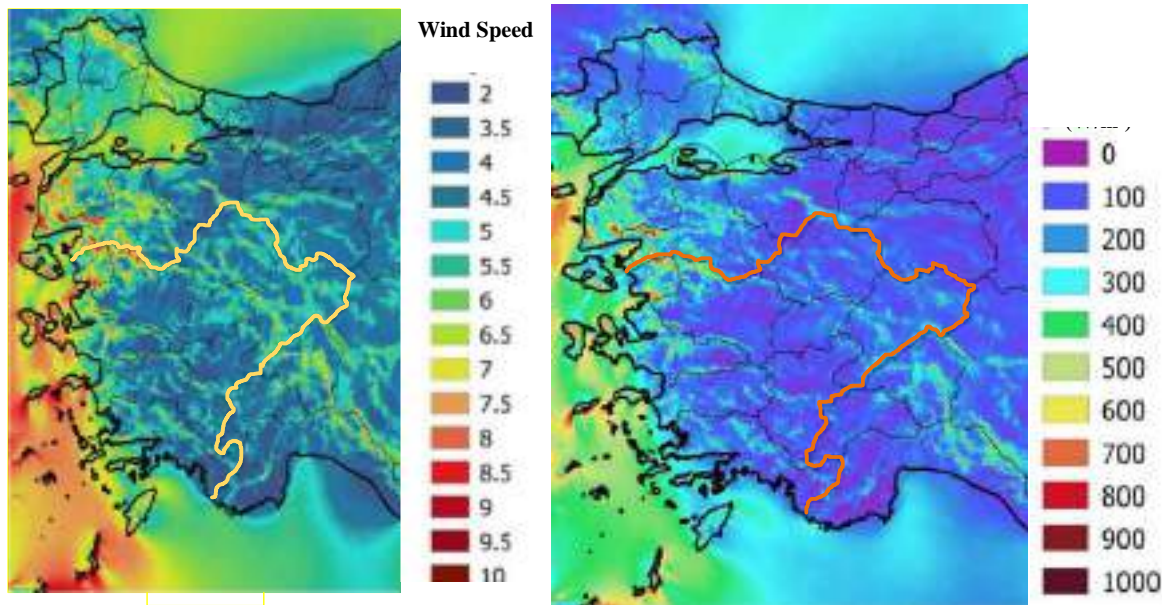


Figure 1. Annual mean wind speed (left column) and annual mean wind power density (right column)

2.2. Plant Generations

Turkey's rapid economic and population growth in the last two decades has increased both its energy demand and its dependence on energy imports. Turkey has restructured its energy system in order to rationalize the growth in energy demand, lower energy prices for consumers, and slow the increase in energy imports. For this purpose, oil and gas exploration has been directed, diversified the infrastructure related to oil and gas supply sources, and increased renewable energy generation. When we examine the worldwide electricity generation in this area in 2021, it is seen that 37.88% of the electricity produced is met from renewable energy sources[20]. In order to achieve this generation, facilities with an installed capacity of 3063 GW were established around the world[3]. Wind power plants constituted 26.9% of these established facilities[21]. When we examine Turkey in this field, the

total electricity generation capacity in 2021 is 99820 MW. Facilities generating electricity from renewable energy sources accounted for 53.7% of this capacity[22]. When we analyze it in terms of wind capacity, it is seen that 10.6% of the total installed power consists of wind power plants.

3506.8 MW of the wind farm in Turkey is located in the Aegean Region. This capacity in the Aegean Region is approximately 33% of Türkiye's wind power plants. This study, it is aimed to examine the wind energy potential of the Aegean region, which is one of the regions with an important installed power, and the provinces in this region. For this purpose, firstly, plant generations in the Aegean Region were requested from Türkiye Elektrik Üretim A.Ş. With the positive result of this demand, 2022 generations of 86 facilities in the Aegean Region were obtained. The distribution of installed power of these facilities according to the provinces is shown on the map in Figure 2.



Figure 2. The installed power distribution of WPP in the Aegean Region by provinces

In addition, some statistical properties of the hourly total generation of the obtained data by provinces are given in Table 1.

Table 1. Statistical characteristics of total generation of provinces

	İzmir	Manisa	Aydın	Afyonkarahisar	Uşak	Denizli	Muğla
Installed Power	1742,5	701,6	397,3	323,8	61,5	66,0	214,0
Mean	696,5	271,0	130,4	102,9	17,4	22,8	72,6
Standard deviation	524,6	210,4	99,3	94,8	16,9	24,6	57,9
Maximum	1724,5	695,9	372,2	343,2	61,0	75,0	214,9
Minimum	0,1	-0,9	-0,7	-0,8	-5,0	0,0	-3,9
Time	01.01.2022-01.01.2023						

The hourly total generation of the provinces in the Aegean Region is given in Figure 3. In the figure given, the hourly total generation of İzmir, Manisa, Aydın, Afyonkarahisar, Muğla, Uşak, and Denizli provinces are shown in blue, red, green, purple, claret red, gray, and black colors, respectively.

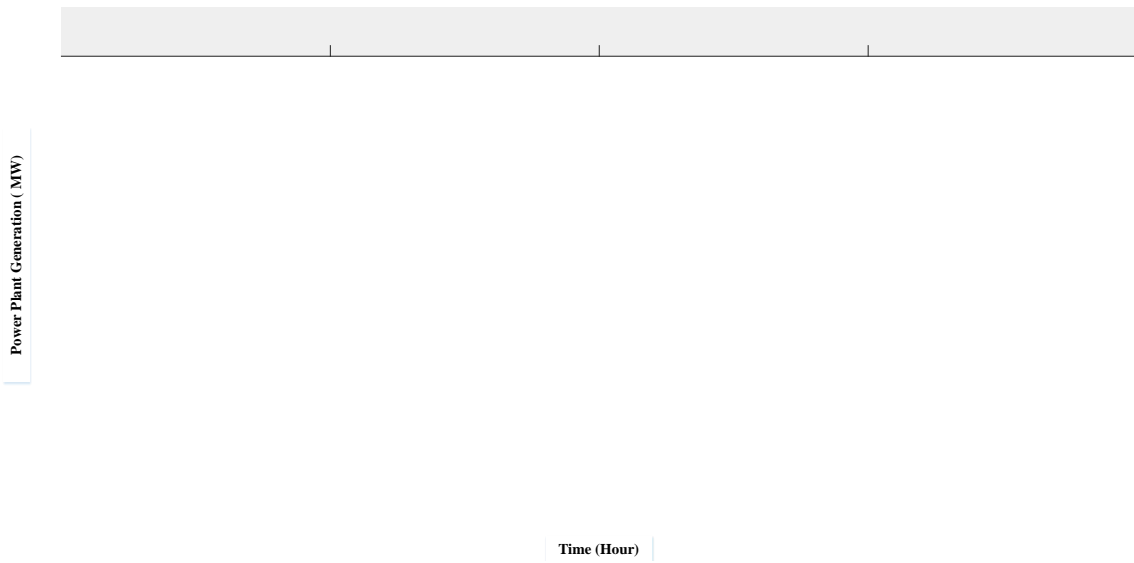


Figure 3. Hourly total WPP generation by provinces

2.3. Wind Power Calculation

As a result of the sun's heating of the earth in different time periods, low and high-pressure centers are formed on the earth's surface. The wind is formed as a result of the airflow between low and high-pressure centers and the rotation of the earth around its axis (Coriolus Force)[23], [24]. Measuring the speed and direction of the wind is of great importance for both meteorology and RES. In order to measure the speed of the wind in a region, stations with a tower height of 10 meters are usually installed. However, in real applications, the rotor height of wind farms generally varies between 80-100 meters. Equation 1 is used to calculate wind speeds at different altitudes according to the wind speed at the reference point.

$$V_t = V_r \left(\frac{h_t}{h_r} \right)^x \quad (1)$$

V_t , V_r , h_t , and h_r given in Equation 1 define theoretical speed, real speed, theoretical height, and real height, respectively. x is the surface roughness coefficient. Wind turbines convert the kinetic energy of wind energy in motion into mechanical energy. The basic definition of the kinetic energy of an air mass m moving with a velocity V is given in Equation 2[25].

$$E_{kinetik} = \frac{1}{2}mv^2 \quad (2)$$

The wind turbines are rotated by hitting the blades of the air mass with p ($p = 1,225 \text{ kg/m}^3$) density at V speed, t time, and radius r . In this way, wind energy is converted into mechanical energy. The mathematical expression of wind power created by deriving the kinetic energy equation given in Equation 2 is given in Equation 4[26], [27].

$$P_{güç} = \frac{1}{2}p\pi r^2 v^3 \quad (3)$$

In theoretical applications, wind power is calculated according to Equation 3. However, when we consider the various losses, it is seen that not all the energy in the area swept by the wind turbines can be converted into mechanical energy by the turbines in real applications. Depending on the difference between the wind speed coming to the wind turbine blades and the wind speed, the wind power also

varies. According to the Betz limit theory, with today's technology, a maximum 59.26% of the theoretical power of wind turbines can be used. According to this definition, the wind turbine power equation is given in Equation 4 ($C_p = \text{Betz Limit}$).

$$P_{güç} = \frac{1}{2} \rho \pi r^2 v^3 C_p \quad (4)$$

2.4. Capacity Factor in Wind Power Plants

Before wind power plants are installed, it is of great importance for the investor-operator to determine the wind energy technical capacity factor and technical potential of the region to be installed. Capacity factor (Equation 5); defines how much energy a power plant produces or can produce by using the installed power for 1 year (365x24=8760 hours)[28], [29]. In other words, the ratio of the total energy produced by a wind turbine within a specified period to the total power that the turbine will obtain by operating at nominal power for the same time period is defined as the capacity factor[30].

$$K_F = \frac{\text{One Year Total Real Energy}}{\text{Total Energy Required by the Turbine to Produce in a Year at Nominal Power}} \quad (5)$$

The feasibility studies carried out before the investment in wind power plants allows optimum operation of existing resources and maximum benefit from these resources. Because, according to the feasibility study, financial and technical issues (depreciation period, turbine selection, etc.) can be predicted. In addition, the first parameter taken into consideration in power plant installations is the capacity factor. According to this parameter, investment calculations are made according to which class turbine will be selected in the facility and the selected turbine model.

When the technical characteristics and technical potentials of wind power plants are taken into account, it is seen that the capacity factors are also high in the areas where the wind speed is high. But there are rare exceptions to this situation. That is, while the capacity factor is low, electricity generation is high. This is explained by the use of turbines with a stronger capacity and a nominal power value[30].

According to Akkaş, the capacity factor is an important parameter for the technically and economically viable and sustainable wind power plants that are established or planned to be established[30].

3. RESULTS

3.1. Evaluations by WPP Generation

In the study, the annual mean, maximum, and minimum capacity factors of the provinces were calculated by considering the generation in 2022 of the facilities located in the provinces of the Aegean region, and these calculated values are given in Table 2. The maximum and minimum capacity values given in the table are the capacity factors of any facility in that province. If we explain this situation with an example; The maximum capacity factor of İzmir is 73.3%. In other words, one of the facilities in İzmir operates with a capacity factor of 73.3%. Since there is only one facility in Uşak and Denizli provinces, the maximum, minimum, and mean capacity factors in these provinces are equal. The province with the highest capacity factor in the Aegean Region is İzmir with 39.9%. The province with the lowest capacity factor in the Aegean region is Uşak with 29.3%. When we evaluate the Aegean Region in terms of facility generation and installed power in general, it shows that the facilities established in the region operate with a capacity factor of 30% or more.

Table 2. Maximum, minimum, and mean WPP capacity factors of the provinces

	Total Installed Power (MW)	Total Generation (MWh)	Mean Generation (MWh)	Mean Capacity Factor %	Maximum Capacity Factor %	Minimum Capacity Factor %	Number of Plants
İzmir	1742,6	6102040,3	696,6	39,9	73,3	29,9	52
Manisa	701,7	2374348,9	271,0	38,6	48,9	30,8	10
Aydın	397,3	1142728,1	130,4	32,8	44,7	24,7	11
Muğla	214,0	636813,8	72,7	33,9	48,0	23,1	7
Uşak	61,5	152631,1	17,4	29,3	28,3	28,3	1
Denizli	66,0	199933,0	22,8	34,5	34,5	35,0	1
Afyonkarahisar	323,8	902219,3	103,0	31,8	38,9	26,6	4

4. CONCLUSION

With the developing industry and technology, there has been a great increase in energy demand. More conventional energy sources have been used to meet the increasing energy demand. As a natural consequence of this situation, an increase in environmental and climatic problems has also been observed. For this reason, states have turned to renewable energy sources in order to reduce the effects of environmental and climatic problems that have been increasing in recent years. In this context; The Aegean region is a region with a high energy potential in terms of wind energy, one of the renewable energy sources. For new investments to be made in this region, the province with the best capacity factor should be chosen so that the depreciation period is minimum and the energy production is maximum. In this study, the average capacity factors of the provinces were examined by evaluating the real production of 86 facilities established in the region. As a result of the examinations, the average annual capacity factors of İzmir, Manisa, Aydın, Muğla, Uşak, Denizli, and Afyonkarahisar provinces were calculated as 39.9%, 38.6%, 32.8%, 33.9%, 29.3%, 34.5%, and 31.8%, respectively. According to these data, the annual average capacity factor of the Aegean Region is 34.4%. The province with the highest annual average capacity factor in the region is İzmir. The province with the lowest annual average capacity factor is Uşak with 29.3%. According to these results, it is predicted that giving priority to İzmir in site selection for new facilities to be established in the Aegean Region will be beneficial for the investor.

REFERENCES

- [1] S. Zhang, C. Wang, P. Liao, L. Xiao, and T. Fu, "Wind speed forecasting based on model selection, fuzzy cluster, and multi-objective algorithm and wind energy simulation by Betz's theory," *Expert Syst. Appl.*, vol. 193, no. January, p. 116509, 2022, doi: 10.1016/j.eswa.2022.116509.
- [2] E. Günay and S. Yıldırım, "Yenilenebilir Enerji Kapasitesi Açısından Türkiye'nin Durumu," in *V. International Kahramanmaraş Management, Economy and Politics Congress*, pp. 21-31, (2022).
- [3] IRENA, *Renewable Capacity Statistics 2022*. 2021.
- [4] IRENA, "IRENA 's Renewable Energy Roadmap - Renewable energy policy targets for REmap countries," 2020.
- [5] "T.C. Enerji ve Tabii Kaynaklar Bakanlığı." <https://enerji.gov.tr/bilgi-merkezi-enerji-elektrik#> (accessed May 01, 2023).
- [6] A. Ucar and F. Balıoğlu, "Assessment of wind power potential for turbine installation in coastal areas of Turkey," *Renew. Sustain. Energy Rev.*, vol. 14, no. 7, pp. 1901-1912, 2010, doi: 10.1016/j.rser.2010.03.021.
- [7] E. Koç and M. C. Şenel, "Dunyada ve Turkiyede Enerji Durumu," *Engineer and Machinery*, pp. 1-4, 2013.

- [8] M. E. Şahin, "Açık Deniz Rüzgâr Sistemleri Üzerine Bir İnceleme ve Danimarka Modeli," *Recep Tayyip Erdoğan University Science and Engineering Science. Journal.*, vol. 1(1), no. 1, pp. 54-67, 2020.
- [9] TÜREB, "2018 Turkish Wind Energy Statistics," 2019.
- [10] A. Koç, H. Yağlı, Y. Koç, and İ. Uğurlu, "Dünyada ve Türkiye' de Enerji Görünümünün Genel Değerlendirilmesi," *Engineering and Machinery Journal.*, vol. 59, no. 692, pp. 84-112, 2018.
- [11] GAZBİR, "Dünyada ve Türkiye' de Enerji Durumu," 2017.
- [12] H. Gençel and İ. Tarhan, "Capacity Factor Analysis for Some Wind Power Plants in the Çanakkale Region, One of the Important Transition Places of Wind Energy," pp. 120-139, 2019.
- [13] C. Yıldız and M. A. Akgül, "Efficiency-based comparison of offshore solar and wind power generation on the Mediterranean coast of Turkey," *BAUN Fen Bil. Enst. Derg.*, vol. 25, no. 1, pp. 122-136, 2023, doi: 10.25092/baunfbed.
- [14] W. Dong, G. Zhao, S. Yüksel, H. Dinçer, and G. G. Ubay, "A novel hybrid decision making approach for the strategic selection of wind energy projects," *Renew. Energy*, vol. 185, pp. 321-337, 2022, doi: 10.1016/j.renene.2021.12.077.
- [15] Ş. Kavcıoğlu, "Renewable Energy and Turkey," *Finance. Journal of Research and Studies.*, pp. 209-227, 2019, doi: 10.14784/marufacd.623399.
- [16] B. Kapusiz and Y. Uzun, "Wind Energy in the World and Turkey," no. November, 2022.
- [17] M. C. Şenel and E. Koç, "General evaluation of the wind energy situation in the world and in Turkey," *Eng. Mach.*, vol. 56, no. 663, pp. 46-56, 2015.
- [18] KPMG, "Energy Sectoral Overview," 2019.
- [19] TMMOB, "Electric Energy Statistics in Turkey," 2020.
- [20] "Global Electricity Review 2022 | Kor." <https://ember-climate.org/insights/research/global-electricity-review-2022/> (accessed May 19, 2023).
- [21] İ. Karadöl, C. Yıldız, and M. Şekkel, "Determining optimal spatial and temporal complementarity between wind and hydropower," *Energy*, vol. 230, 2021, doi: 10.1016/j.energy.2021.120790.
- [22] C. Hakyemez, "Türkiye Sınai Kalkınma Bankası Aylık Enerji Bülteni," 2022.
- [23] V. Femin, R. Veena, I. Petra, S. Mathew, and J. Hazra, "Modelling the ramping behaviour of wind turbines," 2016, doi: 10.1109/COGEN.2016.7728967.
- [24] L. Söder *et al.*, "Review of wind generation within adequacy calculations and capacity markets for different power systems," *Renew. Sustain. Energy Rev.*, vol. 119, no. November 2019, 2020, doi: 10.1016/j.rser.2019.109540.
- [25] H. Demolli, A. S. Dokuz, A. Ecemis, and M. Gokcek, "Wind power forecasting based on daily wind speed data using machine learning algorithms," *Energy Convers. Manag.*, vol. 198, no. July, p. 111823, 2019, doi: 10.1016/j.enconman.2019.111823.
- [26] Q. Cheng *et al.*, "Complementary operation with wind and photovoltaic power induces the decrease in hydropower efficiency," *Appl. Energy*, vol. 339, no. March, p. 121006, 2023, doi: 10.1016/j.apenergy.2023.121006.
- [27] Q. Li, J. Wang, and H. Zhang, "Comparison of the goodness-of-fit of intelligent-optimized wind speed distributions and calculation in high-altitude wind-energy potential assessment," *Energy Convers. Manag.*, vol. 247, no. 217, p. 114737, 2021, doi: 10.1016/j.enconman.2021.114737.
- [28] L. Wang, T. H. Yeh, W. J. Lee, and Z. Chen, "Benefit evaluation of wind turbine generators in wind farms using capacity-factor analysis and economic-cost methods," *IEEE Trans. Power Syst.*, vol. 24, no. 2, pp. 692-704, 2009, doi: 10.1109/TPWRS.2009.2016519.
- [29] M. H. Albadi and E. F. El-Saadany, "Wind turbines capacity factor modeling - A novel approach," *IEEE Trans. Power Syst.*, vol. 24, no. 3, pp. 1637-1638, 2009, doi: 10.1109/TPWRS.2009.2023274.
- [30] A. A. Akkaş, "Rüzgar Enerjisi Sistemlerinin Performans Değerlendirmesi," *Rüzgar Enerj. Sempozyumu*, no. April, pp. 75-84, 2001, [Online]. Available: <http://www.ruzgarsempozyumu.org/wp-content/uploads/2014/08/008.pdf>.

8 JULY 2023

REGISTRATION (Face to Face)

OPENNING CEREMONY (Face to Face/Online)

Prof. Dr. Orhan Aydın

Assoc. Prof. Dr. Gökhan Çuvalcıoğlu

KEYNOTE SPEAKER

The Role of Engineering and Applied Sciences in Developing Innovative Energy Solutions

Prof. Dr. İbrahim Dinçer (Face to Face/Online)

Chair: Gökhan Çuvalcıoğlu

COFFEE BREAK

1. SESSION

HALL-A (Face to Face)-Mathematics

Chair: **Şehmus Fındık**

Generalization of Almost Primary and Nilary Ideals in Noncommutative Rings

Alaa Abouhalaka

Connected, Compact, and Sober Objects in ConLim

Kübra Çevik, Ayhan Erciyes

Dna Codes From Reversible Group Codes By A Virus Optimisation Algorithm

Adrian Korban, **Serap Şahinkaya, Deniz Üstün**

Fractional ECFGM(1,1) model with an application

Ümmügülsüm Erdinç, Halis Bilgil

HALL-B (Face to Face)-Engineering

Chair: **Buğra Sarper**

A Hybrid Deep Reinforcement Learning Algorithm Application For Vehicle Routing Problem

Meltem Atmı, Tolunay Göçken

Optimization of Gurney flap over NACA 0018 by using Surrogate Modeling

Emre Güler, Mehmet Erdem, Şihmehmet Yıldız, Melike Nikbay

The Comparison of Hydrodynamics Designs of Different Geometries in Restricted and Unrestricted Fluidal Mediums with Potential Flow and CFD

Munir Suner, S. Aydın Salci, K. Suleyman Yigit

KEYNOTE SPEAKER

From Type-1, to Type-2 and Type-3 Fuzzy Systems: Theory and Applications

Prof. Dr. Oscar Castillo

Chair: Gökhan Çuvalcıoğlu

2. SESSION

HALL-A (ONLINE)-Mathematics

HALL-B (ONLINE)-Engineering

Chair: **Gökhan Çuvalcıoğlu**

Generators of F/R' Leibniz algebras

Zeynep Özkurt

Clique Matching Neighborhood Polynomial of Graphs

Aldison M. Asdain, Rosalio G. Artes Jr.

Fren simplicial homotopy to crossed module homotopy

Hatice Gülsün Akay

Local Lower Separation Axioms In Q-Reflexive Spaces

Samed Özkan

An Application Of Controlled Sets in Medical

Diagnosis

Sinem Tarsuslu(Yılmaz), Gökhan Çuvalcıoğlu

Chair: **Buğra Sarper**

Measurements And Evaluation Of Electric Field Exposure Generated By Modem in Home Environment

Mustafa Mutlu

The Effects Of Collector Plate Material On Fiber Fineness in Electrospinning

Gonca Şimşek Gündüz

Masked And Unmasked Face Recognition On Unconstrained Facial Images Using Hand-Crafted Methods

Ali Torbati, Önsen Toygar

Classification of Brain Tumors on MRI Images Using Deep Learning Architectures

Samaneh Sarfarazi, Önsen Toygar

9 JULY 2023

INVITED SPEAKER

On the Scattering Problem for a Non-Self-Adjoint Boundary Value Problem

Hanlar Reşidoğlu

Chair: Gökhan Çuvalcıoğlu

COFFEE BREAK

Online Poster

Effect of production method on selected bioactive compounds and antioxidant activity of Japanese quince and quince fruit tinctures

Natalia Marat, Marzena Danowska-Oziewicz, Magdalena Polak-Śliwińska, Agnieszka Narwojsz

1. SESSION

HALL-A (Face to Face)-Mathematics

Chair: **Şehmus Fındık**

Best Approximation of Fixed Point Results in Generalized Metric Spaces

Nesrin Manav Tatar

Approximate Solutions Of The Modified Kratzer Potential Plus Screened Coulomb Potential in N-Dimensions

Aysel Özfidan

A Novel Methodological Framework To Identify The Criteria For Decision-Making Problems in Neutrosophic Fuzzy Environment

Ömer Faruk Görçün

HALL-B (Face to Face)-Engineering

Chair: **Buğra Sarper**

Corporate Carbon Footprint Calculation And Evaluation Of Mersin University Çiftlikköy Campus

Hasret KARAKAYA, Yasin ÖZAY, Nadir DİZGE

Active Packaging Films Incorporated With Essential Oils in Nanoemulsion Formulation

Natalia Marat, Aleksandra Purkiewicz, Didem Demir, Yasin Özay, Gulden Goksen

Smart Film Production By Including Bioactive Compounds

Aleksandra Purkiewicz, Natalia Marat, Didem Demir, Yasin Özay, Gulden Goksen

Using Fuzzy-Logic In Market Conditions For Efficient Portfolio Selection In The Casablanca Stock Exchange Abdelhamid Hamidi Alaoui	Determination Of Priority Areas For A Possible Underground Dam Around The Harşit Stream Basin Tuğba BOZKUŞ ; Yusuf KAYA
--	---

COFFEE BREAK

2. SESSION	
HALL-A (ONLINE)-Mathematics	HALL-B (ONLINE)-Engineering
Chair: Gökhan Çuvalcıoğlu	Chair: Deniz Üstün
A Maximal Type Of Zagreb Index Büşra Aydın , Nihat Akgüneş	Biofuel Utilization in The Aviation Industry Emine Kahramaner , Özlem Ateş Duru
A Note On Higher Order Pell 2 ^s -IONS Hayrullah Özımamoğlu	Interaction Between Ret Protein Kinase And Curcumin And Resveratrol: A Molecular Docking Perspective Deniz Karataş
Some Properties Of Leonardo Sedenions Hayrullah Özımamoğlu	Second Order Model Reduction Of Higher Order Systems And Pid Controller Design Ali Yüce
Revolutionizing Matrix Computations: A Practical Approach For Efficient Calculation Of Matrix Sign Function Gül Karaduman	Automotive Industry Spare Parts Stock Management Abc Analysis Based Ahp Method Application Elife İrem Kal , Emel Yontar
Applications Of Selection, Determination And Decision Making in Education With The Help Of Fuzzy Logic Ali Sınar , Erhan Çetinkaya, Ahu Meryem Çuvalcıoğlu	
Examples And Applications Of Decision Making in The Field Of Education Using Intuitionistic Fuzzy Sets Erhan Çetinkaya , Ali Sınar, Ahu Meryem Çuvalcıoğlu	

LUNCH

INVITED SPEAKER

Challenges of PVT and Nano-based Thermal Property Enhancement of PVT-PCM Systems

Md. Hasanuzzaman

Chair: Buğra Sarper

POSTER FACE TO FACE

On An Eigenproblem Of The Fractional Sturm-Liouville Boundary Value Problem

Zeynep Geçit

3. SESSION

HALL-A (Face to Face)-Mathematics

HALL-B (ONLINE)-Engineering

Chair: **Şehmus Fındık**

Chair: **Serap Şahinkaya**

Approximation By Bivariate Complex Stancu-Schurer Polynomials in Compact Disks

Nesibe Manav Mutlu

Evaluation Of Environmental, Social And Economic Performances Of 81 Provinces Of Turkey With Data Envelopment Analysis

Gökçen Bayram, Ayşe Hande Erol Bingöler, B. Gültekin Çetiner

Approximation By Generalization Of Bernstein-Schurer Operators

Nursel Çetin, **Nesibe Manav Mutlu**

A Literature Survey Based On The Tabu Search Heuristic Method For The Solution Of The Multi-Dimensional And Multi-Objective Knapsack Problem And Variations

Gürkan Güven Güner

On Translation Surfaces

Beyhan Yılmaz, Aykut Has

The Evaluation Of The Criteria To Be Taken into Account When Selecting Online Shopping Sites Based On Industry 4.0 With Using Dematel Method

Zeynep Durmaz, Erdem Aksakal

Fractional Approach To Some Fundamental Concepts Of Surface

Aykut Has, Beyhan Yılmaz

Optimizing CO2 Laser Cutting Parameters Of Polyethylene Polymeric Material Using Hybrid Entropy-Topsis Approach

Oğuzhan Der, Gökhan Başar, Muhammed Ordu

Subprojectivity Domain of Finitely Generated Modules

Arslan Yasin Shibeshi, Yılmaz Durğun

COFFEE BREAK

4. SESSION

HALL-A (ONLINE)-Mathematics		HALL-B (ONLINE)-Engineering	
Chair: Feride Tuğrul		Chair: Serap Şahinkaya	
Novel Inequalities For Generalized Fractional Integrals Applied To Synchronized Convex Functions Abdullah Akkurt , Hüseyin Yıldırım		A Solution To The Solid Transportation Problem Using Lr Flat Numbers Nuran Budak , Nuran Guzel	
On Kconformable Fractional Operators Sümeyye Ermeydan Çiriş , Hüseyin Yıldırım		A Compromise Solution To The Multi-Objective Solid Transportation Problem With The Uncertain Parameters Sedanur AKTÜRK , Nuran GÜZEL	
A Petrov-Galerkin Method For Solving The Generalized Equal Width Equation Yusuf Tatlisu , Seydi Battal Gazi Karakoc		Thermal Diffusion-Based Boriding Effect On Hvf-Sprayed Aisi 316l Stainless Steel Coating Bülent Ermiş , Harun Mindivan	
On Analytical Solutions Of Space-Time Fractional Variant Boussinesq Equation With Beta Derivative Nagehan Özdemir , Ayten Özkan		Sign Language Recognition Mobile Application For Turkish Language Erdem Demiroğlu , Furkan Ayakdaş, Asude Tanribuyurdu, Gülsüm Akkuzu Kaya	

COFFEE BREAK

5. SESSION

HALL-A (ONLINE)-Mathematics		HALL-B (ONLINE)-Engineering	
Chair: Arif Bal		Chair: Buğra Sarper	
Mixed İnteger Linear Programming Model For Optimizing University Exam Schedules Hamza Abunima , Burhan Pektaş, Nazmiye Kopacak, Özlem Şimşek		The Effects Of Cylindrical And Partial Pin Fins On The Cooling Performance Of A Minichannel Heat Sink Dondu Nur Turk , Kayhan Dagidir, Bugra Sarper, Orhan Aydın	
Complex Matrix Version Of Hybrid Numbers		A Performance Analysis Comparison Of Machine Learning Algorithms in Detection Of Heart Disease	

Çağla Ramis , Yasin Yazlık	Bahar Demirtürk, Bekir Can Telkenaroğlu
Generalized Kantorovich-Schurer-Type Operators Nursel Çetin	Investigation Of The Effect Of Nanoparticle Additives On The Refractive Index And Density Of Gasoline Mehmet Selman Gökmen , Mehmet Fatih Parlak, Hasan Aydoğan
Exact Solution Of The Schrodinger Equation in The Topologically Massive Space-Time Ali Tarsuslu , Kenan Söğüt	Simple Ways For Obtaining Transformation Matrices Of Serial Manipulators Samet Yavuz

10 JULY 2023

1. SESSION

HALL-A (Online)-Mathematics

HALL-B (Online)-Engineering

Chair: **Gökhan Çuvalcıoğlu**

Chair: **Aysel Özfidan**

A Fuzzy Soft Set-Based Approach To Identify Academic Dishonesty And Misconduct
Esra Korkmaz

Effect Of Different Build Orientations On Mechanical Properties Of Parts in Additive Manufacturing Technology
Derya Karaman And Hüccet Kahramanzade

Locally Recoverable Codes Based On The Matrices Derived From The Magic Squares
Rabia Zengin, Mehmet Emin Köroğlu

Pistachio Species Identification Using Histogram Of Oriented Gradient Descriptors And Support Vector Machine
Birkan Büyükarikan

Cyclic Dna Codes Over Mixed Alphabets
Tulay Yıldırım

An Innovative Approach for Enhancing Traffic Flow: Decentralized Traffic Signal Split Control Method
Serap Ergün

Finite Element Method For The Nonlocal Elliptic Problem With A \mathbb{S} -Kirchhoff-Type Operator
Mahamat Saleh Daoussa Haggat, Mohamed Mbhou

Addressing the Challenge of Traffic Congestion: An Innovative Approach to Optimize Traffic Signal Control for Improved Traffic Flow
Serap Ergün

COFFEE BREAK

2. SESSION

HALL-A (Face to Face)-Mathematics	HALL-B (Online)-Engineering
Chair: Şehmus Fındık	Chair: Münir Süner
On Derivations Of Free Bicommutative Algebras Şehmus Fındık	Applying The Artificial Bee Colony Algorithm: Enhancing The Efficiency Of A Hydrogen-Based Hybrid Renewable Energy System Aykut Fatih Güven
On Fuzzy Boolean Algebra With Respect To New Fuzzy Logic Conjunction Gökhan Çuvalcıođlu, Gül Karadeniz Gözeri	Vislit-Test: Designing Effective Visualization Literacy Assessment Test Elif E. Fırat
(α, β) -Interval Valued Intuitionistic Fuzzy Subgroups Arif Bal , Gökhan Çuvalcıođlu	A Guideline To Designing Crowdsourced Online Experiments For Evaluating Visualization Literacy Elif E. Fırat
Approach To Intuitionistic Fuzzy Sets With Comparative Examples Of Decision Making Methods In Different Fields Feride Tuđrul , Mehmet Çitil, Gökhan Çuvalcıođlu	Numerical Simulation Of Graphene/N-Ws ₂ /A-Si:H(I)/P-Csi/Ag Hit Solar Cells Nahide Karabulut , Büşra Aydın, Çađlar Duman

COFFEE BREAK

3. SESSION

HALL-A (Online)-Mathematics

HALL-B (Online)-Engineering

Chair: **Feride Tuğrul**

Chair: **Münir Süner**

A New Approach For Score Function On Q-Rung Orthopair Fuzzy Sets

Ali Köseoğlu

Investigation Of Convection Heat Transfer Coefficient Effects On Thermal Energy Storage Performance With Pcm/Graphite Matrix Composite

Sare Mitincik, Mustafa Yusuf Yazici

Convex Independent Common Neighborhood Polynomial Of Graphs

Amelia L. Arriesgado, Rosalio G. Artes Jr.

Impact Sliding Wear Behaviour Of Thermally Oxidized Ti-6Al-4V Alloy

Ayşenur Eğercioğlu, Harun Mindivan

On A General Inclusion Theorem

Hikmet Seyhan Özarslan And **Bağdagül Kartal**

Analysis Of Heating And Cooling Degree Day Values For Tra2 Region Provinces

Galip Kaltakkiran

Solvability And Guh Stability Results Of Fuzzy Nonlinear Abc-Fractional Coupled System

Aziz El Ghazouani, M'hamed Elomari And Said Melliani

Investigating The Time-Domain Sensitivities To Nonlinear Hydrodynamic Interactions Of A Resonant Micro-Cantilever With Glycerol-Water Solutions in Multi-Frequency Operations

Cağrı Yılmaz

On Modeling on Multiplicative Calculus for Population Growth

Yusuf Ziya Altay, Aslı Bucak, **Sertaç Gökteş**

LUNCH

INVITED SPEAKER

ON INTUITIONISTIC FUZZY PRIMARY DECOMPOSITION OF INTUITIONISTIC FUZZY IDEALS

POONAM K. SHARMA

Chair: Gökhan Çuvalcıoğlu

POSTER FACE TO FACE

Robustness Control Circuit for Logic Circuit Integrations with PIC and Arduino Microcontrollers

Mehmet Ersin Aytekin, Dönay Kayahan

Structural Analysis Development Study Of The Rear Cover Used in The Trailer Vehicle

Onur Can Kırıt, Mehmet Vurgun

Reducing The Use Of High-Strength Sheet Metal in Timber Carrier Semi-Trailer Vehicles

Mehmet Vurgun, Onur Can Kırıt

R58-03 Application in Aluminum Chassis

Mustafa YILMAZ, Akın ZENGİN, Onur Can KIRIT, Necip Ahmet KÖROĞLU

4. SESSION

HALL-A (Online)-Mathematics

Chair: **Arif Bal**

A Note On Fuzzy Product Rule
Tahir Ceylan

Fixed-Point Theorems Via Fuzzy-Interpolative Kannan Type Contraction
Meryem Şenocak

Positive Toeplitz Operators Between Harmonic Bloch Spaces On The Ball
Ömer Faruk Doğan

Existence Theorems For Set-Valued Operators in Wc-Banach Algebras
Cesim Temel And **Müberra Selah**

HALL-B (Face to Face)-Engineering

Chair: **Veysel Alcan**

An Encoding –Decoding Algorithm Based On Narayana Numbers
Engin Eser, **Bahar Kuloğlu** And Engin Özkan

New Number Sequences Built On Hybrid Numbers
Mine Uysal And Engin Özkan

A New Approach To Gadovan Numbers
Engin Özkan, **Engin Eser**, Mine Uysal

Microwave Energy-Based Hybrid Nanomaterial Preparation Approach For Energy Storage Purposes
Selçuk Poyraz

COFFEE BREAK

5. SESSION

HALL-A (Online)-Mathematics		HALL-B (Face to Face)-Engineering	
Chair: Şehmus Fındık		Chair: Buğra Sarper	
An Action Of Dihedral Group Nazar Şahin Ögüslü		Multi-Objective Optimizations Of Circular And Square Ducts Under Laminar Flow And Constant Wall Temperature Conditions Muhammet Nasif Kuru	
Invariant Algebras in Polynomial Rings Nazar Şahin Ögüslü		Evaluation Of The Effects Of Visual And Somatosensory Inputs On Balance in The Elderly By Using Machine Learning Veysel Alcan	
Multiplication Rules For Pointwise Inner Automorphisms in Lie Algebras Ela Aydın		Theoretical Investigation Of Alternative Fuels Which Can Be Used On Ships Münir Süner, Buğra Sarper, Servet Uzel, Nedim Kizilkaya	
Fekete-Szegö Problem For Two New Subclasses Of Bi-Univalent Functions Defined By Bernoulli Polynomial Yunus KORKMAZ, İbrahim AKTAŞ			

COFFEE BREAK

6. SESSION

HALL-A (Online)-Mathematics		HALL-B (Online)-Mathematics	
Chair: Feride Tuğrul		Chair: Münir Süner	
Fractional Prey-Predator Model With Linear Functional Response, Prey Refuge, Fear And Carry-Over Effect Ercan Balcı		On Reliability Analysis Of Reference Intervals in Medicine Gülşen Kiliç	

An Almost Unbiased Ridge Estimator in Beta Regression Yasin Asar	On Isolated Subsemigroups Of Order-Decreasing Transformation Semigroups Melek Yağci
Investigating Solitary Wave Solutions Of The Benjamin-Ono Equation For Modelling Internal Waves in Deep Water Gülşen Kiliç, Serbay Duran , Birgül Binzet	Relative Controllability Of The μ -Caputo Fractional Delayed System With Impulses Mustafa Aydın
	Brief Qualitative Properties Of The Regularized Prabhakar Fractional System Mustafa Aydın

11 JULY 2023

1. SESSION

HALL-A (ONLINE)-Mathematics

Chair: **Feride Tuğrul**

Generalized Symmetric Bi-Derivations Of $Up(Bcc)$ -Algebras

Damla Yilmaz

Modeling And Analysis Of Capacitated Nonlinear Network Traffic Assignment Problem

Hasan Dalman

A Dynamic Approach To The Effect Of Harvesting

Seval Işık, Figen Kangalgil

Role Of The Weak Allee Phenomena On A Predator-Prey Model

Figen Kangalgil, **Seval Işık**

HALL-B (ONLINE)-Engineering

Chair: **Buğra Sarper**

The Influence Of The Lactation Period And The Type Of Modified Milk On The Content Of Essential Amino Acids in Human Milk And Infant Formula

Aleksandra Purkiewicz, Kinga Szajkowska, Jacek Nowakowski, Renata Pietrzak-Fiećko

On The Exponential Stability Of Stationary And Perturbed Implicit Systems

Nor El-Houda Beghersa, Mehdi Benabdallah, Mohamed Hariri

Elimination Of Actuation Singularities Of Kinematically Redundant Rpr-Rpr Planar Parallel Robots

Mustafa Özdemir And **Muhammed Yasir Çubuk**

INVITED SPEAKER

HALL-A

TOPOLOGICAL INDICES OF FUZZY GRAPH

MADHUMANGAL PAL

Chair: Şehmus Fındık

HALL-B

POSTER ONLINE

Design of Load Lifting Eyebolts and Standardization with Static Tests

Yasin AYGÜL

On A One Type Fractional Sturm-Liouville Problem

Pınar TÜRKMEN

COFFEE BREAK

2. SESSION

HALL-A (ONLINE)-Mathematics

HALL-B (ONLINE)-Engineering

Chair: **Feride Tuğrul**

Chair: **Buğra Sarper**

On Infra Fuzzy-Soft Topological Spaces

Arife Atay

Solving Nonlinear She Equations Using Harris Hawks Optimization Algorithm

Yasin Bektaş

On Leap Zagreb Indices Of A Special Graph Obtained By Semigroups

Yaşar Nacaroglu

The Necessity Of Using Recycled Waste Aggregate in Turkiye

Eren Yağmur

The Gradient And Partial Derivatives Of Bicomplex Numbers: A Commutative-Quaternion Approach

Ali Atasoy

A Review On Latest Developments in Assembly And Temporary Shelters For Natural Disasters

İrem Karakaya, Alev Taşkin

Comparison Of Predictors/Estimators in General Linear Models With Stochastic Restrictions

Nesrin Güler And **Melek Eriş Büyükkaya**

Carbon Footprint Calculation And Mitigation Strategies For The Transportation Against Climate Change: Pestel Analysis

Şölen Zengin, Fatma Ersoy Duran, Emel Yontar

Numerical Solutions Of Conformable Time-Fractional Klein-Gordon Equation With Proportional Delay By The Novel Method

Halil Anaç

Deciding Applicability Of Blockchain İn Avionics Systems

Ayşenur Sayıl, Harun Çelik

3. SESSION

HALL-A (ONLINE)-Mathematics	HALL-B (ONLINE)-Engineering
Chair: Arif Bal	Chair: Buğra Sarper
Approximation Of Max-Product Truncated Baskakov Operators By Fuzzy Numbers Ecem Acar And Sevilay Kırıcı Serenbay	Process Improvement With Value Flow Mapping Method For Low Density Polyethylene Recycling Processes Emre Can Temiz , Emel Yontar
Geodetic Index Of Graphs Glee Ann L. Tampipi And Rosalio G. Artes Jr.	Investigation Of The Capacity Factor Of The Ege Region Wind Power Plants According To The Real Productions İsrafil Karadöl
Induced Path Polynomials Of The Join And Corona Of Graphs Cerina A. Villarta , Rolito G. Eballe And Rosalio G. Artes Jr.	Comparison Of Reactivity Feedback Coefficients Obtained From Mcnp6.2 And Serpent Monte Carlo Codes Elif Ahsen Baştuğ And Bahram R. Maleki
Statistical Cauchyness With Deferred Cesáro Mean in Asymmetric Context Zeynep Hande Toyganözü	Numerical Investigation Of The Thermal Performance Of A Liquid Cooled Battery Pack Soner Birinci , Mehmet Sağlam, Bugra Sarper, M. Yusuf Yazici And Orhan Aydın
Existence Results for Antiperiodic Ψ -Caputo Fractional Differential Equations with p-Laplacian Operator Walid Benhadda , M. El-Omari, A. Kassidi, A. El Mfadel	

LUNCH

4. SESSION

HALL-A (ONLINE)-Mathematics	HALL-B (ONLINE)-Engineering
Chair: Arif Bal	Chair: Münir Süner
Solvability Of A System Of Third-Order Difference Equations Merve Kara, Şule Devocioğlu	Quality Classification of Ceramic SanitaryWare Products with Machine Learning Techiques Sedanur Şimşek , Erdener Özçetin
Properties Of Generalized Semi Closed Sets in The Topology	Computational Aeroacoustic Modeling Of Supersonic Cavity Flows Using Open-Source Flow Solvers

Havva Taşkıran , Ayhan Erciyes	Ramazan Kaba , Melike Nıkbay, Baha Zafer
Some Numerical Approaches For Computing The Hankel Transform Meryem Güney , Zekeriya Ustaoglu	Production Of Sucker Rod And Determination Of Its Mechanical Properties And Localization Of This Product Kürşat Kahya, Dergah Uysal , Gökhan Acıyiyen
	Detection Of Effect Of Smart Robot Automation On Quality And Efficiency in Production Kürşat Kahya, Seren Geçgel , Seda Yücel

COFFEE BREAK

5. SESSION

HALL-A (ONLINE)-Mathematics	HALL-B (ONLINE)-Engineering
Chair: Gökhan Çuvalcıoğlu	Chair: Münir Süner
Approximate Solutions Of The Integro-Partial Fractional Equation Involving Tempered Ψ -Caputo Fractional Derivative Sami Baroudi , M'hamed Elomari, Ali El Mfadel And Abderrazak Kassidi	Investigation Of The Effect Of Types And Particle Sizes Of Reinforcements On Composite Hardness Of Al6061 Alperen Dindar , Merve Tur, Türker Türkoğlu, Sare Çelik
Totally Umbilical Semi-Invariant Submanifolds Of Poly-Norden Manifolds Şerife Nur Bozdağ	A Performance Analysis Of Attack Individual Pension Funds By A System Dynamics Simulation Approach Muhammed Ordu
Some Fixed Point Applications Of F-Modular Metric Nesrin Manav Tatar, Zehra Dogan , Duran Turkoglu	Ultrasonic Pilot Reactor Design: Temperature, Pressure And Rotary Control Can Be Used in The Production Of Hygroscopic Materials Sinan Köse , Fatma Ulusal, Salih Hakan Yetgin
Open-Loop Control Vs Closed-Loop Control in Smart Irrigation: A Game Theoretical Perspective Ali Hamidoğlu	The Use Of Unmanned Aerial Vehicles in The 3d Documentation Of Historical And Cultural Heritage: The Case Of Ceyhan Kurtkulagi Caravanserai Enis Arslan , Ali İhsan Şekertekin

COFFEE BREAK

6. SESSION

HALL-A (ONLINE)-Mathematics		HALL-B (ONLINE)-Engineering	
Chair: Arif Bal		Chair: Münir Süner	
Preconditioning Linear Systems Using Kronecker Sum Decomposition Youssouf Mezzar		Faults And Suggestions Detected In Distribution Panel And Transformers in Power Plants Hale Bakir	
Nonlinear Differential Equations According To The Bishop Parallel Transport Frame Fatma Bulut		Prediction Of Covid-19 Cases Using Unidirectional Lstm, Bidirectional Lstm, And Deep Neural Network Applications Baha Şen, Büşra Demirbaş	
A Generalization Of The Linear Positive Operators By Using The Special Polynomials Kadir Kanat, Melek Sofyalioglu, Verda Karadaş			

COFFEE BREAK

7. SESSION

HALL-A (ONLINE)-Mathematics		HALL-B (ONLINE)-Mathematics	
Chair: Gökhan Çuvalcıoğlu		Chair: Münir Süner	
Decompositions And Inverses Of Some Lower Triangular Matrices Cahit Köme And Kadir Hilal		Compositions Of Permuting N-Derivations With Commutativity For Associative Rings Mehsin Jabel Atteya	
On A New Class Of Hyperbolic Fibonacci Functions Via Some Special Polynomials Sure Köme And Yasin Yazlik		Some Results On Deferred Cesaro Statistical Convergence Of Order A in The Probability Spaces Uğur Değer, Kübra Uzun	
On Some Natural Geometric Differential Operators Razvan M. Tudoran		Spacelike F-Rectifying Curves in Minkowski Space Hülya Gün Bozok, Önder Korkmaz	
The Selfadjoint Schrödinger Operator On The Half Line With A Real-Valued Compactly Supported Potential Mehmet Ünlü		The Comparison Between Effects Of Heterogeneous And Homogeneous Double Layered Compressible Elastic Media On Dark Solitary Sh Waves Ekin Deliktaş Özdemir	

Contra Continuity For Λ -Strong B-I-Closed Sets Seyfettin Fidan , Aynur Keskin Kaymakci	Approximate Solutions Of Some Fredholm Integral Equations Associated With Lucas Polynomials Çağla Türkoğlu
Almost Supra B-Continuous Functions Fatma Talas , Aynur Keskin Kaymakci	Similarity Measure in Bipolar Fuzzy Sets And its Application To Multi-Attribute Decision Making Method Gözde Sever , Zariife Zararsiz

CLOSING CEREMONY

Chair: Gökhan Çuvalcıoğlu